Tomas Bata University in Zlín
Faculty of Technology

Doctoral Thesis

Preparation of (bio)polymer matrices for substance transfer and study of their release

Příprava (bio)polymerních matric pro přenos látek a studium jejich uvolňování

Author: **Ing. Monika Muchová**

Degree programme: Chemistry and Materials Technology (P2808)

Degree course: Technology of Macromolecular Compounds (2808V006)

Supervisor: Assoc. Prof. Ing. *et* Ing. Ivo Kuřitka, Ph.D. *et* Ph.D.

Consultant: Mgr. Jan Vícha, Ph.D.

Zlín, October 2023

ACKNOWLEDGEMENT

I would like to convey my sincere gratitude to my supervisor, Assoc. Prof. Ing. et Ing. Ivo Kuřitka, Ph.D. et Ph.D., for the continuous support during my doctoral study and research, imparting knowledge and sharing his expertise with me. I would also like to extend my thanks to my consultant Mgr. Jan Vícha, Ph.D. for his motivation, patience, widening of the knowledge, guidance, and encouragement. I would also like to thank Ing. Lukáš Münster, Ph.D., for help with experimental work and enrichment of knowledge.

I am grateful to my colleagues and friends at the Centre of Polymer Systems for their assistance, advice, and companionship during my studies.

My special thanks are devoted to Kateřina Štěpánková for being my soulmate and emotional support. I would like to thank Alžběta Důbravová for endless positivity and support throughout my research journey.

Special thanks belong to my family for all the support, patience, encouragement, strength, and never losing hope in me.

I would like to thank the Centre of Polymer Systems and the Faculty of Technology of the Tomas Bata University in Zlín for their financial support during my studies. This work was supported by Internal grant agency of TBU in Zlín projects no. IGA/CPS/2023/006, IGA/CPS/2022/002, IGA/CPS/2021/002, IGA/CPS/2020/003. Further, the work was supported by procts of the Ministry of Industry and Trade of The Czech Republic within the framework of the programme OP PIK, project no. CZ.01.1.02/0.0/0.0/20_321/0025211, and by the Czech Science Foundation (GA ČR), project no. 23-07361S.

ABSTRACT

The thesis focuses on the study of hydrogel films prepared from the oxidized polysaccharide crosslinkers and polyvinyl alcohol (PVA) aimed at biomedical applications, particularly drug delivery. Initially, the role of the matrix (PVA) characteristics was studied in hydrogels crosslinked by 2,3-dialdehyde cellulose (DAC) and designed for the transdermal delivery of biologically active compounds. Hydrogel structure, properties, and drug release kinetics were investigated. Optimization was achieved by varying the amounts of DAC crosslinker and weight average molecular weight (M_w) of PVA. The best results were obtained for hydrogel films using 0.25% wt. DAC and PVA with M_w=130 kDa which had high porosity, drug loading capacity, mechanical properties, and skin adhesion among all tested samples. Next, different types of oxidized dialdehyde polysaccharide crosslinkers (DAP) based on cellulose, dextran, dextrin, and hyaluronic acid were compared on the selected PVA matrix, from which PVA/DAPs hydrogel films were created. The goal was to formulate a structure/function relationship and to select the best crosslinkers for a given application. The properties of PVA/DAP hydrogels were compared based on the density of -CHO groups, the structure of the crosslinkers, the molecular weight, and the size of the crosslinker nano-assemblies formed spontaneously in their solutions. All prepared hydrogel films with different amounts of DAC and M_w PVA crosslinker (PVA /DAC) and PVA/DAPs films were analyzed based on mechanical, viscoelastic properties, porosity, swelling, water content, network parameters, and cytotoxicity. Crosslinkers based on linear polysaccharides (cellulose, hyaluronate) performed more reliably, while the presence of branching could be both beneficial (dextran) and detrimental (dextrin) at lower crosslinker concentrations.

Keywords: *crosslinkers, polyvinyl (alcohol), hydrogels, polysaccharides, biocompatibility*

ABSTRAKT

Práce je zaměřena na studium hydrogelových filmů připravených z oxidovaných polysacharidových síťovacích činidel a polyvinylalkoholu (PVA) se zaměřením na biomedicínské aplikace, zejména podávání léčiv. Zpočátku byla studována role matrice (PVA) zesíťované 2,3-dialdehydcelulózou (DAC) v hydrogelech navržených pro transdermální podávání biologicky aktivních sloučenin. Byly zkoumány vlastnosti hydrogelu, struktura a kinetika uvolňování léčiva. Optimalizace bylo dosaženo změnou množství zesíťovacího činidla DAC a hmotnostní průměrné molekulové hmotnosti (M_w) PVA. Nejlepších výsledků bylo dosaženo u hydrogelových filmů s použitím 0,25 % hm. DAC a PVA s M_w=130 kDa, které měly vysokou poréznost, kapacitu nanášení léčiva, mechanické vlastnosti a adhezi ke kůži u všech testovaných vzorků. Dále byly porovnány různé typy oxidovaných dialdehydových polysacharidových síťovacích činidel (DAP) na bázi celulózy, dextranu, dextrinu a kyseliny hyaluronové na vybrané PVA matrici, ze které byly vytvořeny PVA/DAPs hydrogelové filmy. Cílem bylo formulovat vztah struktura/funkce a vybrat nejlepší síťovací činidla pro danou aplikaci. Vlastnosti PVA/DAP hydrogelů byly porovnány na základě hustoty -CHO skupin, struktury síťovacích činidel, molekulové hmotnosti a velikosti nano-souborů síťovacích činidel, které se spontánně vytvořily v jejich roztocích. Všechny připravené hydrogelové filmy s různým množstvím DAC a M_w PVA síťovadla (PVA/DAC) a PVA/DAPs filmy byly analyzovány na základě mechanických, viskoelastických vlastností, porozity, bobtnání, obsahu vody, síťových parametrů a cytotoxicity. Síťovací činidla na bázi lineárních polysacharidů (celulóza, hyaluronát) fungovala spolehlivěji, zatímco přítomnost větvení by mohla být prospěšná (dextran) i škodlivá (dextrin) při nižších koncentracích síťovacích činidel.

Klíčová slova: *síťovadla, polyvinylalkohol, hydrogely, polysacharidy, biokompatibilita*

TABLE OF CONTENT

1. INTRODUCTION

Biopolymers are biodegradable materials made from renewable sources by living organisms[1,2]. The repeating units of saccharides, nucleic acids, or amino acids form the backbone of their molecules, and sometimes, side chains also contribute to their functions. Some natural polymers such as polysaccharides provide energy for cell activity and function as structural components in living systems, other polymers produced by microorganisms, plants or animals manipulate basic biological information such as proteins and nucleic acids. In addition to their importance in biology, materials such as chitin, collagen, cellulose, or starch have over time proven their use for various applications in packaging, food, textile, medical, agricultural, and other industries[1]. Utilization of biopolymers has increased significantly across almost all aspects of life as a result of the ongoing health and environmental issues of synthetic polymers.

Hydrogel-based biomaterials are receiving ever-increasing attention due to their similarity to living tissues in terms of mechanical properties, porosity, and high water content. Due to their ability to capture, store, and release substances, hydrogels are excellent materials for various drug delivery applications as well as wound dressings[3–5].

An important aspect of the use of hydrogels in pharmacy is their low toxicity, biocompatibility, and suitable mechanical properties. While synthetic polymer-based hydrogels have well-defined structures and properties, they also have drawbacks. For instance, fully synthetic hydrogels, such as PVA hydrogels crosslinked with organic dialdehydes like glutaraldehyde[6], have a relatively high level of toxicity due to the use of low molecular weight crosslinking compounds. On the other hand, purely biopolymer-based hydrogels have better biodegradability, but in the swollen state, they often have poor mechanical properties. One possible answer is the use of hybrid hydrogels made from two polymers of natural and synthetic origin[7]. These have better-defined properties and can be optimized more easily[3–5]. Polysaccharides such as cellulose, hyaluronan, dextran, and dextrin are potential candidates as they can be obtained from renewable sources, contain vicinal diols in their structure, and can be selectively oxidized to aldehyde groups to prepare dialdehyde polysaccharides (DAPs) [8–10], which are perfect for crosslinking matrices rich in hydroxyl groups, like PVA[11]. Here, we investigate the synthesis, properties, and applications of DAP/PVA hydrogels.

2. HYDROGELS

Hydrogels are three-dimensional cross-linked structures that can absorb large amounts of water based on their hydrophilic nature [12–14]. Their hydrophilicity arises from the presence of hydrophilic groups such as -OH, -COOH, -$CONH_2$, -CONH-, -SO_3H etc. They can also have a main chain made of a water-soluble polymer, such as derivatives of poly(ethylene oxide), or can be based on ionomers, glycopolymers, acrylic, acrylamide, N-vinyl-2-pyrrolidinone, or poly(vinyl alcohol)[13].

2.1 Characterization and structure

One of the most basic divisions of hydrogels is according to the method of cross-linking, namely permanent (chemical hydrogels), which contain covalent bonds between macromolecules, and reversible (physical) hydrogels, which contain molecular entanglements stabilized by ionic bonds, hydrogen bonds, and hydrophobic interactions. Hydrogels can also be divided based on the origin of the used polymer, i.e. whether it is a biopolymer or synthetic polymer. Hydrogels based on natural polymers generally have better biodegradability and biocompatibility. On the other hand, material properties or degradation can be more easily controlled with synthetic materials. By combining both types, we obtain biohybrid gels that include the advantages of natural and synthetic hydrogels [12,15]. The origin of hydrogels and used natural/synthetic polymers is also related to their biological degradability, according to which we can divide hydrogels into degradable or nondegradable. In addition to the above classifications, hydrogels can be further divided based on their properties, reactions to external stimuli, charges, and other characteristics, which are summarized in Figure 1 [14,16,17].

The structure of the hydrogel network is determined by the presence of polymer chains that are covalently or physically linked into a 3D arrangement. Polymer chains can be formed from a homopolymer or copolymer, and those can form a single connected 3D network or an interpenetrating polymer network, i.e. two or more networks that are physically entangled with each other but not connected by covalent bonds[12]. Based on the structure of the polymer network, its interaction with the solvent, and the type of polymer, the properties of the hydrogel are given. For example, crosslinks between different polymer chains result in different viscoelastic behavior and give the gel its structure and elasticity[17,18]. The properties of crosslinkers are thus paramount in designing hydrogels for given applications. Among the most important properties of a hydrogel is its ability to bind water, which depends on the density of the hydrogel network and the content of the hydrophilic monomer. Important parameters that ensure water absorption are the compatibility between the polyelectrolyte and water and the osmotic pressure created by the high concentration of ionic groups in the gel [18].

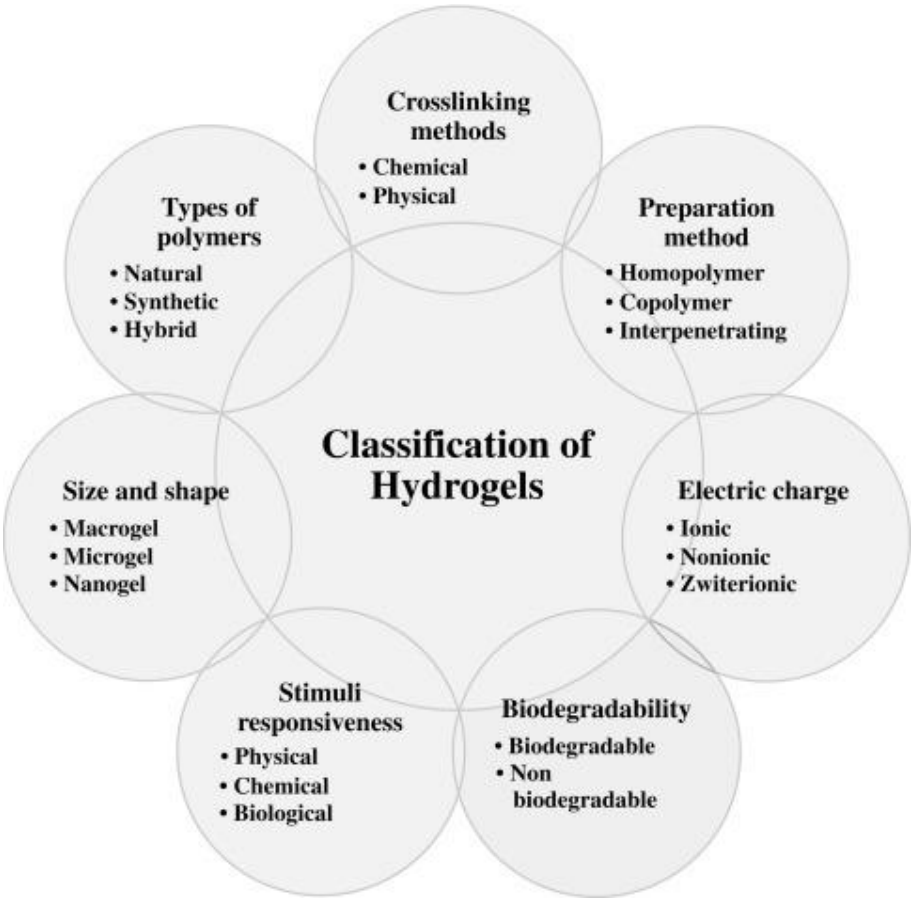

Figure 1 *Classification of hydrogels*[19]

The structure of the hydrogel network is characterized by the volume fraction in the swollen state (υ_2,s), which indicates the percentage of the gel matrix in the gel volume, the number-average molecular weight of the polymer chains between the crosslinks (M_c), and the network mesh size (ξ) which describes the distance between individual chains and allows the diffusional movement of solute molecules. By obtaining and comparing these parameters for a given type of hydrogel, it can be shown how effective a given crosslinker is. [12,15].

2.2 Hydrogel applications

Hydrogels have been used in biomedicine since 1960 when Wichterle and Lim created the first contact lenses using a hydrogel based on poly 2-hydroxyethyl methacrylate[20]. Nowadays, hydrogels are widely used mainly for engineering, biological, and pharmaceutical purposes[21].

Tissue engineering

In tissue engineering, hydrogels are mainly used as scaffolds, i.e. three-dimensional structures that facilitate cell organization and respond to stimuli to guide the development of specific tissues, but can also be used as space-filling

agents or carriers for bioactive substances. Hydrogel scaffolds can be used to (re)construct almost every tissue in the body, including cartilage, bone, and smooth muscle[22]. The most widely used synthetic polymers are polylactic acid and its copolymers[23], polyethylene glycol[24], and polyvinyl alcohol[25]. Of the natural materials, collagen, gelatin, alginates, chitosan, dextran, or hyaluronic acid are the most widely employed[26].

Wound healing

An ideal wound dressing must meet several conditions, such as good biocompatibility with tissues, maintaining a moist wound environment for cell hydration and absorption for wound exudate, having sufficient physical and mechanical strength to prevent the penetration of external bacteria, and, last but not least, having appropriate microstructure and biochemical properties to support cell adhesion, proliferation, and differentiation. Hydrogels are excellent wound dressings as they fulfill all of these criteria. To enhance the mechanical and biochemical properties of hydrogels, various bioactive compounds can be used[27,28]. For the production of antibacterial hydrogels, polymers with natural antibacterial properties are used, or antibacterial agents such as metallic nanoparticles, carbon-based nanomaterials, and nanofibers are incorporated into the hydrogel[29]. One example of a natural polymer with significant antibacterial properties is chitosan[30,31]. Chitosan represents the deacetylated form of chitin and is the second most widespread polysaccharide in the world after cellulose. It is found in the exoskeletons of crustaceans, insects, and fungi. It's a natural linear polysaccharide composed of N-glucosamine and N-acetylglucosamine units[32]. Chitosan is soluble in water only under diluted acidic conditions with a pH below 6. This property is due to the protonated free amino group on glucosamine, which enhances the molecule's solubility[33]. Antioxidant hydrogels are prepared using polymers containing polyphenols, such as gallic acid, which can capture free radicals through their hydroxyl groups or aromatic rings[34]. Another option is the incorporation of antioxidant agents based on catechol and amino acid structures[35]. These substances help neutralize free radicals and protect tissues from damage caused by oxidative stress. Hydrogels based on methacryloyl and chitosan are used as adhesive materials for wound healing[30,36].

Drug delivery

Based on their physical properties, such as their high porosity and affinity to aqueous environments, hydrogels are suitable for drug delivery applications. Their controllable porosity allows for the incorporation of drugs into the gel matrix and, subsequently the controlled release of drugs through the gel network[37]. Hydrogel delivery systems can be classified based on their size. For instance, macroscopic hydrogels are typically on the scale of millimeters to centimeters and are used for transepithelial delivery and localized placement within the body in the form of injectable hydrogels, including *in situ* gelling

hydrogels, shear-thinning hydrogels, and similar applications[38]. Among the most used are synthetic polymers such as poly(vinyl alcohol)[39] and poly(hydroxylalkyl methacrylate)[40] and biopolymers such as alginates[41], collagen[42], or chitosan[43]. Temperature-responsive systems that gel at body temperature, such as gelatin or synthetic poly(N isopropylacrylamide) (PNIPAm),[44] or shear-thinning hydrogels, which have a low viscosity under shear stress during injection the hydrogel, but quickly recovers its initial stiffness after removal of shear stress in the body, are ideal for implantations due to minimal invasiveness of the procedure. One example is modified alginate hydrogels[45].

Microgels and nanogels are particle-based hydrogels with dimensions in the range of micro or nanometers. They are also suitable for oral and systemic administration of drugs[38]. For example, nucleotide-based nanogels for gene therapy to treat cancer[46] have been developed.

2.3 Release of substances from hydrogel systems

The permeability of substances that are not bound to the hydrogel network through an equilibrium swelled-state hydrogel is based on diffusion. Several criteria influence the diffusion behavior of these substances. One of them is the mesh size, which depends both on the concentrations of the polymer and the crosslinker, as well as on the external effects of temperature and pH. Due to network heterogeneity and polymer polydispersity, most hydrogels have a wide mesh size distribution [12,38]. Mesh size can be calculated based on the established shear or Young's modulus or degree of swelling [47,48]. The hydrogel mesh size can also be obtained using the Flory-Rehner equilibrium swelling theory [49,50]. The classical theory of rubber elasticity relates the shear modulus G to the mesh size r_{mesh} by [38]:

$$r_{mesh} = \left(\frac{6RT}{\pi N_{AV} G}\right)^{1/3} \quad (1)$$

where R is the gas constant, T is the absolute temperature, and N_{AV} is Avogadro´s number.

To directly characterize the mesh size, techniques such as confocal microscopy, electron microscopy, atomic force microscopy, small-angle X-ray scattering (SAXS), and small-angle neutron scattering (SANS)[38,51,52] exist.

The size of the mesh determines the method of drug diffusion. If the mesh size is significantly larger than the drug, diffusion is mostly unhindered, and small drug molecules freely migrate through the network. By increasing the polymer or crosslinker concentrations, the mesh size can be decreased. As the drug size approaches the mesh size, its release begins to slow down considerably. If the mesh size is smaller than the drug, the drugs remain trapped inside the mesh. To release drugs, network degradation, swelling, or network deformation is required[38].

In network degradation-controlled release, the mesh size increases as the network degrades, thereby allowing drugs to diffuse out of the hydrogel. Degradation could occur in the main chain of the polymer or at the crosslinks e.g. by hydrolysis or enzymatic activity. Hydrogels based on polysaccharide crosslinkers such as alginate, chitosan, and cellulose, which are oxidized with sodium periodate, typically undergo mass erosion, and the rate of degradation can be controlled by the degree of oxidation.

A second method for controlled drug release is the directed swelling of hydrogels. As the hydrogel swells, the mesh size increases. External parameters that influence the swelling are temperature, glucose, pH, ionic strength, light, and electric fields[38]. For example, pH-responsive swelling is important for anticancer systems. As the hydrogel passes through the intestinal tract, the pH becomes basic compared to the stomach, and thus, the mesh can be designed to swell as much as possible to allow rapid drug diffusion in the intestine or column[13]. Hydrogels based on acidic or basic groups are used for such purposes. A disadvantage of swelling-controlled drug release can be a slow water diffusion response. Therefore, to achieve a faster response, diffusion can be improved by reducing the size of the hydrogel or creating interconnected macropores within the hydrogel.

A final method of controlled release is through mechanical deformation of the network, which can increase the size of the network by changing its structure, thus triggering convective flow in the network and thereby creating a pulsatile release[38]. Mesh deformation can be caused by mechanical deformation induced by ultrasound or magnetic fields.

The empirical Ritger-Peppas equation is utilized to describe the kinetics of substance release from hydrogel systems[38,53–55]:

$$\frac{M_t}{M_\infty} = \mathrm{kt}^{\mathrm{n}} \tag{2}$$

where M_t is the mass of the drug released at time t, M_∞ is the total mass of the drug released, k is the kinetic constant, and n is the diffusion exponent. The size of the exponent n depends on the type of transport, the shape of the hydrogel, and the polydispersity of the polymer. If $n = 0.5$, the drug is released by Fickian diffusion. If $n=1$ surface erosion dominates. In general, real systems often have n between 0.5 and 1 because more than one mechanism controls release in a given system.

To achieve positive therapeutic results, it is necessary to know which way and at what time the hydrogel releases the drug. Simultaneously, at the time of drug exhaustion, hydrogel should ideally have the ability to degrade to prevent surgical removal[38].

2.4 Transdermal drug delivery

The skin, as the largest organ of the human body, serves as the first line of defense against the external environment. Its surface area reaches approximately 1.5–2.0 m^2 and constitutes around 15% of the total body weight of an adult individual[56]. The human skin is composed of three main layers, which are shown in the Figure 2. The outermost layer is called the epidermis, beneath it lies the dermis, and the final layer is the subcutaneous tissue.

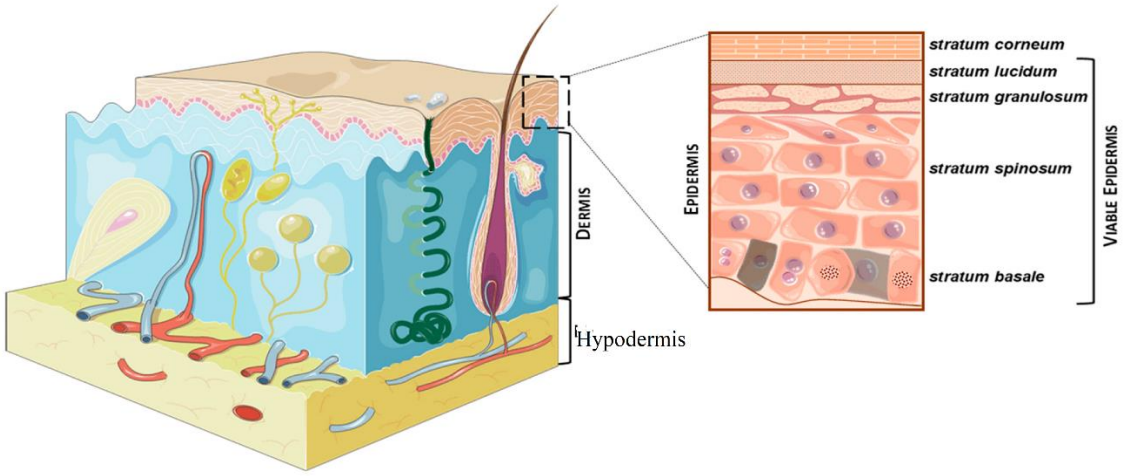

Figure 2 *The structural composition of the skin*[57]

The epidermis, which is the outermost layer of human skin, has a variable thickness of 50-100 μm depending on its location on the body. This layer consists of five distinct layers that work together in the process of skin regeneration[56,58]:

Stratum corneum (SC) – represents the outermost layer of the skin, composed of several layers containing keratin and cornified cells, which lack a nucleus (known as anucleate squamous cells). This layer undergoes gradual renewal every four weeks and provides a barrier function.

Stratum lucidum – Below the *SC* lies a thin translucent layer called the stratum lucidum. It consists of rows of two to three layers of clear and flattened cells whose nuclei have lost their staining ability. This layer is most developed on the palms and soles.

Stratum granulosum – The layer is formed from granules contained within living cells, which accumulate a protein keratohyalin.

Stratum spinosum – The *stratum spinosum* represents an epidermal layer located beneath the *stratum granulosum*. Its name derives from its spiky appearance. The cells are connected by desmosomes, and antigen-presenting Langerhans cells are found within this layer.

Stratum basale - This deepest part of the epidermis, separated from the dermis by the basement membrane, is constantly active in producing keratinocytes, which play a role in keratin production and the formation of a barrier to maintain water and lipid secretion. In this layer, Merkel cells, functional cells of sensory systems, are also present, along with melanocytes producing melanin pigment that safeguards against damage from UV radiation.

The dermis, also known as the corium, is connected to the epidermis at the level of the basement membrane and consists of two layers of connective tissue that are not clearly separated. The upper papillary layer is thinner, richly vascularized, and contains sensory nerve endings. The deeper reticular layer forms the main part of the dermis and is adjacent to the subcutaneous tissue. Unlike the papillary layer, it is thicker and is formed by dense connective tissue composed of collagen fibers, providing elasticity. Additionally, it contains numerous hair follicles, sebaceous and sweat glands, and plays a crucial role in immune function due to the presence of phagocytes, fibroblasts, leukocytes, and mast cells.

The subcutis (Hypodermis) is the deepest layer of the skin, primarily composed of adipocytes, offering thermal insulation and functioning as connective tissue linking the skin, muscles, and bones. As a result, this layer contains a high concentration of proteoglycans and glycosaminoglycans[56,59,60].

The primary function of the skin is to protect the body from various external factors, including physical elements such as UV radiation, mechanical stress, chemical influences, and the penetration of pathogens that could negatively impact health. An important role is played by the acidic protective film on the surface of the skin, composed mainly of lactic acid, free amino acids from sweat, free fatty acids from sebum, and urocanic acid with pyrrolidone carboxylic acid, which are formed during the process of keratinization in the *stratum corneum* of the skin[60]. The skin also plays a role in metabolism, immunity, and body thermoregulation through the sweating process. Additionally, the skin is utilized as a primary site for absorbing various types of drugs for local or systemic delivery, due to the rich network of blood capillaries in the dermis[56]. However, the intercellular organization of the *SC* poses a barrier to the penetration of active substances from topical applications. This structural organization is described by the "brick and mortar" model, where the "bricks" refer to corneocytes interconnected by desmosomes (corneodesmosomes), and the "mortar" consists of intercellular lipids (ceramides, free fatty acids, and cholesterol) forming a cornified envelope surrounding the corneocytes[61,62].

The process of transdermal absorption can be divided into three phases. The first step is penetration, which involves the entry of a substance into a specific layer or structure, such as active components penetrating the *SC*. The second phase is permeation, where there is the passage of a substance from one layer to

another which is structurally different. The third stage is resorption, when active compounds are taken up by the vascular or lymphatic system and absorbed into the body[63].

Transdermal absorption also has several possible pathways for substance absorption through the skin, see Figure 3. In general, these pathways can be divided into two categories: transepidermal and transappendageal routes. The transepidermal route is further divided into two variations: the intercellular pathway, where active substances (hydrophilic, small molecules) diffuse through the lipid matrix of the intercellular space, and the transcellular pathway, where active substances (hydrophobic) penetrate directly through the *SC* cells[56]. Due to the highly impermeable cornified envelope of corneocytes, the majority of substances pass through the intercellular pathway. Another route for drug absorption (especially polar, ionizable, or large macromolecules) is the transappendageal pathway *via* hair follicles or sweat glands in the skin. However, the utilization of this pathway is limited due to a smaller absorption surface area. The choice of a specific path depends on the physicochemical properties of the substance and the condition of the skin itself[57,61,62].

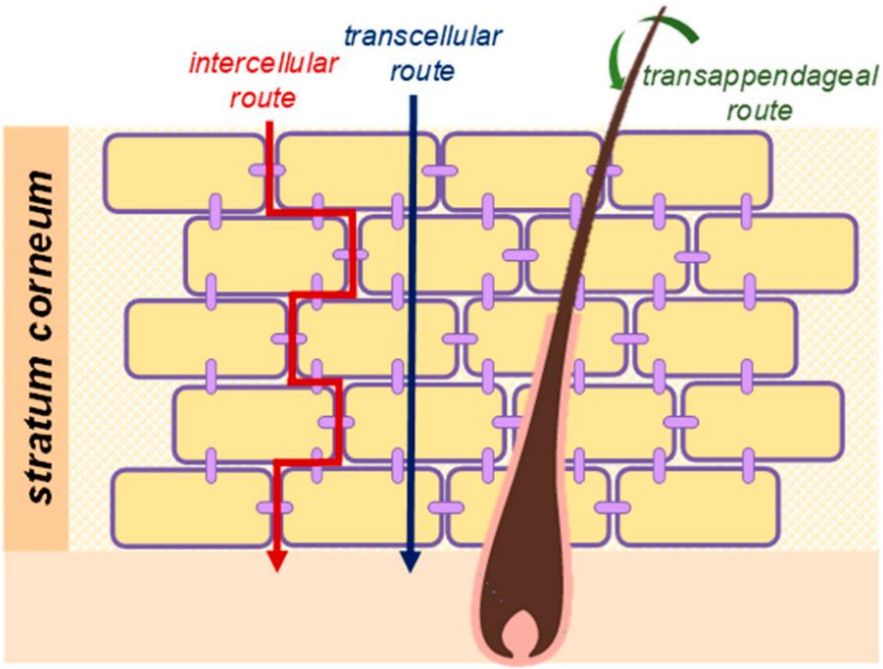

Figure 3 *Pathways for the penetration of drugs through the skin*[57]

2.4.1 Factors influencing transdermal absorption

There are several factors that influence the process of drug absorption into the skin. For example, skin characteristics such as the thickness of the *SC* and the lipid content in different areas of the skin. The presence of capillary blood vessels in specific skin regions can affect the rate of drug absorption into the bloodstream. Additionally, the presence of hair follicles and sweat ducts can enhance drug

permeation into the body. Body temperature is another factor that impacts the dilation of skin blood vessels and blood flow. It's important to note that skin permeability decreases with age[56,64].

Furthermore, substances called enhancers are also used, which disrupt intracellular lipid domains within the *SC* and increase skin permeability. These enhancers can be either physical (such as iontophoresis, electroporation, sonophoresis, and micro-needling)[65] or chemical in origin (like dimethyl sulfoxide DMSO, alcohols, fatty acids, surfactants PAL, biodegradable polymers for active ingredient storage, etc.[65,66]). Considering the composition of the *SC*, the optimal drug molecular size for effective absorption should be less than 600 Da. Drugs should be soluble in both water and oil, and their partition coefficient (Log P) should be between 1 and 3. The melting point of the drug is also important, ideally being below 200 °C[56,67].

2.4.2 Selected biologically active compounds

In this section, selected bioactive compounds of natural origin, which find application in transdermal drug delivery or are utilized in cosmetic applications are discussed, including those used in this work.

Polyphenols

Polyphenols are typically extracted from plants and marine organisms. These substances can be categorized into three main groups based on the number of phenolic units and structural elements that connect the phenolic rings, namely flavonoids, phenolic acids, and non-flavonoids[68]. Flavonoids exhibit significant pharmacological characteristics, including antioxidant, anti-inflammatory, antiproliferative, photoprotective, depigmenting, and anti-aging effects. These properties hold great potential in the treatment of several skin conditions. Due to their lipophilicity, it's challenging to absorb flavonoids orally, thus many topical administration methods have been investigated. The *SC* acts as the principal barrier to skin penetration, and this barrier can be overcome by developing different flavonoid delivery systems, including nanoparticles, lipid nanocapsules, microparticles, microsponges, and others, that improve drug concentration at the target site[69].

Quercetin (QT), also known as 3,3',4',5,7-pentahydroxyflavone (Figure 4), is one of the most extensively studied flavonoids due to its biological effects, including antioxidative, anti-inflammatory, antimicrobial, and anticarcinogenic properties. It is found in various types of fruits and vegetables, especially onions, dill, fennel leaves, oregano, and citrus fruits. QT has proven to be an antioxidant with the potential to support regeneration and can suppress inflammation induced by UV radiation. However, QT's low water solubility and challenges in penetrating the skin pose a challenge that complicates its application. For this reason, nanostructures are utilized to enhance localized QT delivery[68,70].

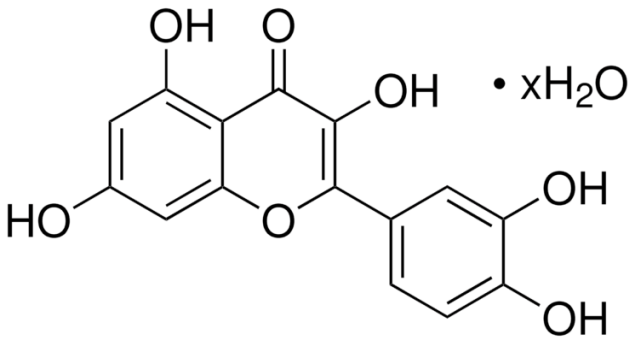

Figure 4 *Structure of Quercetin[71](in hydrated form)*

Rutin is a chemical compound classified as a bioflavonoid glycoside (Figure 5). It is present in plants such as passion fruit, tea, and apple, with buckwheat being among the most significant sources of rutin[72]. Rutin plays an important role in protecting plants from the harmful effects of ultraviolet radiation and pathogens. Rutin has been discovered to have a number of beneficial properties, including antioxidant, cytoprotective, vasoprotective, anticarcinogenic, neuroprotective, and cardioprotective benefits[72,73]. These properties make it useful in wound healing and dressing applications due to its capacity to show antimicrobial and anti-inflammatory behavior, as well as reduce oxidative stress in the affected area[74]. Another important role is its application in hair follicle cell apoptosis therapy, along with substances like spermidine and zeaxanthin. Another study examined its benefits concerning sun exposure in mice and revealed its potential to reduce skin inflammation induced by UVB radiation. Additionally, rutin has been shown to suppress atopic dermatitis and act against skin aging[72].

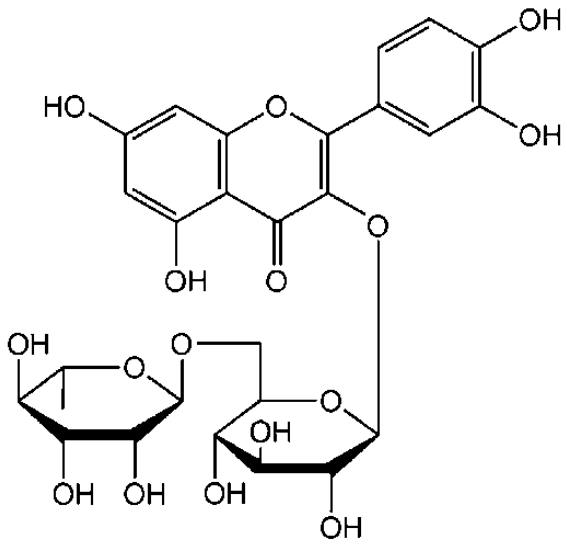

Figure 5 *Structure of rutin[75]*

Curcumin, also known as diferuloylmethane, is a polyphenol obtained from the rhizome of the *Curcuma longa* plant (Figure 6). Traditionally, it has been utilized for various diseases due to its wide range of pharmacological effects. It exhibits antioxidant, anti-inflammatory, antimicrobial, and anticarcinogenic properties, reduces the risk of thrombosis, protects against heart attacks, and possesses hypoglycemic and antirheumatic effects and many others[76,77]. Despite showing these positive effects, its low water solubility, poor absorption, and rapid metabolism and excretion limit its bioavailability. To enhance the bioavailability and stability of curcumin, its incorporation into liposomes[78,79], nanoparticles[80,81], and microemulsions is employed[76,82].

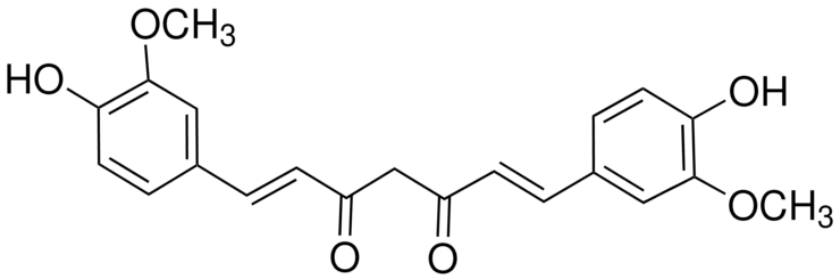

Figure 6 *Structure of curcumin*[83]

Terpenes

Terpenes are derived from five-carbon isoprene units with a molecular formula of $(C5H8)_n$, where $_n$ represents the number of linked isoprene units. Monoterpenes are present in plant oils and are known as essential oils (EO). EO are complex liquid and volatile lipophilic compounds synthesized by aromatic plants through their secondary metabolism. These natural products serve as potent antioxidants and scavengers of free radicals[68]. For instance, Thymol exhibits anti-inflammatory, antioxidant effects[84]. Other examples include tetraterpenes, known as carotenoids. They are lipophilic organic pigments biosynthesized by plants, algae, fungi, and bacteria. These pigments give yellow, orange, or red color to various fruits, vegetables, crustaceans, and certain fish[68] and present in vegetables and fruits, have a preventive effect against aging and carcinogenesis[68,85].

Alkaloids

Alkaloids are organic compounds containing nitrogen in their molecular structure, primarily sourced from plants, and less frequently from fungi and animals. These compounds exhibit various biological effects such as antimicrobial, analgesic, anti-inflammatory, antioxidant, anticancer, and antibacterial properties[68]. An example of this is caffeine (1,3,7-trimethylxanthine-2,6-dione), an alkaloid derived from methylxanthine, which is found in tea leaves, coffee, cocoa beans, guarana, and cola nuts (Figure 7). It finds utility as a

medication or is applied for cosmetic purposes. The benefits of its utilization in skincare cosmetic products involve preventing excessive lipid accumulation in the skin, supporting lymphatic drainage, and protecting the skin from the harmful effects of light[86]. It has also been investigated for potential treatment of various types of cancer[87]. Caffeine is also a stimulant of the central nervous system and is frequently used as a model drug for research on the penetration of hydrophilic substances across the epidermal barrier[86]. Caffeine is a hydrophilic substance, thus it is primarily incorporated into emulsions, gels, and nanoparticles[87,88].

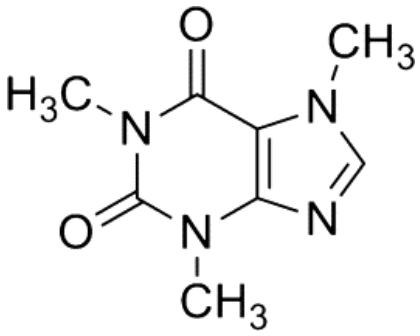

Figure 7 *Structure of caffeine[86]*

Vitamin C

It is a water-soluble vitamin that serves as an essential natural antioxidant (Figure 8). Although most plants and animals are capable of synthesizing vitamin C on their own, humans must obtain it through dietary sources. The biological availability of ascorbic acid in the skin is limited when taken orally, making local application a more effective option. This approach supports collagen formation in skin tissues, prevents malignancy, reduces radiation-induced damage, and accelerates wound healing[89]. Local application of vitamin C has been proven to positively impact burn healing in two ways: contributing to collagen formation in the skin and acting as an antioxidant that eliminates free radicals[90].

Ascorbic acid is present in many cosmetic products. However, the quick oxidation of L-ascorbic acid to dehydroascorbic acid in contact with air, which results in products turning yellow, caused a problem in these formulations. New formulations include chemically modified forms of ascorbic acid produced through hydroxyl group esterification. These derivatives include magnesium ascorbyl phosphate, sodium ascorbyl phosphate, ascorbyl-6-palmitate, and ascorbyl tetraisopalmitate[89]. Further research also examines squalene, the primary component of skin sebum, for its potential benefits[90].

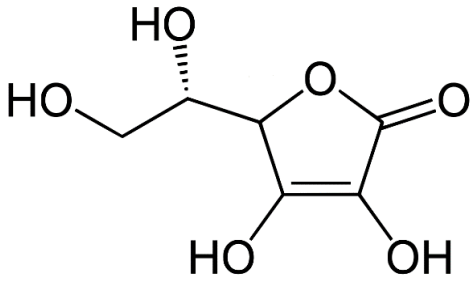

Figure 8 *Structure of vitamin C*[89]

Vitamin B12

Vitamin B12, also known as cobalamin, is found in animal products such as meat and dairy[91]. It plays a crucial role in cellular metabolism, particularly in DNA synthesis, methylation, and mitochondrial metabolism[92]. A deficiency of vitamin B12 is typically treated with subcutaneous or intramuscular injections of cyanocobalamin. As an alternative to this, the method of using microneedles can be employed[91].

Vitamin A

Retinoids are compounds derived from vitamin A that have been used for decades in the prevention and treatment of aging skin (photoaging). They come in both natural and synthetic forms. In cosmetic products, natural retinoids are predominantly utilized. Retinoic acid (tretinoin) is the most extensively researched topical retinoid and acts against the formation of wrinkles and skin aging. Retinoic acid binds and activates the RAR-γ receptor and is generated through enzymatic reactions where retinol is initially converted to retinal through reverse oxidation, followed by further oxidation to retinoic acid. In the USA, it is available by prescription and comes in cream and gel formulations. Commercially available doses come in concentrations of 0.025%, 0.05%, and 0.1%. It reduces skin surface roughness, hyperpigmentation, and fine wrinkles due to histological changes in compactness within the *stratum corneum* and *stratum spongiosum* in the epidermis. However, higher concentrations of retinoic acid are associated with increased irritation[93].

Hydroxy acids (AHA, PHA, BA)

Alpha-hydroxy acids (AHA) are organic carboxylic acids with one hydroxyl group in the α position of an aliphatic or alicyclic molecule. Many AHAs are present in food and fruit and are therefore also referred to as fruit acids. The most famous are glycolic acid, lactic acid, and citric acid. AHAs profoundly affect the keratinization and exfoliation of the *stratum corneum*. Later research showed significant anti-aging impact, and AHAs are still essential components of skin care today[93].

Polyhydroxy acids (PHAs) are structurally similar to AHAs but have two or more hydroxyl groups in the molecule, one of which is in the α position. Many PHAs are endogenous metabolites that are naturally produced by the human body. These include gluconic acid or glucolactone. Glucolactone used in cosmetics has similar effects to glycolic acid, i.e. it acts as a chelating agent and provides increased moisturizing and exfoliating effects. It is compatible with sensitive skin, including rosacea and atopic dermatitis. With the addition of benzoyl peroxide or retinoids, they act against acne[93].

Bionic acids (BA) consist of two components: polyhydroxy acids attached to a sugar molecule. This group includes lacticobionic acid and maltobionic acid. Lacticobionic acid incorporates gluconic acid (PHA), which is linked via an ether bond to galactose. Similarly, maltobionic acid is connected to a glucose molecule. These bionic acids are hygroscopic because they include many hydroxyl groups. They easily attract and hold water, capable of forming a gel-like matrix. Additionally, bionic acids have chelating and antioxidant effects[93].

3. DIALDEHYDE POLYSACCHARIDES

Polysaccharides are formed of monosaccharide units that are linked by glycosidic bonds. Polysaccharides are very abundant in nature and are easily derived from various natural sources such as algae (alginate), higher plants (cellulose), microorganisms (dextran), or animals (chitosan). Thus, they offer a wide development potential due to their excellent properties, which include natural abundance, biocompatibility, biodegradability, chemical reactivity, etc[26]. Due to the existence of various functional groups in the structure of polysaccharides, such as carboxyl, hydroxyl, and amino groups, the chemical properties of polysaccharides can be changed by chemical modifications. In particular, polysaccharides containing vicinal diol(s) can be selectively oxidized to introduce aldehyde groups to prepare dialdehyde polysaccharides[10,26].

3.1 Preparation, structure and properties

Dialdehyde polysaccharides (DAPs) are generally prepared by regioselective oxidation of source polysaccharides that contain neighboring (vicinal) -OH groups using periodate salt, which introduces a pair of reactive aldehyde groups into each oxidized unit [94,95]. This reaction is shown in Figure 9[96].

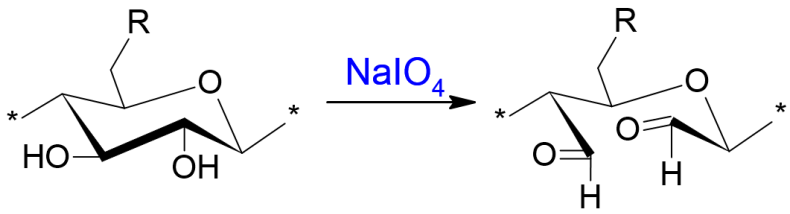

Figure 9 Periodate oxidation of polysaccharide featuring vicinal diol group at C2 and C3[96]

The structures of DAPs are closely linked to the architecture of source polysaccharides. The structures of source polysaccharides used in this work and respective dialdehydes are given in Figure 10 [96].

Cellulose is one of the most abundant polysaccharides worldwide and can be found in various plants, tunicates, and bacteria. It is composed of linear chains of anhydroglucose units (AGU) linked by β-(1→4) glycosidic bonds. The oxidation of cellulose by periodate is characterized by cleavage of the C2–C3 bond of AGU, leading to the formation of 2,3-dialdehyde cellulose (DAC) [95]. It is thus highly regioselective.

Dextrin is a product of the hydrolysis of starch or glycogen. Due to the presence of α-(1→4) and α-(1→6) glycosidic bonds, dextrin forms a branched structure, see Figure 10. Depending on its molecular weight, it is partially or fully soluble in water. Oxidation of dextrin with periodate produces 2,3-dialdehyde dextrin (DXI) in a way analogous to DAC.

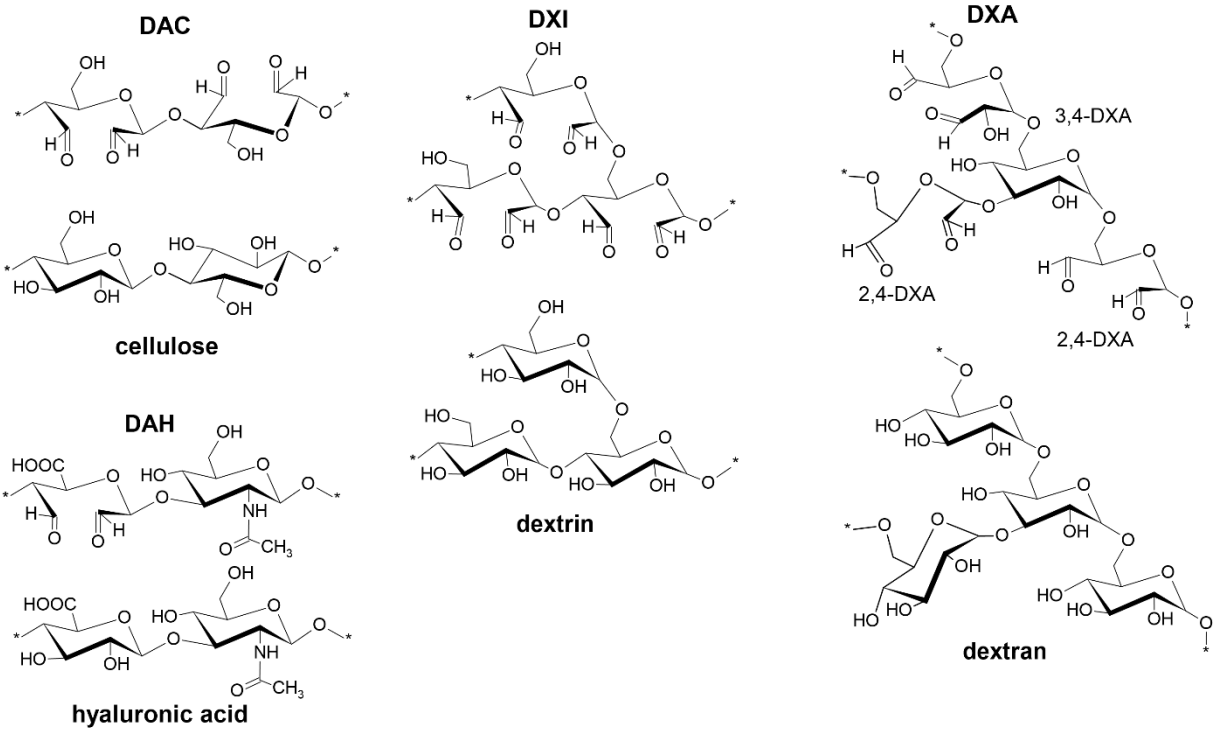

***Figure 10**: Structures of source polysaccharides and corresponding dialdehydes*[96]

Complex glucans called dextrans are produced by microorganisms, particularly bacteria from the species Leuconostoc and Streptococcus. They are composed of AGU chains linked mainly by α-(1→6) glycosidic bonds with a degree of α-(1→3) branching. The structure and properties of dextran differ not only for different species of bacteria but also for different strains [97]. Because α-(1→6) bonded units contain three neighboring -OH groups, oxidation of dextran leads to a mixture of 3,4-, 2,4- and 2,3 dialdehyde dextrans (DXA) [98,99]. In contrast, AGUs with α (1→3) branching lack any vicinal hydroxyl groups and are therefore entirely resistant to periodate oxidation[94].

D-glucuronic acid and N-acetyl-D-glucosamine connected by alternating β-(1→4) and β-(1→3) glycosidic links form the anionic linear polysaccharide known as hyaluronic acid (HA). Compared to cellulose, only the D-glucuronic acid units contain vicinal diols and are oxidized, because the glycosidic link at position C3 protects the N-acetyl-D-glucosamine units from periodate oxidation, see Figure 10. This reduces the maximum amount of -CHO groups per unit of HA mass to 5 mmol/g, i.e. by a factor of 2.5 compared to cellulose/DAC (12.5 mmol/g). HA is abundant in the human extracellular matrix, synovial fluid, cartilage, muscle connective tissue tissues, skin, etc. [100,101]

3.2 Applications

Based on the presence of reactive aldehyde groups, DAPs are used for different purposes. For instance, DAC is used as a filling for cellulose-based columns in aqueous chromatography[102], an absorbent of heavy metal ions and dyes[103], a material for protein immobilization[104], a carrier for drug delivery[105], material in tissue engineering[106], and has applications in wound dressings[96]. DAH has been used, for example, as a crosslinker for hydrogels intended for chronic wound treatment and tissue regeneration[107,108]. Oxidized dextran is used for wound healing as a crosslinking agent for polymers containing amine groups, such as chitosan[109]. Applications of dextrin derivatives are mostly limited to cyclodextrins, which are used as carriers for hydrophobic types of drugs[110], improving the ability of hydrogels to load drugs and control their release[111].

In general, dialdehydes are also known crosslinkers that are capable of two main types of crosslinking reactions: i) the formation of Schiff's bases with substrates containing -NH_2 groups (chitosan)[112] and ii) the formation of hemiacetal bonds between -CHO groups of aldehyde and -OH groups of the matrix that makes them ideal for crosslinking polymers rich in hydroxyl groups like PVA[11], which is discussed in more details in section 6.2. This work focuses on oxidized cellulose, dextran, dextrin, and hyaluronic acid and their use as crosslinkers for PVA.

4. POLY(VINYL ALCOHOL) BASED HYDROGELS

Poly(vinyl alcohol) (PVA) is a linear semi-crystalline polymer that consists of a main carbon chain containing hydroxyl (-OH) functional groups (Figure 11). It is obtained by hydrolysis of polyvinyl acetate (PVAc). By controlling the hydrolysis step, different degrees of hydrolysis (DH) of the PVA polymer can be prepared, which thereby affects the behavior of the polymer, such as solubility, crystallinity, and chemical properties. For example, low DH PVA shows higher solubility in water at low temperatures compared to high DH. Therefore, the temperature must be increased above ~70°C to dissolve high DH PVA in an aqueous system[25,113].

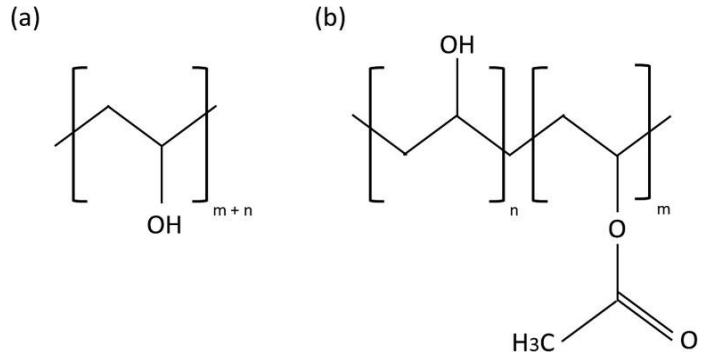

Figure 11 *Molecular structures of (a) fully hydrolyzed polyvinyl alcohol (PVA), where each monomer has a hydroxyl group, and (b) incompletely hydrolyzed PVA molecular structure, where some PVA units still contain acetyl groups[113]*

Poly(vinyl alcohol) is one of the most widespread and used materials for hydrogel applications, due to its biocompatibility, biodegradability, low toxicity, etc.[114,115] Based on these properties, PVA can be used for various purposes such as the formation of films, hydrogels, fibers, scaffolds, composites, or polymer membranes[113].

PVA is a hydrophilic and water-soluble polymer, due to the content of -OH groups in its backbone. On the other hand, solubility in water can reduce its mechanical properties, which can limit its use. This limitation can be overcome by cross-linking hydroxyl groups to form hydrogels[116].

4.1 Preparation of PVA-based hydrogels

PVA-based hydrogels can be prepared in different ways that determine their network parameters and physico-chemical properties.

The first method is physical crosslinking using freeze-thaw-induced crystallization or high-temperature (energy) processing, where network nodes are formed through prolonged heating. During the freeze-thawing process, the mechanical properties of the hydrogel increase with increasing temperature, the number of freeze-thawing cycles, the concentration of the polymer solution, and

the molecular weight of PVA[117] . The advantage is the absence of a crosslinking agent. On the other hand, partial degradation of PVA caused by higher temperatures can lead to the formation of unsaturated bonds, chain splitting, and thus to covalent interactions. These hydrogels have worse mechanical properties in the swollen state, due to weak and less stable physical crosslinking[118,119].

The second method is chemical crosslinking, using agents such as epichlorohydrin, various aldehydes (formaldehyde, glutaraldehyde, benzaldehyde, etc.), anhydrides (EDTA dianhydride) or boric acid[120,121]. A common feature of crosslinking agents is their synthetic origin (except boric acid) and relatively high toxicity. The low molecular weight of crosslinking agents also enables easy penetration through various barriers into the living organism. The resulting hydrogels must therefore be intensively washed before use and can still be toxic to organisms upon long-term exposure. Therefore, an important step in the preparation of synthetic hydrogels is their intensive purification and removal of all potentially toxic reactive components that may be trapped in the gel network[119].

4.2 Applications

PVA hydrogels find a wide range of biomedical applications, from serving as articular cartilage replacements to a controlled release of pharmaceutical substances[122]. They are also used in the food industry, in the cosmetic industry, and in sanitary products. For instance, poly(vinyl alcohol) hydrogels are utilized for the treatment of atopic dermatitis[123] or as superabsorbents in hygiene products[37].

There are countless specific applications of cross-linked PVA hydrogels in many different fields due to the improvement of the physical and mechanical properties of PVA by the presence of other synthetic polymers or biopolymers[124]. For example, there are PVA-based double network hydrogels that serve as absorbers of heavy metal ions in waste-water treatment[125] or PVA-based membranes that are used in various separation processes[126,127].

A lot of attention is focused, especially in the field of biomedicine[117,128–131]. For example, the work of A. Kumar and S.S. Han (2017) deal with advances in the production of PVA-based hydrogels in tissue engineering applications[25]. Another work by E.A. Kamoun et al. (2021) discussed modern perspectives of electrospun nanofibrous PVA hydrogel membranes, which are mainly used in wound dressing applications [132]. G. Rivera-Hernández et al. (2021) focus on the field of drug delivery, suggesting a cancer treatment strategy using hydrogels, microparticles, or nanoparticles that are capable of encapsulating, protecting, and transporting and targeted delivery of a therapeutic agent[39]. Last but not least, an overview of the use of PVA hydrogels by Baker et al. (2012) includes their use in contact lenses, artificial cartilage, and orthopedics[122].

5. AIM OF DOCTORAL THESIS

This work deals with the study of the preparation of hydrogels based on modified polysaccharides as crosslinkers for transdermal/systemic administration of biologically active substances, and the study of the influence of their properties and structure on the kinetics of drug release.

The aim is to investigate the impact of the PVA matrix on the prepared hydrogels and to optimize their properties for transdermal delivery of substances. Additionally, the research aims to examine the influence of crosslinking agent structures on the properties of the hydrogels.

A synthetic polymer matrix (PVA) and modified polysaccharides as crosslinkers were chosen for hydrogel preparation. These polysaccharides are regioselective oxidized to the appropriate aldehydes capable of crosslinking the selected matrice. First, dialdehyde cellulose (DAC) was found effective for cross-linking PVA matrices resulting in hydrogels with potential application for transdermal delivery of substances. Then, four different dialdehyde polysaccharides (DAP) crosslinker types based on cellulose, dextran, dextrin, and hyaluronic acid were selected to obtain deeper insight in the principles generally governing crossling of PVA matrices by the modified polysaccharides. The main research direction of the thesis can be divided into two objectives:

1. Preparation and study of the PVA/DAC hydrogels to evaluate the effects of the crosslinking agent concentration and used PVA polymer on the resulting hydrogel properties. The loading of selected model bioactive substances into prepared materials and determination of the kinetics of substance release.

2. Analysis and study of the influence of the PVA matrix and different crosslinker properties and structure on the characteristics of hydrogels, namely their mechanical and viscoelastic properties, porosity, swelling, water content, and network parameters.

6. EXPERIMENTAL PART

6.1 Materials

For the matrix evaluation study, hydrogels were prepared using poly(vinyl alcohol) (PVA) with 88% degree of hydrolysis and different M_w (130 and 31 kDa, respectively, Sigma Aldrich Co.). Alpha cellulose (M_w = 109 kDa) (Sigma Aldrich Co.) oxidized by sodium periodate ($NaIO_4$) (Penta, Czech Republic) to 2,3-dialdehyde cellulose (DAC) served as a crosslinker. Following source polysaccharides were employed in the study of the role of crosslinker structure PVA/DAPs hydrogels: cellulose SigmaCell type 20 (weight-average molecular weight M_w = 76 kDa, degree of polymerization DP = 468, polydispersity index PDI = 4.7; Sigma Aldrich Co.), dextran from Leuconostoc spp. (M_w = 71, DP = 449, PDI = 1.9; Sigma Aldrich Co.), dextrin from corn starch type I (M_w = 52 kDa, DP = 325, PDI = 2.3; Sigma Aldrich Co.), and sodium hyaluronate (M_w = 1.5 MDa, DP = 3740, PDI = 4.3; Contipro Ltd., Czech Republic). Poly(vinyl alcohol) PVA with 88% degree of hydrolysis (M_w=130 kDa) served as a matrix. Other chemicals involved in modifications and characterizations can be found in relevant papers.[96,133] All chemicals were of analytical purity and were used as received without further purification. Throughout the experiments, demineralized water with a conductivity of less than 0.1 μS/cm was used.

6.2 Sample preparations

6.2.1 Preparation of dialdehyde cellulose (DAC) for the matrix evaluation study

DAC was produced by oxidizing alpha cellulose by NaIO4 using a 1:1.2 M molar ratio of reactants (DAC : periodate) following earlier works[119,134,135]. In summary, 10 g of cellulose was suspended in 250 mL of water containing 16.5 g of sodium periodate and stirred in the dark for 72 hours at 30 °C. The oxidation was stopped by adding 10 mL of ethylene glycol and the resulting product was washed and filtered. The raw DAC was then suspended in 175 mL of water, solubilized at 80 °C for 7 hours, and cooled before being centrifuged for 10 minutes.

6.2.2 Preparation of dialdehydes polysaccharides (DAPs) for the study of the role of crosslinker structure

The general procedure for preparing DAP is as follows. Individual DAPs, namely cellulose, hyaluronate, dextrin, and dextran, were oxidized with $NaIO_4$ according to earlier works[119,134,135] into their respective 2,3-dialdehyde derivatives (DAC, DAH, DXI, and DXA). To achieve this, 1 gram of each polysaccharide was dissolved in 50 mL of water, and 1.65 g of sodium periodate was used as the oxidizing agent. The reaction mixtures were left to stir in the dark for different time intervals depending on the type of polysaccharide used. Specifically, DAC

was stirred for 72 hours, DAH for 24 hours, DXI for 8 hours, and DXA for 4 hours, all at a temperature of 30 °C. Reactions were stopped by the addition of 1 mL of ethylene glycol. The insoluble DAC was centrifuged and homogenized. DXI, which was partially soluble, was dialyzed for a day against demineralized water. The DAC suspension and DXI sample were then solubilized in an oil bath under reflux, at 80 °C for 2 hours. The resulting solutions were purified by filtering and centrifugation to eliminate any residual insoluble material. Subsequently, they were dialyzed again for a day using 14 kDa MWCO dialysis tubing. All of the purified materials were then frozen using an ethanol ice bath and lyophilized, resulting in dialdehyde polysaccharide powders (DAPs). The dialdehyde polysaccharide powders were utilized as crosslinkers for different PVA matrices.

6.2.3 Hydrogel preparation

The hydrogels are formed through a reaction between the crosslinker and the matrix involving the -CHO and -OH groups of the dialdehydes and PVA in an acidic environment. The dialdehyde polysaccharides (DAP) react with the hydroxyl groups of PVA to form hemiacetal bonds (Figure 12).

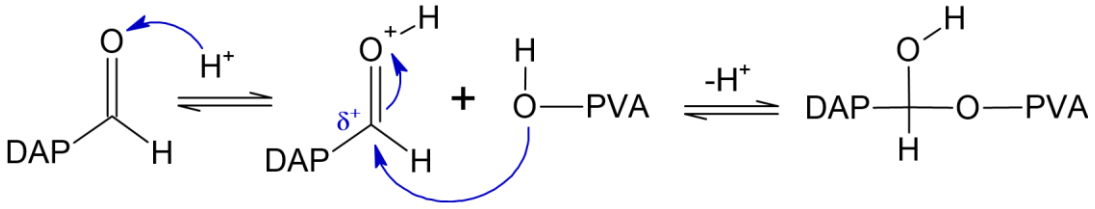

Figure 12 *The mechanism of hemiacetal bond formation between PVA and DAP*[96]

To prepare hydrogel samples for the matrix evaluation study, 10 g of two types of PVA (with molecular weights of 31,000 and 130,000 g/mol) were separately dissolved in 80 mL of water at a temperature of 90 °C. Then, a catalyst (10 mL of 1.3 M HCl) and a specific amount of DAC (either 0.25 wt% or 1 wt% with respect to the weight of PVA) were added to the mixtures. The resulting reaction mixtures were mixed thoroughly and poured onto Petri dishes (with a diameter of 140 mm) and dried at 30 °C until a constant weight was reached. The thin films obtained were washed with water to eliminate any non-crosslinked material, and circular samples with diameters of 15 and 50 mm were cut out and stored in an aseptic medium (70% ethanol solution) until use.

The following general procedure was used for the study of the role of crosslinker structure: 10 g of PVA was dissolved in 80 mL of water heated to 80 °C. Subsequently, the acidic catalyst (10 mL of 1.3 M HCl) was added and the solutions were thoroughly mixed. Then, solutions of DAPs were added to the acidified PVA solutions. These DAP solutions contained either 1.25 mmol/g of -CHO groups (equivalent to 0.1 wt% of crosslinker for DAC, DXI, and DXA, and

0.25 wt% for DAH, which has fewer -CHO groups per unit of mass), or 12.5 mmol/g (equivalent to 1 wt% of crosslinker for DAC, DXI, and DXA, and 2.5 wt% for DAH). The reaction mixtures were stirred for 30 minutes and then poured onto Petri dishes (d = 140 mm), and allowed to crosslink upon drying at 30 °C. The prepared films were then washed with water for a week to remove non-crosslinked material, and disc-shaped samples of 15 mm in diameter were cut out.

6.3 DAPs characterization

FTIR, degree of oxidation (DO), Gel Permeation Chromatography (GPC), and dynamic light scattering (DLS) techniques were used to characterize specific crosslinkers, including DAC, DAH, DXI, and DXA. The cytotoxicity of crosslinkers was done in cooperation with Prof. Humpolíček at CPS. The characterization of DAPs are described in more detail below.

6.3.1 FTIR analysis

The lyophilized DAPs powders were analyzed qualitatively using Fourier-transform infrared (FT-IR) spectroscopy. The analysis was carried out using a Termo Scientific Nicolet 6700 FT-IR instrument equipped with a diamond crystal in the attenuated total reflectance (ATR) mode. The range of wavelengths analyzed was 4000-700 cm^{-1}, with a resolution of 4 cm^{-1} and 64 scans. The analysis was performed with the suppression of atmospheric gases to ensure accurate results.

6.3.2 Determination of the degree of oxidation

To characterize the DAP, the oxime reaction was utilized. The procedure involved dissolving 0.1 g of each DAP in 30 mL of demineralized water and adjusting the pH to 4.0 using 0.1 M HCl. A solution of HAHCl was basified using 0.1 M NaOH to pH 4.0 and mixed with each acidified DAP solution. The resulting mixtures were stirred in closed containers at room temperature for 24 hours. The conversion of aldehyde to oxime was determined by observing the consumption of 0.1 M NaOH. This method was adapted from Veelaert et al. (1997)[136].

6.3.3 GPC analysis

To determine the molecular weight of the prepared dialdehydes, they were converted to double-oxidized corresponding dicarboxylated derivatives (DCP) including DCDXA, DCH, DCDXI, and DCC. This conversion was necessary as DCP is more stable and has a more defined composition compared to DAP. To prepare DCP, $NaClO_2$ was used with a $NaClO_2$ to –CHO molar ratio of 1:4. The concentration of $NaClO_2$ was 0.2 M and the oxidation reactions were carried out in the presence of 0.5 M CH_3COOH. The secondary oxidation started with the dropwise addition of $NaClO_2$ solution into the acidified solution of the given dialdehyde. The reaction was performed for 7 hours at 30 °C in the dark. Subsequent addition of 10 M NaOH to pH 8 terminated the oxidation reaction.

The products were purified by dialysis against demineralized water using 14 kDa MWCO dialysis tubing, and the pH of all samples was adjusted to 7.4 with 0.1 M NaOH after dialysis. The solutions were then filtered, flash-frozen, and lyophilized. This method has been used previously with good results[135].

To analyze the molecular weight of the samples, a Waters HPLC Breeze chromatographic system was used, which included a refractive index detector (Waters 2414, drift tube T= 60 °C) and a Tosoh TSKgel GMPWXL column (300 mm × 7.8 mm × 13 μm, T = 30 °C). The mobile phase used for the analysis was composed of 0.1 M $NaNO_3$ and 0.05 M $Na_2HPO_4 \cdot 12H_2O$ aqueous solution. The molecular weight was calibrated using a Pullulan polysaccharide calibration kit SAC-10 with a range of M_w 342–805,000 g/mol provided by Agilent Technologies, Inc.

6.3.4 DLS analysis

To determine the zeta potential (ζ) and hydrodynamic radius (d_h) of DAP solutions, dynamic light scattering (DLS) analysis was carried out using a Zetasizer Nano ZS90 instrument from Malvern Instruments, UK. The analysis was conducted on concentrated DAP samples of 1 mg/mL at 25°C, utilizing a DTS1070 cell and the Smoluchowski model.

6.4 Hydrogel characterization methods

Several techniques were used to investigate the characteristics of the prepared hydrogels, including network parameters, viscoelastic properties, BET, and SEM analysis, which are described below[96,133]. In addition, drug release kinetics and transdermal absorption were measured for the PVA/DAC hydrogels for transdermal drug delivery (see section 7.1). For the role of DAP crosslinker structure in PVA hydrogels (section 7.2), the crosslinker structure, molecular weight, aldehyde group density, and size of the formed crosslinker nano-assemblies were studied. Cytotoxicity at CPS in collaboration with a group of Prof. Humpolíček at CPS was determined for all prepared hydrogels.

Network parameters

The network parameters were determined using a swelling experiment. Disc-shaped hydrogels with a diameter of 15 mm were washed in water for a week with regular water changes to remove excess reactants. The swollen discs were then gently dried to remove excess water, weighed, and further dried at 30°C in the oven until a constant weight was achieved. The Flory-Rehner equilibrium swelling theory was used to estimate the network parameters of the hydrogels[50]. This method has been described in detail in my previous works[119,134].

Measurement of viscoelastic properties

Properly prepared hydrogel discs with a diameter of 15 mm were tested using an Anton Paar MCR 502 rotary rheometer (Anton Paar, Austria) equipped with a D-PP15 shaft. To avoid any movement of samples, a roughened aluminum plate and a base plate with glued sandpaper were used. The testing was performed at room temperature for the matrix evaluation study and 37 ◦C for the role of crosslinker structure study. All hydrogel samples were measured in oscillatory mode in a frequency sweep from 1 to 10 Hz by applying a constant strain of 1%. In the chosen range of oscillatory measurement, the complex modulus G* was calculated as the square root of the sum of the square of the storage and loss modulus. The tan δ is defined as the ratio between loss and storage modulus (G″/G′) and gives a measure of viscous to an elastic component of the material.

BET and SEM analysis

Before conducting scanning electron microscopy (SEM) analysis and measuring specific surface area using multipoint Brunauer-Emmet Teller (BET) analysis, hydrogel samples were first lyophilized to form cryogels. The cryogels of PVA/DAP and PVA/DAC were then analyzed using a scanning electron microscope Nova NanoSEM 450 (FEI, Czech Republic) with a 5 kV accelerating voltage. To prevent the charge accumulation effect, all samples intended for SEM analysis were sputtered by gold and palladium nanoparticles. BET analysis was performed on samples degassed for 24 hours, and absorption/desorption isotherms recorded at 77 K were evaluated using a Belsorp-mini II high-precision surface area analyzer (BEL Japan Inc., Japan).

Drug release kinetics and transdermal absorption

The release kinetics and transdermal absorption of two model drugs, caffeine and rutin were examined in a study of the matrix evaluation of hydrogels.

Sample preparation – drug loading of hydrogel samples

Hydrogel samples were loaded with biologically active compounds by putting them into 50 mL of stock solutions containing 0.1 mg/mL (rutin) or 10 mg/mL (caffeine) and shaking for 72 hours at 37 °C.

Drug release kinetics

The samples of each hydrogel were put in separate, closed containers with 10 mL of demineralized water, and the containers were shaken at 37 °C in the dark. The UV-VIS spectrometer Perkin Elmer Lambda 1050 (Perkin Elmer Inc., USA) was used to evaluate aliquots of 1 mL at predetermined intervals all over 96 hours, using characteristic peaks at 353 nm (rutin) and 273 nm (caffeine).

Transdermal absorption

The skin absorption tests for caffeine were conducted in accordance with the OECD Test Guideline for Skin Absorption: In vitro method, using pig ear skin. Skin samples of 3 x 3 cm were collected from the inner region of the auricle after shaving the pig's ear lobe. These samples were then placed in test cells and checked for skin integrity using a multimeter, with samples below 5 mΩ resistance being excluded. The skin samples were then combined with disc-shaped hydrogel samples, which were previously loaded with caffeine by shaking for 120 hours at 37°C in 10 mg/mL caffeine. The testing was carried out using an automated diffusion cell system, with a continuous flow of receptor liquid (PBS buffer and 0,05% gentamicin sulfate) through samples being collected for 24 hours at a constant flow rate of 2 mL/h. The fractions collected at specific times (1–24 hours) after the measurements were stored at –20 °C until analysis. Following filtering, the samples were subjected to liquid chromatography analysis using an HPLC chromatograph equipped with a UV-VIS detector. The caffeine was isocratically separated on a Kinetex C18 100A column (150 x 4.6 mm, 2.6 m) using a mobile phase composed of 0.2% HCOOH and methanol in a 75/25 ratio. The flow rate was 0.7 mL/min, and the temperature was set to 30°C. The caffeine was detected using a wavelength of 272 nm.

7. RESULTS AND DISCUSSION

A variety of combinations of hydrogels were successfully prepared and analyzed. The results, discussions, and conclusions will be analyzed separately for each type of study followed below.

7.1 PVA/DAC hydrogels for transdermal drug delivery

7.1.1 Preparation of the PVA/DAC hydrogels

Four different PVA/DAC hydrogels were prepared with varying concentrations of DAC and molecular weights of PVA, as shown in Table 1. Disc-shaped hydrogel samples are shown in Fig 13. Due to the poor physical properties of sample L-31, which were attributed to crosslinker concentrations and low PVA molecular weight, only network parameters were examined for this sample. The three other types of samples, L-130, H-130, and H-31, were, however, successfully characterized using all previously mentioned techniques (6.4).

Table 1 *Designation of PVA/DAC samples, M_w of PVA used and their composition*[133].

Sample	PVA M_w (kDa)	PVA (g)	DAC (wt.%)	DAC (g)
L-31	31	10	0,25	0,025
L-130	130	10	0,25	0,025
H-31	31	10	1	0,1
H-130	130	10	1	0,1

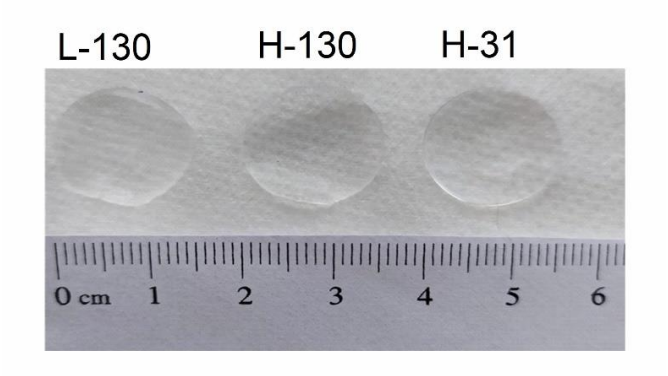

Figure 13 *Photograph of PVA/DAC samples*[133]

7.1.2 Characterization of the prepared hydrogels

Network parameters

The Flory-Rehner equilibrium swelling theory was used to estimate the network parameters of the hydrogels,[50] for details see relevant works[119,134].

The swelling and equilibrium water content (EWC) of PVA/DAC hydrogel samples (L-130, H-130, L-31, H-31) depend on the amount of crosslinker and the M_w of PVA (Table 2). Generally, a lower amount of crosslinker and a lower M_w of PVA lead to greater swelling and EWC. Thus, sample L-31 has the largest swelling, equal to almost 80-times of its dry mass. On the other side, sample H-130 swells only about 3.5-times. In contrast, the gel fraction grows when the concentration of DAC and M_w of PVA increase, therefore sample H-130 shows the largest gel fraction and sample L-31 the smallest. On the other hand, increasing the M_w of PVA decreases M_c (increases ρ_c) in the H-series (1% of DAC), but the opposite trend is observed in the L-series (0.25% of DAC). The difference is probably caused by differences in residual physical interactions, such as chain entanglements and hydrogen bridge networks between PVA macromolecules, as well as chemical crosslinks between PVA and DAC[119]. In particular, for the H-130 sample, where longer PVA chains offer significantly more crosslinking hotspots, it is probable that chemical crosslinking is more pronounced. Overall, the amount of crosslinker DAC plays a significant role in the network parameters of hydrogels, but the M_w of PVA further emphasizes this relationship.

Table 2 *Network parameters calculated for the PVA/DAC hydrogel samples[133]*

Sample	**Swelling (%)**	***EWC* (%)**	**Gel fraction (%)**	***M_c* (g/mol)**	**ρ_c (μmol/cm^3)**	**ξ (Å)**
L-31	7900 ± 800	99 ± 1	12 ± 1	12380 ± 20	103 ± 1	508 ± 17
H-31	707 ± 17	88 ± 1	48 ± 1	6410 ± 160	198 ± 5	169 ± 4
L-130	1150 ± 90	92 ± 1	59 ± 2	20700 ± 1900	62 ± 6	350 ± 30
H-130	351 ± 6	78 ± 1	89 ± 1	2890 ± 90	440 ± 14	93 ± 2

Viscoelastic properties

The dependence of storage modulus (G′) and loss modulus (G″) on angular frequency is given in Figures 14A and 14B. According to Figure 14A, the G′ values of the PVA/DAC hydrogel samples range from about 2100 Pa for sample H-130 to about 150 Pa for sample L-130. Corresponding G″ values range (Figure 14B) from about 190 Pa to 4.3 Pa. The crosslink density of PVA/DAC hydrogel samples clearly affects the G′ and G″ values, which are higher for denser mesh and lower for sparser mesh because the first type has a higher elasticity than the other one, which has more viscous behavior.[134] The L-130 sample with the lowest crosslink density displays the lowest G′ and G″ values, indicating more viscous-like behavior, while the most elastic is sample H-130. Viscoelastic properties of the hydrogels are similarly influenced by the M_w of PVA as lower M_w leads to lower G′ and G″ values, as can be seen from a comparison of H-31 and L-130 samples. The decreased M_w of PVA resulted in a nearly 70 % decrease in G′ values.

The complex dynamic modulus (G*) (Figure 14C) and damping factor (tan δ) (Figure 14D) show analogous correlations with the amount of crosslinker and M_w of PVA. Sample H-31, prepared with the same amount of crosslinker as H-130, has viscoelastic properties closer to L-130, highlighting the significant impact of the PVA matrix on hydrogel rheological properties.

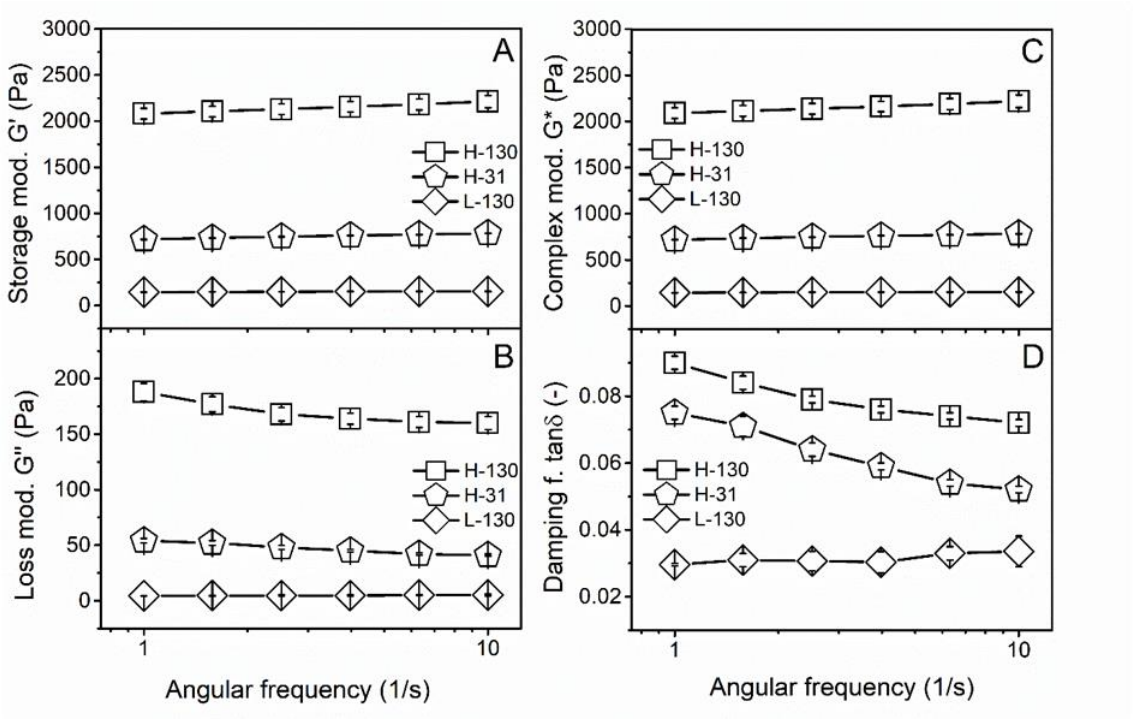

Figure 14 *Dependence of the G˙ (part A) and the G¨ (part B) of PVA/DAC hydrogel samples on the angular frequency and dependence of the calculated complex modulus (G*, part C) and the damping factor (tanδ, part D) on the angular frequency*[133].

BET and SEM analysis

PVA/DAC hydrogels were lyophilized and their specific surface area (α_{BET}), total pore volume (V_p), mean pore diameter and adsorbed volume of nitrogen (V_a) was measured, see Fig. 15. In comparison to samples H-130 (2.0 ± 0.1 m^2/g) and H-31 (2.2 ± 0.1 m^2/g), sample L-130 has a α_{BET} value that is an order of magnitude higher (31.1 ± 0.9 m^2/g) (Figure 15A). The results demonstrated that decreasing DAC concentrations significantly increased the hydrogels' specific surface area (BET), total pore volume (V_p), and V_a, with sample L-130 displaying the highest values (Figure 15). This can be explained by the extent of cavitation induced by the lyophilization process, which is indirectly connected to the hydrogel's capacity to absorb water. Interestingly, the mean pore diameter did not follow the same trend, with the H-series cryogels having fewer larger pores and L-130 containing a larger number of smaller pores. This is attributed to the molecular weight of the PVA used, which influences the mean pore size. SEM confirmed that the surface of the L-130 cryogel was highly porous in agreement with α_{BET} values, while the H-31 sample had slightly larger surface pores than the H-130 sample (Figure 15C).

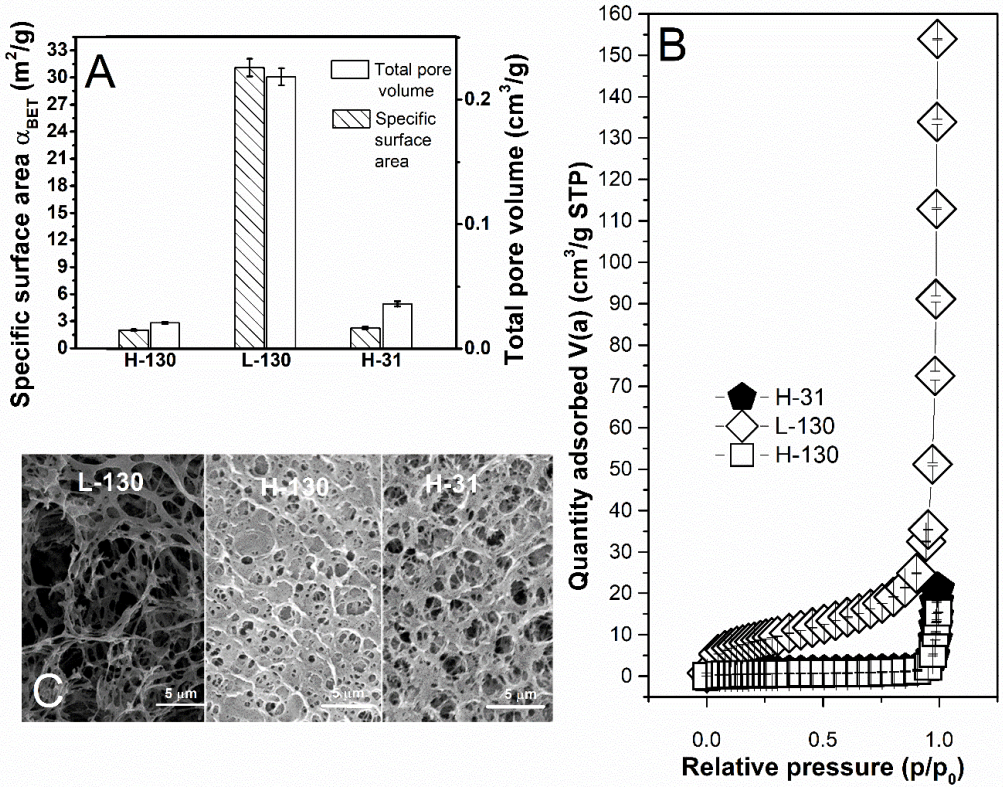

Figure 15 *The specific surface area α_{BET}, and total pore volume (V_p) of the prepared PVA/DAC cryogels (part A), the dependence of the amount of nitrogen adsorbed per mass of the cryogels on the relative pressure p/p_0 (part B), and SEM images of individual PVA/DAC samples taken at a magnification of 30.000 (part C)* [133].

Cytotoxicity

The biological evaluation was performed in collaboration with a group of Prof. Humpolíček at CPS. It consisted of two parts. Firstly, the cytotoxicity of hydrogel extracts in culture media was determined according to ISO 10993-12.[96,133] Secondly, the cell growth and morphology in the presence of hydrogels were observed, both in the media and directly on the gel surface.

The cytotoxicity of hydrogel extracts in culture media was determined, and all materials were found to be non-toxic according to ISO 10933-5 (Figure 16).

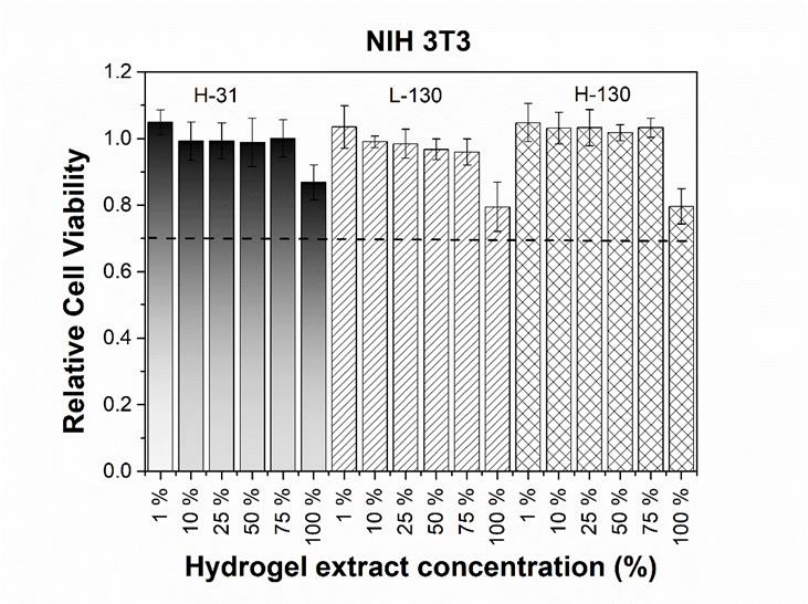

Figure 16 *Various amounts of PVA/DAC hydrogel extracts and their relative cell viability*[133]

The effect of hydrogel samples on cell growth and morphology was investigated by incubating samples with an NIH-3T3 mouse fibroblastic cell line for 96 hours. The MTT assay and microscopic observation were used to quantify cell viability and morphology. The results showed that the presence of hydrogel samples had no significant effect on cell growth or morphology. The cells reached confluence at the same time and their viability was the same as for cells not treated with hydrogels (Figure 17, top). Additionally, the fibroblasts retained their typical elongated shapes (micrographs in Figure 17, bottom), and no degradation of hydrogels was observed during the tests or after one week of in vitro conditions. To assess the cells' growth and morphology in direct contact with the hydrogel, however, was impossible since they did not adhere to the hydrogel surface. Although the results suggest that hydrogel films are suitable for topical applications, additional tests are necessary to claim biosafety *in vivo*.

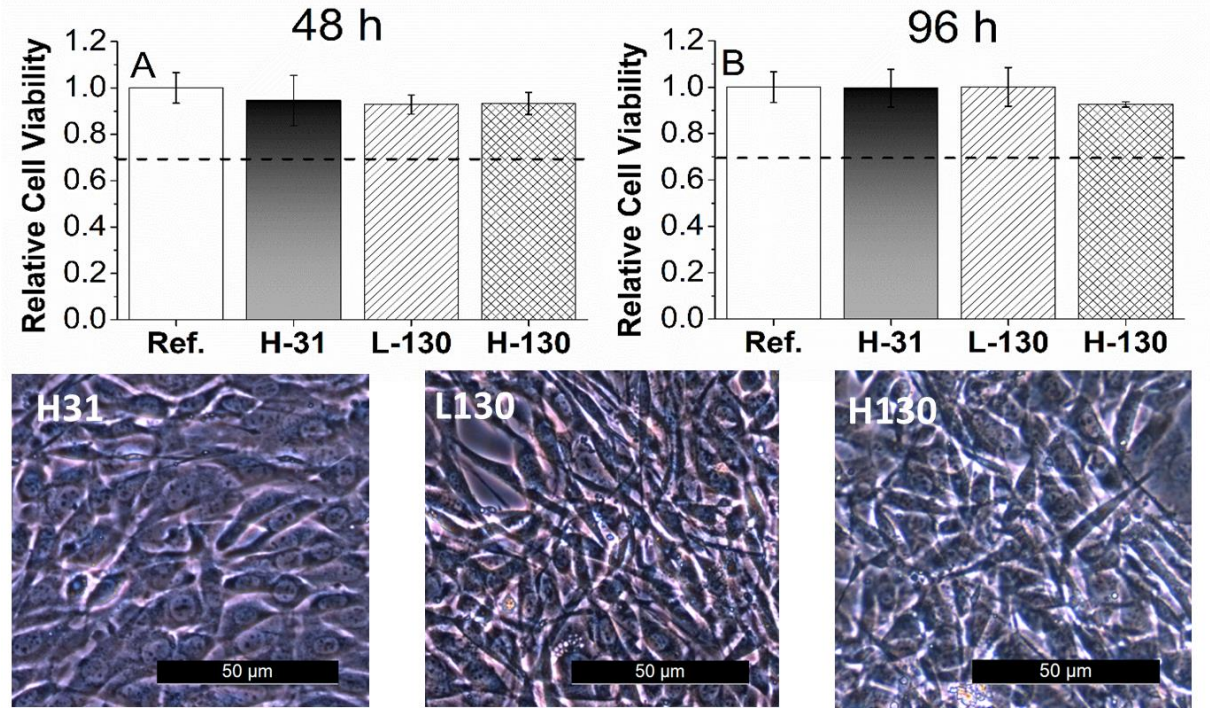

Figure 17 *Relative cell viability of cells incubated in the presence of PVA/DAC for 48 and 96h and micrographs of cells after 96 h*[133]

7.1.3 Drug release and transdermal absorption performance of prepared PVA/DAC hydrogels

The kinetics of release and transdermal absorption of two model drugs, caffeine and rutin, were investigated using a UV-VIS spectrometer at 353 nm (rutin) and 273 nm (caffeine)[96,133]. The hydrogel samples were loaded by the selected compounds and tested as described above (6.4).

The release rates of caffeine, which is a relatively small molecule, were identical for all three hydrogel materials tested (Figure 18B). For larger rutin molecules, there were minor differences in the release kinetics among the samples, with the fastest release observed in the H-31 sample (Figure 18A). These differences may be related to the lower molecular weight of PVA and its influence on pore size, but further tests would be needed to confirm this observation. The relatively low thickness of the hydrogel films may have minimized the impact of the hydrogel network on drug release rates. This could be improved by employing thicker films or changing the drug loading process. However, the observed release kinetics, which includes fast initial release rates (up to 80–90%) of compounds released in 8 h), seem to be well suited for topical drug delivery applications, where the expected time of application is in the order of hours.

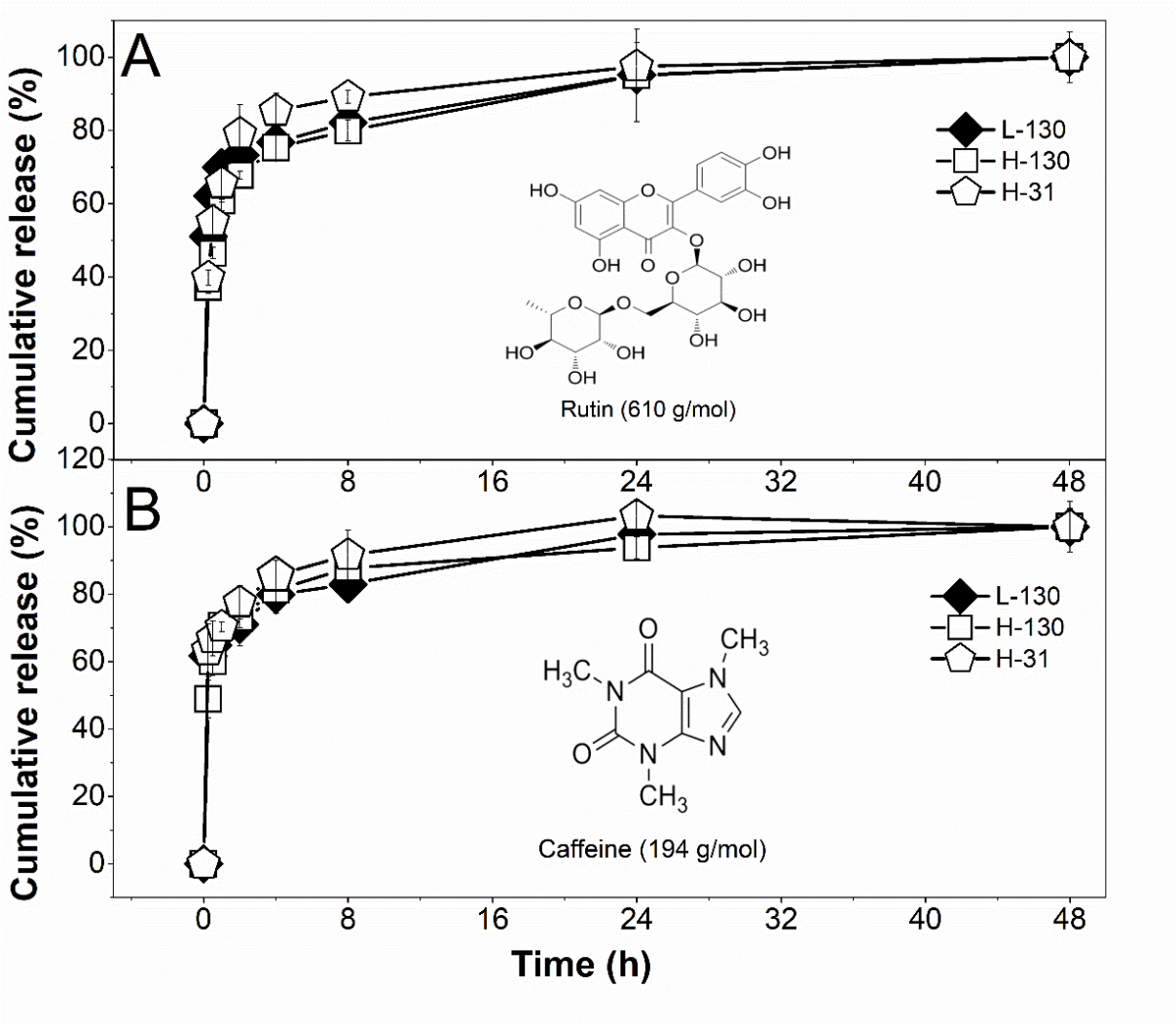

Figure 18 *Cumulative release of rutin (part A) and caffeine (part B) from PVA/DAC hydrogels*[133]

Transdermal absorption

The skin absorption tests for caffeine were conducted following the OECD Test Guideline. The measurement was tested using an automated diffusion cell system, with a continuous flow of receptor liquid. The amount of caffeine absorbed through the skin was analyzed by liquid chromatography using an HPLC chromatograph equipped with a UV-VIS detector using a wavelength of 272 nm [96,133].

Although all samples were loaded using the same technique, the total caffeine dose differs between samples due to their different EWC, gel fractions, and equilibrium swelling. Sample L-130 had the highest caffeine load (around 900 μg), whereas sample H-130 was able to absorb a small amount (about 500 μg), (Table 3). Aqueous caffeine solution containing 250 μg of caffeine was used as a reference.[137].

Table 3 *Caffeine amount present in the samples (μg) and the dose of caffeine per cm² of skin*[133].

Sample	Total dose of caffeine (μg)	Dose per cm² (μg/cm²)
L-130	896 ± 8	1134 ± 10
H-31	660 ± 6	832 ± 7
H-130	495 ± 1	625 ± 1
Reference	250	320

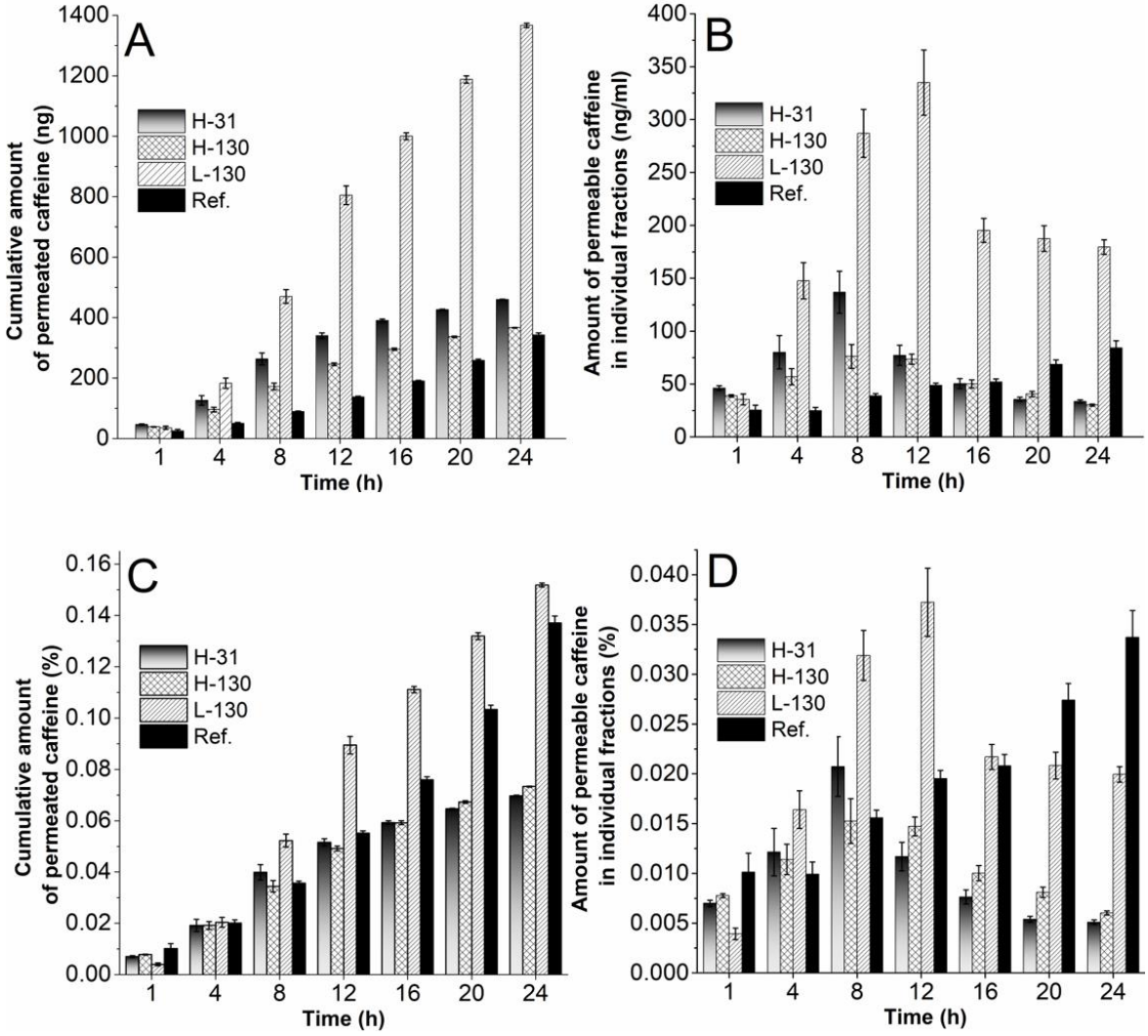

Figure 19 *The cumulative amount of penetrated caffeine [ng] (part A), the time-dependent quantity of permeated caffeine [ng/mL] (part B), the total amount of transdermally absorbed caffeine relative to applied dose [%] (part C), and the time profile of caffeine absorption relative to applied dose [%] (part D)* [133].

Results showed that penetration of caffeine through the skin was slow, with only between 0.07% and 0.2% of the total dose crossing the skin barrier within 24 hours (Figure 19 C, D). According to Trauer et al.[137], this is due to an absence of blood supply to the skin during the *in vitro* study. Caffeine absorption through the skin of a living organism would be much faster. Moreover, the hydrophilic nature of caffeine presents a significant challenge to its penetration through the stratum corneum. This is consistent with the results of several other studies, including those by Bonina et al.[138], Santander-Ortega et al.[139], and Pilloni et al.[140], where it was also discovered that caffeine transdermal absorption was relatively low, typically in the range of tenths of a percent of the applied dose, despite of the various carriers used. Despite this low amount, the L-130 sample, which had the lowest elasticity and best adhered to the skin, had the highest overall amount of caffeine absorbed (1400 ng/0.15%), whereas only 350–450 ng (0.06-0.07%) of caffeine was absorbed from H-series samples over 24 hours. The amount of caffeine permeated from the L-130 sample is approximately twice larger than from H-series samples, Fig. 19 C, D.

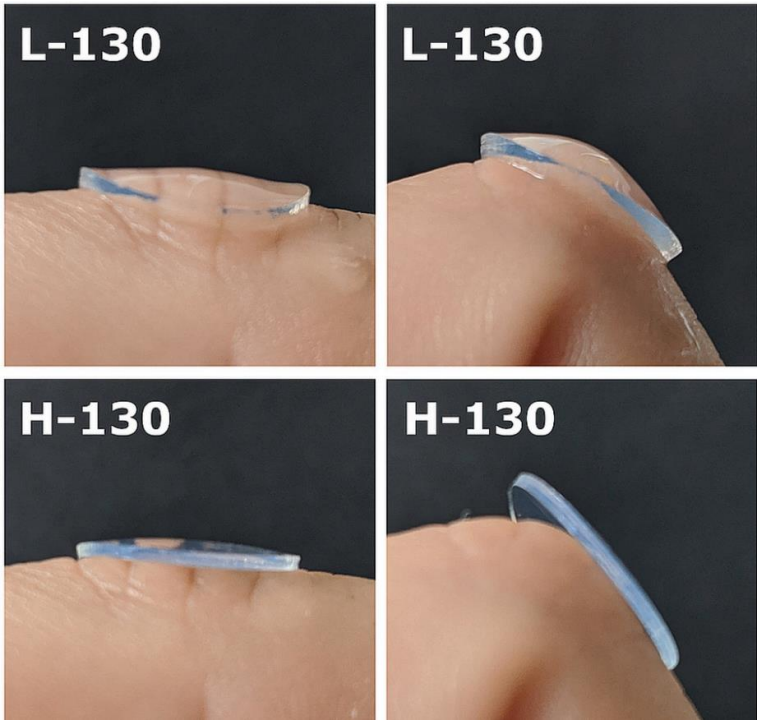

Figure 20 *The comparison between H-130 and L-130 hydrogels on an uneven skin surface*[133]

Wound dressing applicability note

The samples showed no significant signs of cytotoxicity and all of them seem to be suitable for topical applications, although additional tests are necessary to claim full biosafety *in vivo*. Besides transdermal application, wound dressing application may be considered as well. Comparing individual hydrogel samples,

easy handling and best adherence to the skin would be the criterium for material selection. Hence, selected samples of L-130 and H-130 hydrogels were tested on the uneven skin surface to visualize the compliance of the material to the human skin under real condition. The result is depicted in Figure 20 demonstrating superiority of the L-130 hydrogel.

Concluding remarks

The hydrogel L-130 was identified as the most promising candidate for transdermal delivery of biologically active substances without the need for skin-penetration enhancers. Its physical properties allow easy handling and adherence to the skin, which enhances its transdermal drug delivery properties. Next, the role of crosslinker structure and properties was examined.

The results presented in section 7.1 were published in an article **Muchová, M.**; Münster, L.; Capáková, Z.; Mikulcová, V.; Kuřitka, I.; Vícha, J. Design of Dialdehyde Cellulose Crosslinked Poly(Vinyl Alcohol) Hydrogels for Transdermal Drug Delivery and Wound Dressings. *Materials Science and Engineering: C* **2020**, *116*, 111242. https://doi.org/10.1016/j.msec.2020.111242 which is attached as **Appendix I**.

7.2 The role of DAP crosslinker structure in PVA hydrogels

7.2.1 Preparations of PVA/DAPs hydrogels

The hybrid hydrogel samples prepared in this study are designated as PVA/DAP and are categorized and named DAC, DXI, DXA, or DAH based on the type and concentration of the crosslinker used, with -L and -H indicating lower (0.1/0.25 wt%) or higher (1/2.5 wt%) concentrations, respectively. Some of the swelled PVA/DAP hydrogel samples (H series) were also subjected to a 3-hour treatment in closed reaction flasks with demineralized water heated to 70 °C (labeled as DAP-HT), to enhance the role of chemical crosslinks by disrupting hydrogen bonding in residual crystallites formed between PVA chains during drying. PVA/DAPs hydrogel disc-shaped samples are shown in Figure 21.

Figure 21 *Photographs of PVA/DAPs hydrogels samples*[96]

7.2.1 Preparation and characterization of DAP crosslinkers

DAPs were prepared as described in (6.2.2). Conditions of periodate oxidation were set to obtain fully oxidized materials[99,135] .Regarding the differences between DAPs, the dialdehydes of cellulose, dextran, and dextrin are composed of similar building blocks (i.e. oxidized glucopyranose units) and thus share very similar structural patterns. However, the four DAPs retain unique back bone and side

group structural features of their source compounds and the properties of DAPs are to a large extent given by the architecture and characteristics of source polysaccharides, they differ significantly. Therefore, the molecular weight, DO, FT-IR, size of nano-assemblies formed by DAPs in the solution and their cytotoxicity were analyzed before the preparation of hydrogels.

The gel permeation chromatography analysis (GPC)

To determine the molecular weight of the prepared dialdehydes, they were converted to corresponding doubly-oxidized dicarboxylated derivatives (DCP) namely DCDXA - dicarboxy dextran, DCH - dicarboxy hyaluronate, DCDXI - dicarboxy dextrin, and DCC - dicarboxy cellulose. This conversion was necessary, as DCPs are more stable and have a better-defined composition compared to DAPs, which tend to form hemiacetals and self-crosslinks. This method has also been used previously with good results[135]. To analyze the molecular weight of the samples, a Waters HPLC Breeze chromatographic system with a refractive index detector was used. The highest M_n is found in the DXA at 30 kDa, followed by the DAH at 21 kDa, while the M_n in the DXI and DAC is nearly identical at 12 kDa, see Table 4 for more details.

Table 4 *Number average molecular weight (M_n), weight average molecular weight (M_w), polydispersity index (PDI), degrees of polymerization (DP) of dicarboxy and dialdehyde polysaccharides, their DO, and molar amount of –CHO groups per unit of crosslinker mass (n_{-CHO})* [96]

DCP	***M_w*** **(kDa)**	***M_n*** **(kDa)**	***PDI***	***DP***	**DAP**	***M_w*** **(kDa)**	***M_n*** **(kDa)**	***DO*** **(%)**	***n_{-CHO}*** **(mmol/g)**
DCDXA	84.8	44.1	1.92	420	DXA	58.0	30.2	85±4	12.3±0.4
DCH	47.8	24.8	1.92	103	DAH	41.2	21.4	99±6	5.0±0.3
DCDXI	36.9	16.9	2.17	157	DXI	25.2	11.5	98±1	12.5±0.2
DCC	31.2	16.9	1.84	132	DAC	21.2	11.5	95±2	12.4±0.3

The degree of oxidation

The DO (degree of oxidation) of each DAP, which is defined as a percentage of the total amount of basic structural units that were oxidized to dialdehydes, was determined using oxime reaction[136]. DAC, DAH, and DXI were nearly fully oxidized with a DO greater than 95%, while the maximum DO of DXA was limited to around 85% due to the presence of 15% of oxidation-resistant branched units. This corresponds to: 12.5 mmol/g of -CHO groups in DAC and DXI, while

DXA oxidized to 85% contains 12.3 mmol/g of -CHO groups (Table 4). The presence of oxidation-resistant N-acetyl-D glucosamine units in DAH reduces the maximum -CHO content to 5.0 mmol/g, which is 2.5 times lower than that of the tested homoglycans. Therefore, the amount of DAH crosslinker used in hydrogel preparation was increased by 2.5 times to better assess the impact of molecular weight, structure, and -CHO group density of individual DAPs.

Dynamic light scattering (DLS)

The hydrodynamic radii (d_h) and zeta potentials (ζ) of DAP nano-assemblies formed in their solutions were investigated using DLS (Table 5). The linear DAP molecules (DAC, DAH) formed larger nano-assemblies compared to the branched crosslinkers, despite these having the same (DXI) or even higher (DXA) M_n than their linear counterparts. DAH created the largest nano-assemblies, whereas DAC, despite having an approximately 3x lower molecular weight (M_n), produced outcomes comparable to those of DXA. Interestingly, the size of DXI nano-assemblies was almost 1.5 times smaller than that of DAC with the same M_n. With a polydispersity between 0.35 and 0.4, the size distribution of the DAC, DXI, and DAH nano-assemblies was relatively uniform. The size distribution of DXA assemblies, however, was distinctly bimodal, with the majority (approximately 80%) of the assemblies being larger (d_h 270 nm) and the minority (about 20%) being smaller (20 nm).

Table 5 *The hydrodynamic radii (d_h) and zeta potentials (ζ) of DAPs*[96]

sample	***d_h* (nm)**	**ζ (mV)**
DXA	267 ± 19 (20 ± 3) *	-14.6 ± 1.1
DAH	308 ± 1	-31.0 ± 1.9
DXI	170 ± 11	-23.6 ± 1.5
DAC	250 ± 30	-23.6 ± 1.1

*DXA sample has a bimodal size distribution

Regarding the stability of colloids, their ζ-potential values ranged from -15 mV for DXA to -31 mV for DAH. This is expected because DXA is partly composed of less polar, non-oxidized anhydroglucose units, whereas DAH has one carboxylic group per each fundamental structural unit increasing its negative charge. The stability of the colloids was confirmed by repeating the DLS and ζ-potential measurements one week after their preparation, which gave essentially the same results.

FTIR analysis

The IR spectra of all DAPs show distinctive absorption bands around 1730 cm^{-1} (C=O vibration from -CHO) and 875 cm^{-1} (C-O-C vibration), indicating the presence of both free aldehyde groups and newly formed hemiacetal groups, as you can see in Figure 22. The spectrum patterns of DAC, DXI, and DXA crosslinkers are similar because they are all formed from oxidized glucopyranose units. On the other hand, DAH shows distinctive absorption bands that are connected to the existence of -COOH groups in the glucuronic unit, such as an asymmetric valence -COO vibration at around 1600 cm^{-1} and a deformation vibration -OH from COOH at around 1380 cm^{-1}. The absence of the glucuronic acid fingerprint vibrational band at 893 cm^{-1} in the DAH spectra suggests that the C2-C3 bond has been broken as a result of quantitative oxidation.

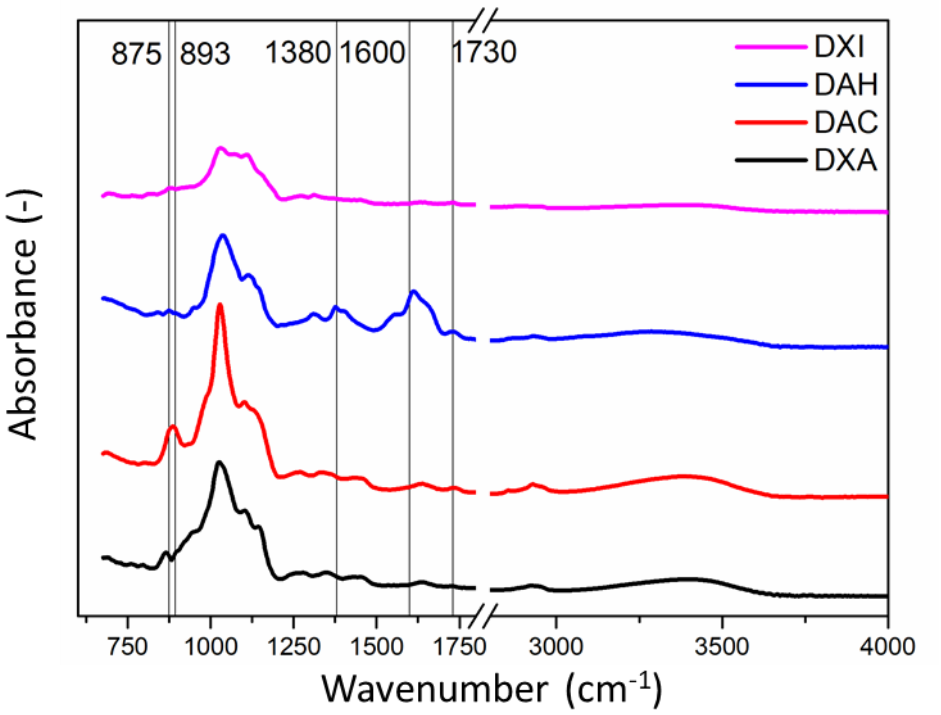

Figure 22 *FT-IR spectra of DAPs*[96]

Cytotoxicity

In collaboration with a group of Prof. Humpolíček at CPS, all DAPs were found to be non-cytotoxic up to 0.1 mg/mL, and some even supported cell growth at lower concentrations (Figure 23). DAH, DXA, and DAC were the least cytotoxic, while DXI was the most cytotoxic. The number of reactive -CHO groups did not correlate with the cytotoxicity of the crosslinking agents, however, which may be due to the size of their nano-assemblies and related differences in transport through the cell wall. Overall, the cytotoxicity of crosslinkers is deemed to be relatively low compared to other crosslinking agents. To put these results into a proper perspective, a comparison to glutaraldehyde (GA) was performed. GA was

found to be highly toxic even at the lowest concentration used (0.05 mg/mL). Speer et al. even reported 99% inhibition of 3T3 fibroblast growth at a GA concentration of 0.003 mg/mL[6]. DAPs are thus several orders of magnitude less toxic.

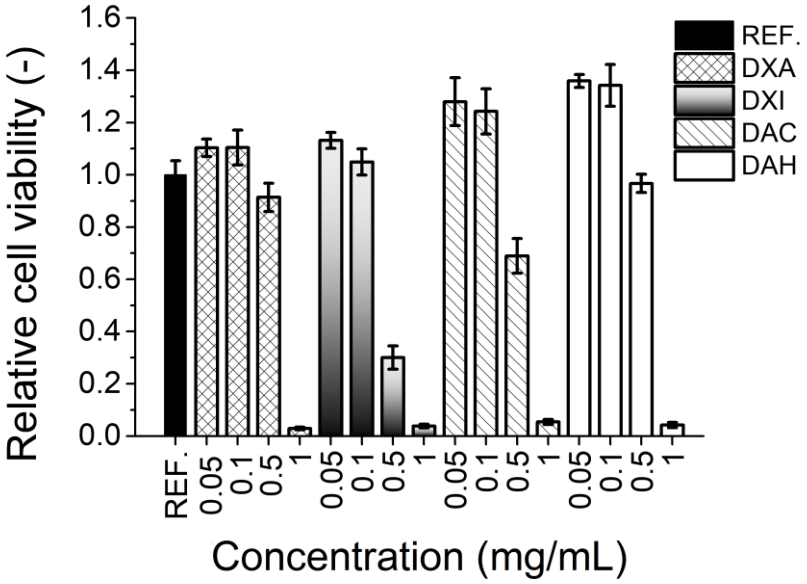

Figure 23 *Relative cell viability containing 0–1mg/mL of DAP for 24 h*[96]

Crosslinkers were subsequently used to prepare hydrogels, whose properties are discussed in the following section.

7.2.2 Characterization of prepared PVA/DAP hydrogels

Network parameters

Network parameters of all types of PVA/DAP hydrogel samples were calculated according to Flory and Rehner[50]. The DAH-H sample showed the largest swelling among the H-series samples (approximately 225%), followed by the DXI-H and DAC-H samples, which both swelled by about 200%, and the DXA-H sample, which swelled by 170% (Figure 24). Similar trends are observed for average molecular weight between crosslinks M_c and the mesh size ξ, whereas the crosslink density (ρ_c) increases in the opposite order (DXA-H has the highest crosslink density).

Heat treatment of the samples leads to a significant increase in hydrogel swelling, up to 480% for DAH-HT. DXA-HT sample had the lowest swelling of 400%. The H-series hydrogels followed the same trend. As a result of heating, other network characteristics also displayed a significant decrease in crosslink density, which is probably due to the disruption of PVA's physical crosslinks, which are created during the preparation of hydrogel films. In the L-series, the highest swelling was observed for DXI (620%), followed by DAH (500%) and DAC (480%), while DXA had the lowest swelling (420%).

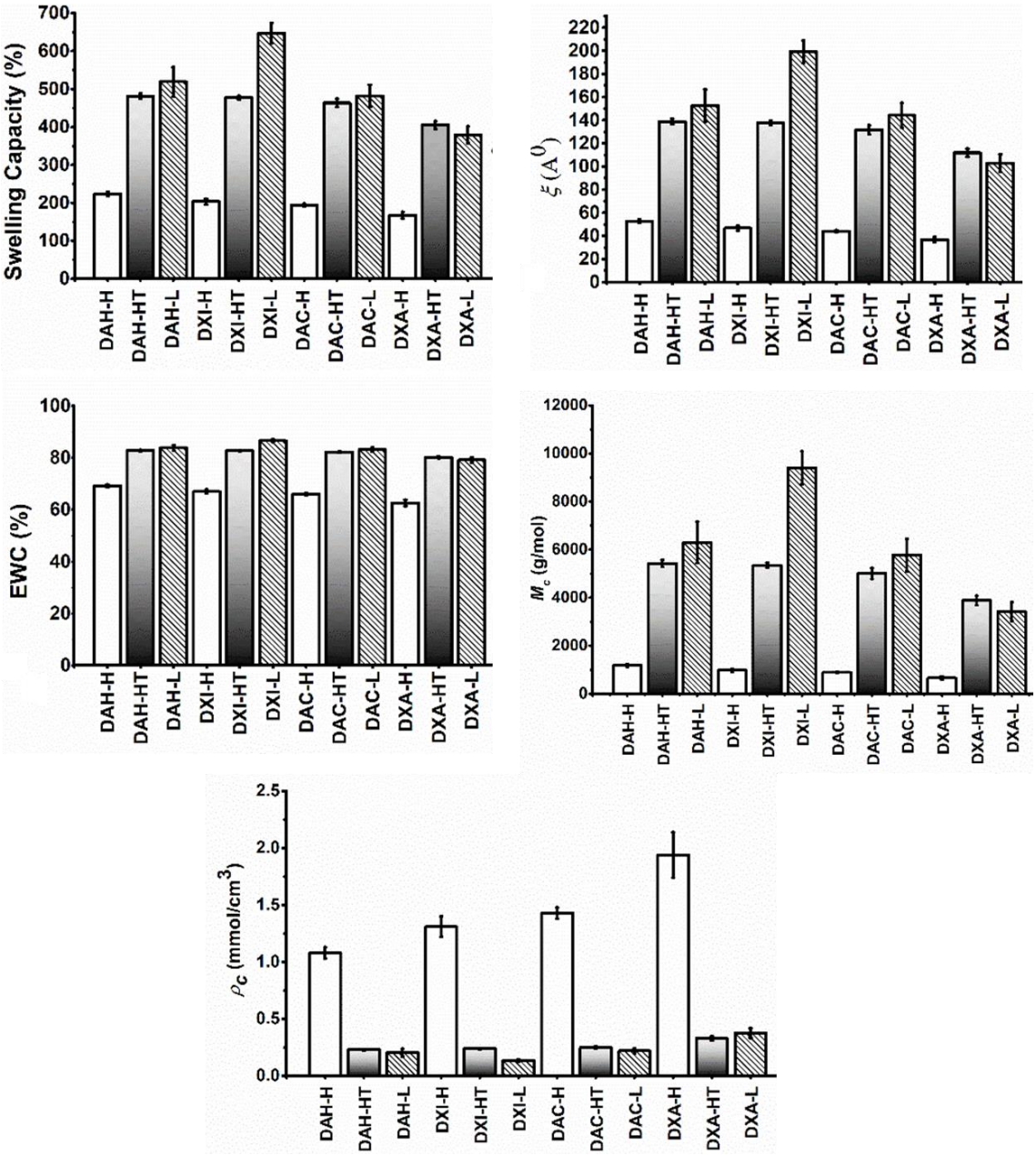

Figure 24 *Network parameters calculated for PVA/DAP hydrogels*[96]

Viscoelastic properties

Graphs in Figure 25 show the storage (G′) and loss (G″) modules of various PVA/DAPs hydrogel samples as a function of different angular frequencies. The higher G′ values than G″ values in all samples demonstrated a higher degree of elasticity than viscosity, which corresponds to hydrogel formation. The G′ values for the H-series samples range from 3500 Pa for the DXA-H sample to 6500 Pa for the DXI-H sample (Figure 25). Note, that the DXA-H sample had the highest crosslink density but the lowest G′ value. This issue is likely caused by the bimodal size distribution of DXA nano-assemblies, see below. G″ values followed the same trend as G′, with DXI having the highest and DXA having the

lowest values. The same trend was reflected in the damping factors, with DXI and DAC being the most elastic, and DAH and DXA having more viscous-like character (Fig 26).

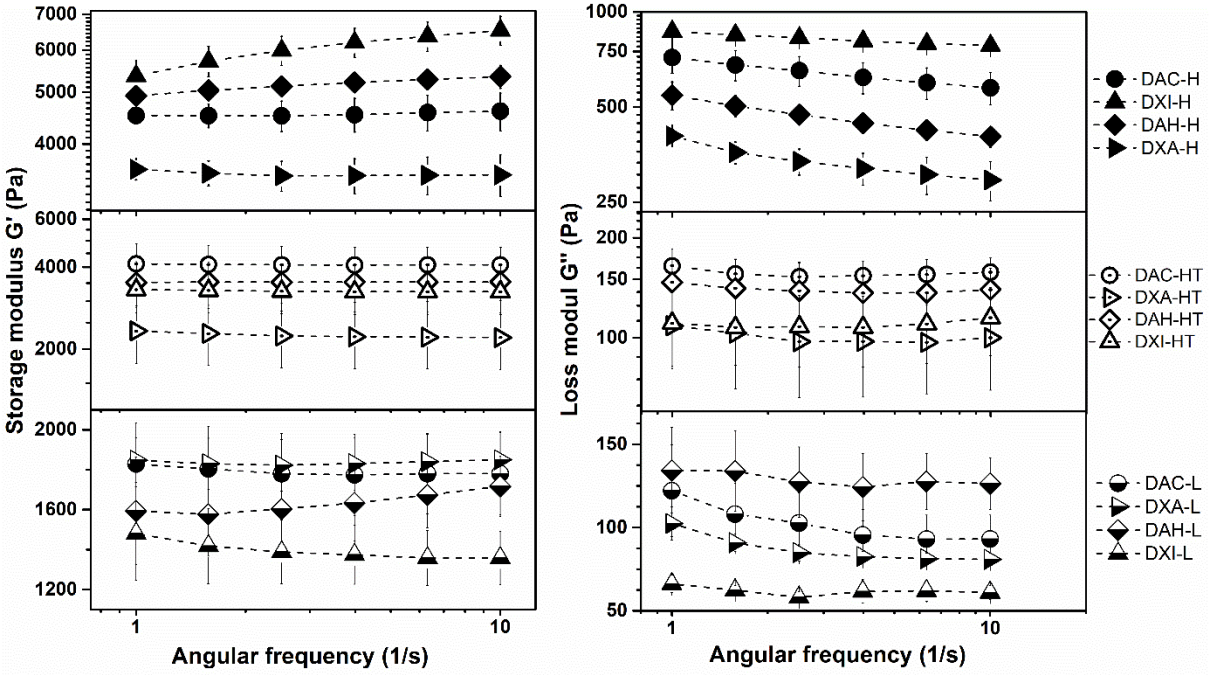

Figure 25 *Dependence of storage modulus and loss modulus of PVA/DAPs on angular frequency*[96]

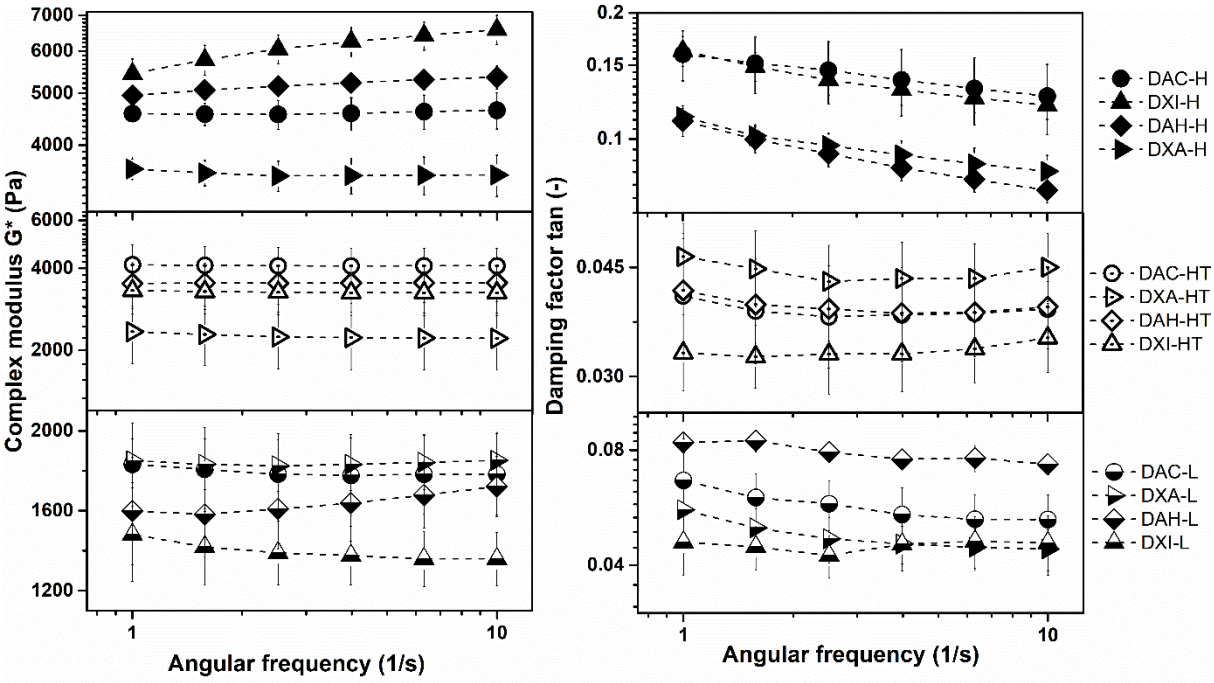

Figure 26 *Complex modulus G* and damping factor tan of PVA/DAPs depend on the angular frequency*[96].

Due to the loss of crosslinking caused by heating, all samples in the HT series showed a decrease in G′, G″, and tan δ, with DAC-HT having the smallest decrease and DXI-HT getting the greatest decrease.

The G′, G″, and tan δ, of the L-series samples were similarly decreased, with DXI-L showing the largest decrease and DXA-L showing the smallest decrease in storage modulus compared to the H-series. The DAH-L showed the lowest decrease in G″ (and thus the highest overall tan δ) among the L-series samples. The values for the other L-series samples were mostly comparable within experimental error.

BET and SEM analysis

The porosity of PVA/DAPs was analyzed using BET and SEM techniques, and the results are shown in Figure 27 for BET and Figure 28 for SEM. The L-series samples were found to be more porous than the H-series samples. Among the H-series samples, DAH-H showed the highest specific surface area (α_{BET}) (3.9 m^2/g) and total pore volume (V_p) values (0.038 cm^3/g), whereas DAC-H had the lowest. The mean pore diameter (d_m) was also found to be highest in DAH-H (~35 nm), and lowest in DAC-H (~27 nm). In all cases, heating the samples increased the α_{BET} and V_p values, with DAH-HT remaining the most porous material. The DXI-L sample was found to be the most porous sample overall, with DXA-L being the least porous of the L-series samples. The decrease in crosslinker amount led to a significant increase in porosity. SEM images of fracture surfaces of lyophilised hydrogels in Figure 28 also support these findings.

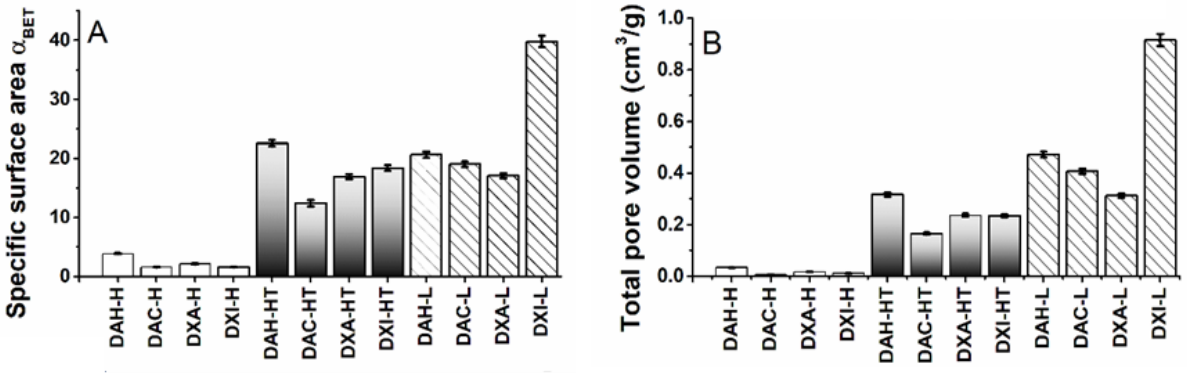

Figure 27 Specific surface area (part A), total pore volume (part B) of PVA/DAPs hydrogels[96]

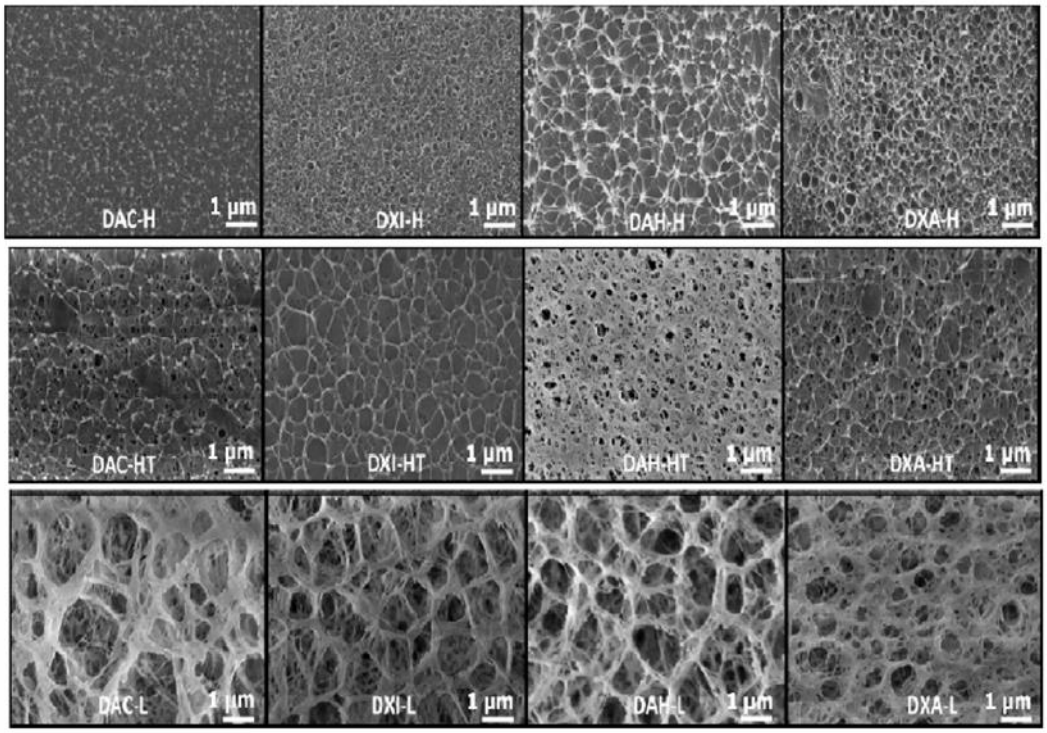

Figure 28 *SEM analysis of lyophilised PVA/DAPs hydrogels*[96]

Cytotoxicity

In collaboration with a group of Prof. Humpolíček at CPS, cytotoxicity was determined according to ISO 10 993-5. Figure 29 displays the results for 100% extracts from hydrogels. Hydrogel extracts are considered non-toxic if the relative cell viability is above 0.7, as indicated by the dashed line in Figure 29.

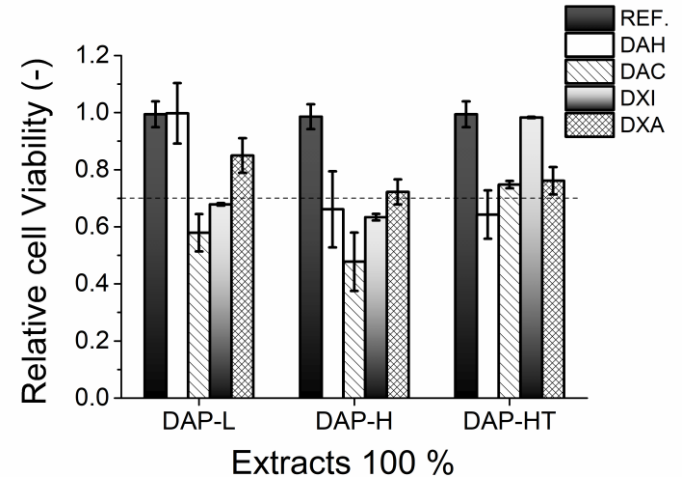

Figure 29 *Cytotoxicity of the PVA/DAPs extracts*[96]

It was discovered that the cytotoxicity of hydrogel extracts is influenced by both the amount of the crosslinker and the heating of the gel matrix and that it partially correlates with the trends shown for free crosslinkers. DAH and DXA-based hydrogels were found to be the least cytotoxic, while DAC and DXI-based

hydrogels were found to be mildly cytotoxic in both L- and H-series. However, heat treatment of hydrogels significantly reduced the cytotoxicity of hydrogel extracts, especially for DXI. This is probably because increased hydrogel swelling at a higher temperature makes it easier to remove unreacted crosslinkers and fragments of the partially crosslinked matrix, therefore reducing cytotoxicity.

7.2.3 Unraveling of DAP crosslinkers' effects in PVA matrix

Based on the obtained data, the following conclusions were reached.

DAC - DAC-based hydrogels have properties that indicate effective chemical crosslinking, such as high storage modulus and damping factors, as well as good retention of rheological properties even after heating and at low crosslinker concentrations, and the porosity of DAC xerogels is among the lowest across all series. The high –CHO group density and large DAC nanodomains, comparable to those of almost three times heavier DXA, contribute to the efficient crosslinking of distant PVA chains as schematically demonstrated in Figure 30. The presence of β-glycosidic bonds in DAC also enhances its crosslinking effectiveness by allowing efficient crosslinking of different PVA chains even by relatively close DAC units. Although the mild cytotoxicity of PVA/DAC hydrogel extracts is a disadvantage, it can be improved by heating. In summary, DAC is an effective crosslinker for hydrogels but may not be the best choice for certain biological applications.

DXI - Although M_n, $n_{\text{-CHO}}$, and the chemical composition of DXI-based hydrogels are essentially comparable to those of DAC, their structural differences (branching) lead to significantly different characteristics. The properties of DXI-based hydrogels degrade rapidly after heating and at low crosslinker concentrations. The observed differences between DXI and DAC are most likely caused by the smaller size of DXI domains rather than molecular weight or -CHO group density. As a result, smaller regions of very high crosslink density are embedded in physically crosslinked PVA network hydrogels (Figure 30). DXI-based hydrogels are the least suitable for biomedical applications since they demonstrate one of the highest observed cytotoxicity of all tested species (but still mild). In conclusion, compared to other tested species, DXI-based hydrogels demonstrate characteristics that make them the least suited for crosslinking.

DAH - Because linear DAH macromolecules are based on heteroglycan, they can only be oxidized by periodate at glucuronic acid units. DAH thus contains fewer crosslinking hotspots per macromolecule compared to AGU derivatives. As a result, the DAH forms a more loosely bound network than DAC, leading to high swelling, lower network density, high porosity, and moderate storage modulus in DAH-H hydrogels. However, DAH-based hydrogels maintain their properties better than DXI-based hydrogels. These do not degrade as quickly as those of DXI-based samples, and even perform similarly to DAC-based hydrogels at low

crosslinker concentrations. This is likely due to the larger size of DAH nano-assemblies and possibly higher M_n of DAH macromolecules, which allows them to crosslink more distant PVA chains (Figure 30). Additionally, DAH-based hydrogels showed the lowest cytotoxicity compared to other samples. In summary, DAH-based hydrogels have a more viscous character, lower cytotoxicity, and higher porosity than other hydrogels, making them a potentially interesting option for scaffolds in tissue engineering. However, to achieve physical properties similar to other crosslinkers, a 2.5 times higher amount of DAH is needed.

DXA - Due to their densest mesh, the DXA-based hydrogels should have the highest storage modulus and damping factors because they have the lowest swelling and highest crosslink density. However, this trend is only observed in the DXA-L sample, while the G′ values of DXA-H and DXA-HT are the lowest within their respective series. This unexpected behavior is attributed to the bimodal size distribution of DXA nano-assemblies, with the small domains (d_h ~20 nm) acting as a "secondary" crosslinker network, binding nearby PVA chains. The DXA hydrogels are promising alternatives to other species for certain applications because they have lower cytotoxicity and better mechanical properties than DAH-based hydrogels, especially at low concentrations.

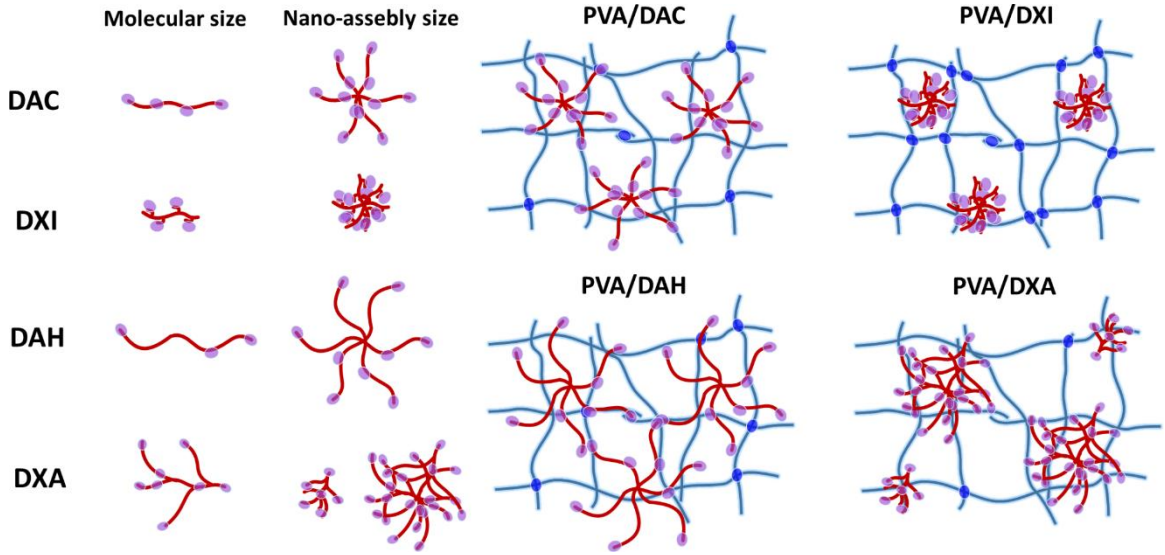

Figure 30 *The size of the crosslinker molecules, $n_{\text{-CHO}}$, hydrodynamic radii, and the predicted crosslinking mode of the PVA network are shown schematically. Crosslinking hotspots are shown in purple, and the PVA matrix's residual physical crosslinks are shown in blue. The number of crosslinking hotspots shown corresponds to the ratio of -CHO groups between crosslinker molecules, while the sizes of individual macromolecules and nano-assemblies reflect the observed M_n and d_h, respectively. For better clarity, the PVA matrix was represented uniformly, showing the same PVA concentration during the crosslinking*[96].

The results presented in section 7.2 were published in an article **Muchová, M**.; Münster, L.; Vávrová, A.; Capáková, Z.; Kuřitka, I.; Vícha, J. Comparison of Dialdehyde Polysaccharides as Crosslinkers for Hydrogels: The Case of Poly(Vinyl Alcohol). *Carbohydrate Polymers* **2022**, *279*, 119022. https://doi.org/10.1016/j.carbpol.2021.119022 which is attached as **Appendix II**.

8. SUMMARY OF OTHER RESEARCH

During my doctoral studies, I also participated in several cooperations with other researchers, mainly in the evaluation of drug loading and release or rheological parameters.

Specifically, I evaluated the cumulative release of cisplatin from various dicarboxypolysaccarides in a research paper by Münster, L.; Fojtů, M.; Capáková, Z.; **Muchová, M.**; Musilová, L.; Vaculovič, T.; Balvan, J.; Kuřitka, I.; Masařík, M.; Vícha, J. Oxidized Polysaccharides for Anticancer-Drug Delivery: What Is the Role of Structure? *Carbohydrate Polymers* **2021**, *257*, 117562 (https://doi.org/10.1016/j.carbpol.2020.117562). This study focused on the modification and characterization of various polysaccharides, namely cellulose, dextrin, dextran, and hyaluronic acid. These polysaccharides were regioselectively oxidized to their respective dicarboxylic derivatives, enabling the binding of the cisplatin as a anticancer drug. The different dicarboxylic derivatives were compared, and their advantages and disadvantages as structural carriers for platinum drugs were investigated. These carriers differed in drug binding site configuration, drug binding efficiency, type of glycosidic bond, presence of branching, and various molecular weight. Subsequently, release kinetics tests and cytotoxicity tests were conducted. It has been observed that the branched structure of dextrin partially inhibits undesirable initial burst release, reduces cellular uptake, and lowers the cytotoxicity of the delivered drug. Conversely, linear polysaccharides such as cellulose and hyaluronate exhibit the most suitable overall combination of structural characteristics for enhanced drug delivery applications. For more details, see the manusctript.

Furthermore, in the work by Münster, L.; Fojtů, M.; **Muchová, M.**; Latečka, F.; Káčerová, S.; Capáková, Z.; Juriňáková, T.; Kuřitka, I.; Masařík, M.; Vícha, J. Enhancing Cisplatin Anticancer Effectivity and Migrastatic Potential by Modulation of Molecular Weight of Oxidized Dextran Carrier. *Carbohydrate Polymers* **2021**, *272*, 118461 (https://doi.org/10.1016/j.carbpol.2021.118461) I worked on the cisplatin loading and release from oxidized dicarboxydextran (DXA) derivates. This study focused on the preparation and characterization of nanogels from dicarboxyl dextran with various molecular weights using a modified method of controlled cleavage of oxidized polysaccharides with sulfamic acid. Subsequently, these prepared dextran derivatives were analyzed using FTIR, GPC, and NMR, and then conjugated with different amounts of cisplatin. Dependencies between drug release rate, cytotoxicity, and migrastatic potential were investigated. It was found that molecular weight plays a significant role, and conjugates with higher molecular weight exhibited increased anti-cancer effectiveness. For more details, see the manusctript.

In a research paper by Důbravová A., **Muchová M.**, Škoda D., Lovecká L., Kimmer D., Kuřitka I., Šimoníková L., Vícha J., Münster L. Efficient affinity

anchoring of gold nanoparticles on chitosan nanofibers via dialdehyde cellulose for reusable catalytic devices, Carbohydrate polymers, under revision I prepared chitosan nanofibers for affinity anchoring gold nanoparticles by employing dialdehyde cellulose (AuDAC). This work introduces an effective approach for anchoring AuNPs onto chitosan nanofibers through covalent bonding using dialdehyde cellulose (DAC). This method demonstrated high binding efficiency and dense decoration of nanofibers with AuDAC. Subsequently, the ability of the material to catalytically reduce 4-nitrophenol (4NP) to 4-aminophenol (4AP) was demonstrated. For more details, see the manuscript.

In a research paper by Káčerová S., **Muchová M**., Doudová H., Münster L., Hanulíková B., Víchová Z.,Valášková K., Kašpárková V., Kuřitka I., Humpolíček P., Vašíček O., Vícha J. Antibacterial, anti-oxidant, conductive, and anti-inflammatory polypyrrole/chitosan/dialdehyde cellulose hydrogel wound dressings, Carbohydrate polymers, under revision, I studied the viscoelastic properties of hydrogels based on water-soluble half N-acetylated chitosan (SCN) with 2,3-dialdehyde cellulose (DAC) and polypyrrole colloidal particles PPy-containing wound dressings. This work focuses on the preparation of composite hydrogel dressings for wound healing, which are conductive and contain bound polypyrrole nanoparticles. The hydrogels are composed of reacetylated chitosan and utilize dialdehyde cellulose (DAC) as a crosslinker. Subsequently, these hydrogel dressings were subjected to comprehensive physicochemical characterizations, including analysis of network parameters, viscoelastic properties, surface analysis, conductivity, cell compatibility, antioxidant activity, wound healing capability, and skin irritation test. The resulting hydrogel dressings demonstrated conductivity, anti-inflammatory properties, non-irritation, and simultaneously promoted wound healing in vitro. For more details, see the under revision manuscript.

9. CONCLUSIONS AND CONCLUDING REMARKS

To draw conclusions of the research, delineate ongoing and future research, and summarise the key findings and their significance presented in this dissertation for both scientific research and socio-economic practice, it is necessary to highlight that the research originated from basic yet abundant resources like cellulose, starch, other natural polysaccharides, and PVA. PVA is a widely available synthetic polymer produced through a well-established and optimised industrial process, available in various degrees of polymerisation and hydrolysis. On the other hand, cellulose and other polysaccharides represent renewable sources onto which an intriguing, yet undemanding on equipment, polymer analogue chemistry was applied yielding polymeric aldehyde compounds with fine-tuned structures.

9.1 Conclusions

The main contributions of my research include i) the preparation of PVA/DAC hydrogels and the study of the effect of the PVA matrix on their properties, and ii) the preparation of PVA/DAPs hydrogels and the study of the structure-function relationship of DAP crosslinkers. These results were published in Materials Science and Engineering: C (**Appendix I**) and Carbohydrate Polymers (**Appendix II**)[96,133], respectively.

*****

In the development of thin hydrogel films of PVA/DAC optimised for topical applications, varying concentrations of the crosslinker, 2,3-dialdehyde cellulose (DAC), and different molecular weights of the matrix component, poly(vinyl alcohol) (PVA), were combined. The standard approach of adjusting the crosslinker quantity to modify hydrogel attributes was supplemented by concurrently altering the molecular weight of another essential hydrogel component, which is a frequently underestimated approach. This additional modification offers another variable in customising the material to specific requirements.

Detailed evaluations showed that increasing the molecular weight of PVA affects the hydrogel network parameters directly at a (macro)molecular scale, such as crosslink density and mesh size, contributing to further stabilisation of the obtained hydrogel. These molecular-level modifications significantly influence the overall characteristics of the hydrogel, most noticeably in their equilibrium swelling capacity and viscoelastic traits. Moreover, the molecular weight of PVA used for creating the hydrogel matrix enhances the physical properties of the L-130 films relative to the L-31 variants, also evidenced by the maintained integrity of L-130 samples during manipulation, in contrast to L-31 samples. Conversely, properties like specific surface area and total pore

volume in lyophilised forms are predominantly determined by the crosslinker concentration, irrespective of the PVA type, although the average pore size is affected by the latter.

The release rates of incorporated pharmaceuticals (rutin and caffeine) are seemingly unimpacted by either the crosslinker concentration or the molecular weight of examined PVA, possibly due to the minimal role of network density in thin-film configurations. Such behavior can be explained in the case of hydrogels, as they are generally characterised by low crosslinking density. The investigated pharmaceuticals are small molecules and, therefore, sensitive to the nearest molecular environment, whereas the long-distance structural parameters do not influence their diffusion. Importantly, all hydrogel formulations exhibited no cytotoxic effects in vitro, preserving cellular proliferation and morphology without promoting cellular adhesion, underscoring their potential in transdermal medication administration and wound care applications. Regarding the prospective fabrication of skin patches and facial masks for the transdermal administration of bioactive substances, the L-130 hydrogel was evaluated as the best choice among prepared materials. This variant, synthesised with a high-molecular-weight PVA matrix and a reduced crosslinker concentration, boasts superior porosity and moisture retention (indicating its drug incorporation capacity) alongside physical properties suitable for its application. It also demonstrates the most effective skin adherence among all tested samples, a necessary part of its performance in transdermal pharmaceutical applications.

In contrast, employing a higher molecular weight PVA with an increased crosslinker concentration results in hydrogels with high elasticity and a more compact network structure. Although these materials are unsuitable for wound dressing and facial masks due to poor skin adherence, their higher elasticity and strength could be used in other applications. Without exploring it in the presented dissertation, it could be suggested to continue in this research direction aiming at drug delivery systems requiring a sustained release over time, utilisation of these hydrogels as scaffolds mimicking mechanical properties of various tissues, or any other application requiring form-stable articles made from hydrogels.

*****

The second part of the dissertation delved into the properties of PVA hydrogels, examining how they are influenced by crosslinking with various dialdehyde polysaccharides (DAPs), such as dialdehydes obtained from cellulose, dextrin, dextran, and hyaluronate, with particular emphasis on the macromolecular and nanoscale structures of these DAPs. The research validated the initial hypothesis, indicating that the intrinsic structural variances

in the original polysaccharides converted into dialdehydes by polymer analogue reactions significantly affected the properties of the resultant hydrogels. Critical factors included: (i) the density of –CHO groups, which also correlated with the original homo/heteroglycan nature of the crosslinker, (ii) the configuration (branched versus linear) and molecular weight of the crosslinker, and (iii) the dimensions of nano-assemblies that the crosslinker forms spontaneously in solution.

The density of –CHO groups within the crosslinker had a predictable impact. This density essentially establishes the number of active crosslinking sites available on each macromolecule, influencing the final properties of the hydrogel. A sparser presence of –CHO groups was associated with increased swelling and porosity of the hydrogel but decreased elasticity.

However, a deeper study of the effects of the structural form and molecular weight of the crosslinker proved more complex behavior due to their intertwined nature. Notably, the effect of molecular weight alone could not fully explain the characteristics of the final hydrogels, especially when crosslinkers with diverse macromolecular architectures were employed. A clear example of this complexity is the comparison between DXI and DAC. Despite identical *Mn* values, the distinct structural arrangements of their macromolecules led to markedly different hydrogel properties. Hydrogels derived from linear DAPs (like DAC and DAH) showed less variability based on concentration or thermal processing than branched DAPs. Conversely, the impact of branching proved to be both beneficial and problematic, being advantageous in some instances (as with DXA) or counterproductive (as seen with DXI) at lower concentrations, depending on the dimensions of the resultant crosslinker nano-assemblies.

The dimensions of the crosslinker nano-assemblies, a parameter influenced by both the molar mass and structural organisation of the crosslinking molecules, had a notable correlation with the modes of crosslinker attachment and, thus, with the characteristics of the resulting hydrogels. While it remains unclear if these nano-structured domains maintain their integrity throughout hydrogel synthesis, the relationship between hydrogel properties and nano-assembly size suggests that these structures are somewhat, at least partially, preserved during crosslinking process. Generally, crosslinkers forming larger nano-assemblies maintained their effectiveness at sparse concentrations due to their capacity to link matrix chains even at considerable distances. In contrast, those constituting smaller assemblies were superior at denser concentrations, contributing to a compact, chemically crosslinked environment supplemented by the physical entanglements among matrix chains, albeit their efficiency deteriorated at diluted concentrations.

In evaluating individual crosslinkers, DAC stood out for its ability in creating effective hydrogels across a spectrum of concentrations, though the reduced porosity and slightly elevated cytotoxicity of DAC-crosslinked hydrogels might narrow its applicability in biological contexts. DXI emerged as the least favourable option owing to the pronounced reliance of DXI-based hydrogels on crosslinker quantity and the toxic nature of the extracts derived. Hydrogels utilising DAH exhibited relatively enhanced porosity, a more viscous nature, and minimised cytotoxicity, presenting them as viable candidates for medical purposes despite potential compromises in mechanical integrity or rheological properties at lesser concentrations. Remarkably, DXA excelled as a crosslinker at minimal concentrations, yielding hydrogels characterised by minimal swelling. This property, coupled with its low cytotoxicity, makes DXA a compelling substitute for DAH-oriented hydrogels in engineering biomaterials demanding superior physical hydrogel properties.

9.2 Ongoing and future research

It must be pointed out that besides results and answers published in the corresponding papers, the dissertation also opens further questions and calls to continue ongoing research. It would be highly interesting to study our materials in the following directions.

- Investigate the long-term stability and degradation of the hydrogel films to assess their practical applications and shelf life.
- Study in detail the release kinetics and sustained release properties of the drug-loaded patches to optimise drug delivery. More examples of active pharmaceutical ingredients belonging to various classes of molecules, ionic species, macromolecules etc. should be added to the research design.
- Conduct *in vivo* studies to evaluate the biocompatibility and cytotoxicity of the hydrogel films for their safe use.
- Investigate the potential applications of the hydrogel films beyond topical use, such as in tissue engineering or as drug delivery systems.
- Investigate the potential applications of the hydrogel films beyond biomedical use, such as in agriculture or as smart material systems.
- Explore other factors such as pH, temperature, or external stimuli.

And eventually look outside the studied material base for other solutions.

- Explore the use of alternative crosslinking agents or methods of crosslinking to further enhance the properties of the hydrogels.

9.3 Contribution to science and practice

The ongoing efforts in biomedical research continually work to meet the requirements of applications such as tissue engineering, drug delivery, and wound healing. In our group, recent studies have focused on exploring polymer-based hydrogels, especially poly(vinyl alcohol) (PVA) hydrogels crosslinked with dialdehyde polysaccharides (DAPs), to understand their practicality and constraints in various applications. The detailed investigations presented in this thesis provide experimental results and conclusions, suggesting that a combination of chosen synthetic and modified natural polymers may lead to enhanced healthcare materials.

The initial study offered a methodical approach, adjusting the crosslinker concentration, specifically 2,3-dialdehyde cellulose (DAC), and varying the molecular weight of PVA to fine-tune the properties of hydrogel films for potential topical applications. This research emphasised the relevance of both crosslinker concentration and the molecular weight of PVA, a detail sometimes overlooked in standard practices. The finding that optimisation of these factors could lead to hydrogels with preferable physical and viscoelastic properties indicated an important development. It pointed out, to deliver the most promising and specific example, the potential of L-130 hydrogel samples in applications like transdermal drug delivery and wound dressings, fulfilling specific healthcare requirements.

Expanding on these rather practically oriented insights, the following study examined the influence of different dialdehyde polysaccharides (DAPs) on PVA hydrogels' properties. This analysis went beyond mere material testing, going deeper into the molecular structural factors that determine the behaviour of hydrogels. The evaluation of cellulose, dextrin, dextran, and hyaluronate derivatives revealed that the unique structural aspects of these polysaccharides significantly affect the performance of hydrogels. This understanding offers a rational framework for eangineering hydrogel components beyond achieving favourable results under laboratory conditions. The research, especially in the second part, has an intention to grasp molecular behaviour of studied compounds to anticipate their application performance.

Among the derivatives, DAC and DXA emerged as particularly effective, showing promise as crosslinkers due to their performance and biocompatibility, essential for medical use. DAC shows potential for diverse biological applications, but its suitability is tempered by certain limitations in cytotoxicity. DAH exhibited promising porosity and minimised cytotoxicity. Nevertheless, it shows worse performance in mechanical and rheological properties at lesser concentrations. In contrast, issues with concentration dependence and cytotoxicity profile of DXI suggest it is less suitable for application in direct contact with the human body. The research highlighted how structural

differences in polysaccharides, once converted into dialdehyde derivatives, play a crucial role, suggesting a need for thoughtful hydrogel design.

*****

This research underlines the importance of understanding the molecular structural factors that influence the final properties of the hydrogels, contributing to advances in biomedical material base solutions. The insights gained here encourage a balanced approach to hydrogel research, considering both chemical composition and physical properties, and stress out the practical implications of specific hydrogel formulations. These contributions can potentially guide the development of future medical products and lead to further improvements in the field of hydrogel healthcare materials. Continuing such research could help in optimising healthcare resources, enhancing patient recovery processes, and improving overall health care outcomes.

REFERENCES

(1) *Handbook of Biopolymer-Based Materials: From Blends and Composites to Gels and Complex Networks*; Thomas, S., Durand, D., Chassenieux, C., Jyotishkumar, P., Eds.; Wiley-VCH Verlag GmbH & Co. KGaA: Weinheim, Germany, 2013.

(2) *Biopolymers and Nanocomposites for Biomedical and Pharmaceutical Applications*; Sharmin, E., Zafar, F., Eds.; Polymer science and technology; Nova Biomedical: Hauppauge, New York, 2017.

(3) Chen, R.; Hunt, J. A. Biomimetic Materials Processing for Tissue-Engineering Processes. *J. Mater. Chem.* **2007**, *17* (38), 3974. https://doi.org/10.1039/b706765h.

(4) Ma, P. X. Biomimetic Materials for Tissue Engineering. *Advanced Drug Delivery Reviews* **2008**, *60* (2), 184–198. https://doi.org/10.1016/j.addr.2007.08.041.

(5) Tibbitt, M. W.; Anseth, K. S. Hydrogels as Extracellular Matrix Mimics for 3D Cell Culture. *Biotechnol. Bioeng.* **2009**, *103* (4), 655–663. https://doi.org/10.1002/bit.22361.

(6) Speer, D. P.; Chvapil, M.; Eskelson, C. D.; Ulreich, J. Biological Effects of Residual Glutaraldehyde in Glutaraldehyde-Tanned Collagen Biomaterials. *J. Biomed. Mater. Res.* **1980**, *14* (6), 753–764. https://doi.org/10.1002/jbm.820140607.

(7) Kamoun, E. A.; Kenawy, E.-R. S.; Chen, X. A Review on Polymeric Hydrogel Membranes for Wound Dressing Applications: PVA-Based Hydrogel Dressings. *Journal of Advanced Research* **2017**, *8* (3), 217–233. https://doi.org/10.1016/j.jare.2017.01.005.

(8) Yan, G.; Zhang, X.; Li, M.; Zhao, X.; Zeng, X.; Sun, Y.; Tang, X.; Lei, T.; Lin, L. Stability of Soluble Dialdehyde Cellulose and the Formation of Hollow Microspheres: Optimization and Characterization. *ACS Sustainable Chem. Eng.* **2019**, *7* (2), 2151–2159. https://doi.org/10.1021/acssuschemeng.8b04825.

(9) Koprivica, S.; Siller, M.; Hosoya, T.; Roggenstein, W.; Rosenau, T.; Potthast, A. Regeneration of Aqueous Periodate Solutions by Ozone Treatment: A Sustainable Approach for Dialdehyde Cellulose Production. *ChemSusChem* **2016**, *9* (8), 825–833. https://doi.org/10.1002/cssc.201501639.

(10) Ding, W.; Wu, Y. Sustainable Dialdehyde Polysaccharides as Versatile Building Blocks for Fabricating Functional Materials: An Overview. *Carbohydrate Polymers* **2020**, *248*, 116801. https://doi.org/10.1016/j.carbpol.2020.116801.

(11) Dai, W. S.; Barbari, T. A. Hydrogel Membranes with Mesh Size Asymmetry Based on the Gradient Crosslinking of Poly(Vinyl Alcohol). *Journal of Membrane Science* **1999**, *156* (1), 67–79. https://doi.org/10.1016/S0376-7388(98)00330-5.

(12) Peppas, N. A.; Slaughter, B. V.; Kanzelberger, M. A. Hydrogels. In *Polymer Science: A Comprehensive Reference*; Elsevier, 2012; pp 385–395. https://doi.org/10.1016/B978-0-444-53349-4.00226-0.
(13) Sperling, L. H. *Introduction to Physical Polymer Science*, 4th ed.; Wiley: Hoboken, N.J, 2006.
(14) Rosiak, J. M.; Yoshii, F. Hydrogels and Their Medical Applications. *Nuclear Instruments and Methods in Physics Research Section B: Beam Interactions with Materials and Atoms* **1999**, *151* (1–4), 56–64. https://doi.org/10.1016/S0168-583X(99)00118-4.
(15) *Hydrogels: Biological Properties and Applications*; Barbucci, R., Ed.; Springer: Milan ; New York, 2009.
(16) *Gels Handbook*; Osada, Y., Kajiwara, K., Eds.; Academic Press: San Diego, 2001.
(17) Hennink, W. E.; van Nostrum, C. F. Novel Crosslinking Methods to Design Hydrogels. *Advanced Drug Delivery Reviews* **2002**, *54* (1), 13–36. https://doi.org/10.1016/S0169-409X(01)00240-X.
(18) H. Gulrez, S. K.; Al-Assaf, S.; O, G. Hydrogels: Methods of Preparation, Characterisation and Applications. In *Progress in Molecular and Environmental Bioengineering - From Analysis and Modeling to Technology Applications*; Carpi, A., Ed.; InTech, 2011. https://doi.org/10.5772/24553.
(19) Ahmad, N.; Pandey, M.; Mohamad, N.; Yi Chen, X.; Amin, M. C. I. M. Hydrogels for Pulmonary Drug Delivery. In *Targeting Chronic Inflammatory Lung Diseases Using Advanced Drug Delivery Systems*; Elsevier, 2020; pp 441–474. https://doi.org/10.1016/B978-0-12-820658-4.00021-2.
(20) Wichterle, O.; Lím, D. Hydrophilic Gels for Biological Use. *Nature* **1960**, *185* (4706), 117–118. https://doi.org/10.1038/185117a0.
(21) Ullah, F.; Othman, M. B. H.; Javed, F.; Ahmad, Z.; Akil, H. Md. Classification, Processing and Application of Hydrogels: A Review. *Materials Science and Engineering: C* **2015**, *57*, 414–433. https://doi.org/10.1016/j.msec.2015.07.053.
(22) Drury, J. L.; Mooney, D. J. Hydrogels for Tissue Engineering: Scaffold Design Variables and Applications. *Biomaterials* **2003**, *24* (24), 4337–4351. https://doi.org/10.1016/S0142-9612(03)00340-5.
(23) Benatti, A. C. B.; Pattaro, A. F.; Rodrigues, A. A.; Xavier, M. V.; Kaasi, A.; Barbosa, M. I. R.; Jardini, A. L.; Filho, R. M.; Kharmandayan, P. Bioreabsorbable Polymers for Tissue Engineering: PLA, PGA, and Their Copolymers. In *Materials for Biomedical Engineering*; Elsevier, 2019; pp 83–116. https://doi.org/10.1016/B978-0-12-816901-8.00004-3.
(24) Leach, J. B.; Schmidt, C. E. Characterization of Protein Release from Photocrosslinkable Hyaluronic Acid-Polyethylene Glycol Hydrogel Tissue Engineering Scaffolds. *Biomaterials* **2005**, *26* (2), 125–135. https://doi.org/10.1016/j.biomaterials.2004.02.018.

(25) Kumar, A.; Han, S. S. PVA-Based Hydrogels for Tissue Engineering: A Review. *International Journal of Polymeric Materials and Polymeric Biomaterials* **2017**, *66* (4), 159–182. https://doi.org/10.1080/00914037.2016.1190930.
(26) Jin, M.; Shi, J.; Zhu, W.; Yao, H.; Wang, D.-A. Polysaccharide-Based Biomaterials in Tissue Engineering: A Review. *Tissue Engineering Part B: Reviews* **2021**, *27* (6), 604–626. https://doi.org/10.1089/ten.teb.2020.0208.
(27) Liang, Y.; He, J.; Guo, B. Functional Hydrogels as Wound Dressing to Enhance Wound Healing. *ACS Nano* **2021**, *15* (8), 12687–12722. https://doi.org/10.1021/acsnano.1c04206.
(28) Hu, H.; Xu, F.-J. Rational Design and Latest Advances of Polysaccharide-Based Hydrogels for Wound Healing. *Biomater. Sci.* **2020**, *8* (8), 2084–2101. https://doi.org/10.1039/D0BM00055H.
(29) Li, S.; Dong, S.; Xu, W.; Tu, S.; Yan, L.; Zhao, C.; Ding, J.; Chen, X. Antibacterial Hydrogels. *Adv. Sci.* **2018**, *5* (5), 1700527. https://doi.org/10.1002/advs.201700527.
(30) Asadi, N.; Pazoki-Toroudi, H.; Del Bakhshayesh, A. R.; Akbarzadeh, A.; Davaran, S.; Annabi, N. Multifunctional Hydrogels for Wound Healing: Special Focus on Biomacromolecular Based Hydrogels. *International Journal of Biological Macromolecules* **2021**, *170*, 728–750. https://doi.org/10.1016/j.ijbiomac.2020.12.202.
(31) Guo, S.; Ren, Y.; Chang, R.; He, Y.; Zhang, D.; Guan, F.; Yao, M. Injectable Self-Healing Adhesive Chitosan Hydrogel with Antioxidative, Antibacterial, and Hemostatic Activities for Rapid Hemostasis and Skin Wound Healing. *ACS Appl. Mater. Interfaces* **2022**, *14* (30), 34455–34469. https://doi.org/10.1021/acsami.2c08870.
(32) Negm, N. A.; Hefni, H. H. H.; Abd-Elaal, A. A. A.; Badr, E. A.; Abou Kana, M. T. H. Advancement on Modification of Chitosan Biopolymer and Its Potential Applications. *International Journal of Biological Macromolecules* **2020**, *152*, 681–702. https://doi.org/10.1016/j.ijbiomac.2020.02.196.
(33) Madihally, S. V.; Matthew, H. W. T. Porous Chitosan Scaffolds for Tissue Engineering. *Biomaterials* **1999**, *20* (12), 1133–1142. https://doi.org/10.1016/S0142-9612(99)00011-3.
(34) Yang, X.; Wang, B.; Sha, D.; Liu, Y.; Liu, Z.; Shi, K.; Liu, W.; Yu, C.; Ji, X. PVA/Poly(Hexamethylene Guanidine)/Gallic Acid Composite Hydrogel Films and Their Antibacterial Performance. *ACS Appl. Polym. Mater.* **2021**, *3* (8), 3867–3877. https://doi.org/10.1021/acsapm.1c00447.
(35) Sun, P.; Jiao, J.; Wang, X.; Chen, L.; Chen, Z.; Zhang, K.; Qu, K.; Qin, X.; Yang, Z.; Zhong, J. L.; Wu, W. Nanomedicine Hybrid and Catechol Functionalized Chitosan as pH-Responsive Multi-Function Hydrogel to Efficiently Promote Infection Wound Healing. *International Journal of Biological Macromolecules* **2023**, *238*, 124106. https://doi.org/10.1016/j.ijbiomac.2023.124106.

(36) Liu, Y.; Wang, Q.; Liu, X.; Nakielski, P.; Pierini, F.; Li, X.; Yu, J.; Ding, B. Highly Adhesive, Stretchable and Breathable Gelatin Methacryloyl-Based Nanofibrous Hydrogels for Wound Dressings. *ACS Appl. Bio Mater.* **2022**, *5* (3), 1047–1056. https://doi.org/10.1021/acsabm.1c01087.
(37) Caló, E.; Khutoryanskiy, V. V. Biomedical Applications of Hydrogels: A Review of Patents and Commercial Products. *European Polymer Journal* **2015**, *65*, 252–267. https://doi.org/10.1016/j.eurpolymj.2014.11.024.
(38) Li, J.; Mooney, D. J. Designing Hydrogels for Controlled Drug Delivery. *Nat Rev Mater* **2016**, *1* (12), 16071. https://doi.org/10.1038/natrevmats.2016.71.
(39) Rivera-Hernández, G.; Antunes-Ricardo, M.; Martínez-Morales, P.; Sánchez, M. L. Polyvinyl Alcohol Based-Drug Delivery Systems for Cancer Treatment. *International Journal of Pharmaceutics* **2021**, *600*, 120478. https://doi.org/10.1016/j.ijpharm.2021.120478.
(40) Li, R.; Guan, X.; Lin, X.; Guan, P.; Zhang, X.; Rao, Z.; Du, L.; Zhao, J.; Rong, J.; Zhao, J. Poly(2-Hydroxyethyl Methacrylate)/β-Cyclodextrin-Hyaluronan Contact Lens with Tear Protein Adsorption Resistance and Sustained Drug Delivery for Ophthalmic Diseases. *Acta Biomaterialia* **2020**, *110*, 105–118. https://doi.org/10.1016/j.actbio.2020.04.002.
(41) Ray, P.; Maity, M.; Barik, H.; Sahoo, G. S.; Hasnain, M. S.; Hoda, M. N.; Nayak, A. K. Alginate-Based Hydrogels for Drug Delivery Applications. In *Alginates in Drug Delivery*; Elsevier, 2020; pp 41–70. https://doi.org/10.1016/B978-0-12-817640-5.00003-0.
(42) Xeroudaki, M.; Thangavelu, M.; Lennikov, A.; Ratnayake, A.; Bisevac, J.; Petrovski, G.; Fagerholm, P.; Rafat, M.; Lagali, N. A Porous Collagen-Based Hydrogel and Implantation Method for Corneal Stromal Regeneration and Sustained Local Drug Delivery. *Sci Rep* **2020**, *10* (1), 16936. https://doi.org/10.1038/s41598-020-73730-9.
(43) Tao, F.; Ma, S.; Tao, H.; Jin, L.; Luo, Y.; Zheng, J.; Xiang, W.; Deng, H. Chitosan-Based Drug Delivery Systems: From Synthesis Strategy to Osteomyelitis Treatment – A Review. *Carbohydrate Polymers* **2021**, *251*, 117063. https://doi.org/10.1016/j.carbpol.2020.117063.
(44) Cao, M.; Wang, Y.; Hu, X.; Gong, H.; Li, R.; Cox, H.; Zhang, J.; Waigh, T. A.; Xu, H.; Lu, J. R. Reversible Thermoresponsive Peptide–PNIPAM Hydrogels for Controlled Drug Delivery. *Biomacromolecules* **2019**, *20* (9), 3601–3610. https://doi.org/10.1021/acs.biomac.9b01009.
(45) Soltani, S.; Emadi, R.; Javanmard, S. H.; Kharaziha, M.; Rahmati, A. Shear-Thinning and Self-Healing Nanohybrid Alginate-Graphene Oxide Hydrogel Based on Guest-Host Assembly. *International Journal of Biological Macromolecules* **2021**, *180*, 311–323. https://doi.org/10.1016/j.ijbiomac.2021.03.086.
(46) Smith, M. H.; Lyon, L. A. Multifunctional Nanogels for siRNA Delivery. *Acc. Chem. Res.* **2012**, *45* (7), 985–993. https://doi.org/10.1021/ar200216f.

(47) Li, J.; Hu, Y.; Vlassak, J. J.; Suo, Z. Experimental Determination of Equations of State for Ideal Elastomeric Gels. *Soft Matter* **2012**, *8* (31), 8121. https://doi.org/10.1039/c2sm25437a.
(48) Drury, J. L.; Dennis, R. G.; Mooney, D. J. The Tensile Properties of Alginate Hydrogels. *Biomaterials* **2004**, *25* (16), 3187–3199. https://doi.org/10.1016/j.biomaterials.2003.10.002.
(49) Rehmann, M. S.; Skeens, K. M.; Kharkar, P. M.; Ford, E. M.; Maverakis, E.; Lee, K. H.; Kloxin, A. M. Tuning and Predicting Mesh Size and Protein Release from Step Growth Hydrogels. *Biomacromolecules* **2017**, *18* (10), 3131–3142. https://doi.org/10.1021/acs.biomac.7b00781.
(50) Flory, P. J.; Rehner, J. Statistical Mechanics of Cross-Linked Polymer Networks II. Swelling. *The Journal of Chemical Physics* **1943**, *11* (11), 521–526. https://doi.org/10.1063/1.1723792.
(51) Waters, D. J.; Engberg, K.; Parke-Houben, R.; Hartmann, L.; Ta, C. N.; Toney, M. F.; Frank, C. W. Morphology of Photopolymerized End-Linked Poly(Ethylene Glycol) Hydrogels by Small-Angle X-Ray Scattering. *Macromolecules* **2010**, *43* (16), 6861–6870. https://doi.org/10.1021/ma101070s.
(52) Krogstad, D. V.; Choi, S.-H.; Lynd, N. A.; Audus, D. J.; Perry, S. L.; Gopez, J. D.; Hawker, C. J.; Kramer, E. J.; Tirrell, M. V. Small Angle Neutron Scattering Study of Complex Coacervate Micelles and Hydrogels Formed from Ionic Diblock and Triblock Copolymers. *J. Phys. Chem. B* **2014**, *118* (45), 13011–13018. https://doi.org/10.1021/jp509175a.
(53) Ritger, P. L.; Peppas, N. A. A Simple Equation for Description of Solute Release I. Fickian and Non-Fickian Release from Non-Swellable Devices in the Form of Slabs, Spheres, Cylinders or Discs. *Journal of Controlled Release* **1987**, *5* (1), 23–36. https://doi.org/10.1016/0168-3659(87)90034-4.
(54) Ritger, P. L.; Peppas, N. A. A Simple Equation for Description of Solute Release II. Fickian and Anomalous Release from Swellable Devices. *Journal of Controlled Release* **1987**, *5* (1), 37–42. https://doi.org/10.1016/0168-3659(87)90035-6.
(55) Lin, C.-C.; Metters, A. T. Hydrogels in Controlled Release Formulations: Network Design and Mathematical Modeling. *Advanced Drug Delivery Reviews* **2006**, *58* (12–13), 1379–1408. https://doi.org/10.1016/j.addr.2006.09.004.
(56) Ramadon, D.; McCrudden, M. T. C.; Courtenay, A. J.; Donnelly, R. F. Enhancement Strategies for Transdermal Drug Delivery Systems: Current Trends and Applications. *Drug Deliv. and Transl. Res.* **2022**, *12* (4), 758–791. https://doi.org/10.1007/s13346-021-00909-6.
(57) Pereira, R.; Silva, S. G.; Pinheiro, M.; Reis, S.; Vale, M. L. D. Current Status of Amino Acid-Based Permeation Enhancers in Transdermal Drug Delivery. *Membranes* **2021**, *11* (5), 343. https://doi.org/10.3390/membranes11050343.

(58) Yousef, H.; Alhajj, M.; Sharma, S. Anatomy, Skin (Integument), Epidermis. In *StatPearls*; StatPearls Publishing: Treasure Island (FL), 2023.
(59) Lai-Cheong, J. E.; McGrath, J. A. Structure and Function of Skin, Hair and Nails. *Medicine* **2009**, *37* (5), 223–226. https://doi.org/10.1016/j.mpmed.2009.03.002.
(60) Rippke, F.; Schreiner, V.; Schwanitz, H.-J. The Acidic Milieu of the Horny Layer: New Findings on the Physiology and Pathophysiology of Skin pH. *American Journal of Clinical Dermatology* **2002**, *3* (4), 261–272. https://doi.org/10.2165/00128071-200203040-00004.
(61) Schneider, M.; Stracke, F.; Hansen, S.; Schaefer, U. F. Nanoparticles and Their Interactions with the Dermal Barrier. *Dermato-Endocrinology* **2009**, *1* (4), 197–206. https://doi.org/10.4161/derm.1.4.9501.
(62) Ruela, A. L. M.; Perissinato, A. G.; Lino, M. E. D. S.; Mudrik, P. S.; Pereira, G. R. Evaluation of Skin Absorption of Drugs from Topical and Transdermal Formulations. *Braz. J. Pharm. Sci.* **2016**, *52* (3), 527–544. https://doi.org/10.1590/s1984-82502016000300018.
(63) Bartosova, L.; Bajgar, J. Transdermal Drug Delivery In Vitro Using Diffusion Cells. *CMC* **2012**, *19* (27), 4671–4677. https://doi.org/10.2174/092986712803306358.
(64) Farage, M. A.; Miller, K. W.; Elsner, P.; Maibach, H. I. Characteristics of the Aging Skin. *Advances in Wound Care* **2013**, *2* (1), 5–10. https://doi.org/10.1089/wound.2011.0356.
(65) Ammala, A. Biodegradable Polymers as Encapsulation Materials for Cosmetics and Personal Care Markets. *Int J Cosmet Sci* **2013**, *35* (2), 113–124. https://doi.org/10.1111/ics.12017.
(66) Williams, A. C.; Barry, B. W. Penetration Enhancers. *Advanced Drug Delivery Reviews* **2004**, *56* (5), 603–618. https://doi.org/10.1016/j.addr.2003.10.025.
(67) Finnin, B. C.; Morgan, T. M. Transdermal Penetration Enhancers: Applications, Limitations, and Potential. *Journal of Pharmaceutical Sciences* **1999**, *88* (10), 955–958. https://doi.org/10.1021/js990154g.
(68) Schilrreff, P.; Alexiev, U. Chronic Inflammation in Non-Healing Skin Wounds and Promising Natural Bioactive Compounds Treatment. *IJMS* **2022**, *23* (9), 4928. https://doi.org/10.3390/ijms23094928.
(69) Nagula, R. L.; Wairkar, S. Recent Advances in Topical Delivery of Flavonoids: A Review. *Journal of Controlled Release* **2019**, *296*, 190–201. https://doi.org/10.1016/j.jconrel.2019.01.029.
(70) Li, Y.; Yao, J.; Han, C.; Yang, J.; Chaudhry, M.; Wang, S.; Liu, H.; Yin, Y. Quercetin, Inflammation and Immunity. *Nutrients* **2016**, *8* (3), 167. https://doi.org/10.3390/nu8030167.
(71) Anand David, A.; Arulmoli, R.; Parasuraman, S. Overviews of Biological Importance of Quercetin: A Bioactive Flavonoid. *Phcog Rev* **2016**, *10* (20), 84. https://doi.org/10.4103/0973-7847.194044.

(72) Ganeshpurkar, A.; Saluja, A. K. The Pharmacological Potential of Rutin. *Saudi Pharmaceutical Journal* **2017**, *25* (2), 149–164. https://doi.org/10.1016/j.jsps.2016.04.025.
(73) Kianersi, F.; Abdollahi, M. R.; Mirzaie-asl, A.; Dastan, D.; Rasheed, F. Identification and Tissue-Specific Expression of Rutin Biosynthetic Pathway Genes in Capparis Spinosa Elicited with Salicylic Acid and Methyl Jasmonate. *Sci Rep* **2020**, *10* (1), 8884. https://doi.org/10.1038/s41598-020-65815-2.
(74) Tran, N. Q.; Joung, Y. K.; Lih, E.; Park, K. D. In Situ Forming and Rutin-Releasing Chitosan Hydrogels As Injectable Dressings for Dermal Wound Healing. *Biomacromolecules* **2011**, *12* (8), 2872–2880. https://doi.org/10.1021/bm200326g.
(75) Mauludin, R.; Müller, R. H. Preparation and Storage Stability of Rutin Nanosuspensions. *Journal of Pharmaceutical Investigation* **2013**, *43* (5), 395–404. https://doi.org/10.1007/s40005-013-0084-1.
(76) Sintov, A. C. Transdermal Delivery of Curcumin via Microemulsion. *International Journal of Pharmaceutics* **2015**, *481* (1–2), 97–103. https://doi.org/10.1016/j.ijpharm.2015.02.005.
(77) Anand, P.; Thomas, S. G.; Kunnumakkara, A. B.; Sundaram, C.; Harikumar, K. B.; Sung, B.; Tharakan, S. T.; Misra, K.; Priyadarsini, I. K.; Rajasekharan, K. N.; Aggarwal, B. B. Biological Activities of Curcumin and Its Analogues (Congeners) Made by Man and Mother Nature. *Biochemical Pharmacology* **2008**, *76* (11), 1590–1611. https://doi.org/10.1016/j.bcp.2008.08.008.
(78) Patra, S.; Roy, E.; Madhuri, R.; Sharma, P. K. Retracted Article: The next Generation Cell-Penetrating Peptide and Carbon Dot Conjugated Nano-Liposome for Transdermal Delivery of Curcumin. *Biomater. Sci.* **2016**, *4* (3), 418–429. https://doi.org/10.1039/C5BM00433K.
(79) Jain, H.; Geetanjali, D.; Dalvi, H.; Bhat, A.; Godugu, C.; Srivastava, S. Liposome Mediated Topical Delivery of Ibrutinib and Curcumin as a Synergistic Approach to Combat Imiquimod Induced Psoriasis. *Journal of Drug Delivery Science and Technology* **2022**, *68*, 103103. https://doi.org/10.1016/j.jddst.2022.103103.
(80) Nair, R. S.; Morris, A.; Billa, N.; Leong, C.-O. An Evaluation of Curcumin-Encapsulated Chitosan Nanoparticles for Transdermal Delivery. *AAPS PharmSciTech* **2019**, *20* (2), 69. https://doi.org/10.1208/s12249-018-1279-6.
(81) Prabhu, A.; Jose, J.; Kumar, L.; Salwa, S.; Vijay Kumar, M.; Nabavi, S. M. Transdermal Delivery of Curcumin-Loaded Solid Lipid Nanoparticles as Microneedle Patch: An In Vitro and In Vivo Study. *AAPS PharmSciTech* **2022**, *23* (1), 49. https://doi.org/10.1208/s12249-021-02186-5.
(82) Scomoroscenco, C.; Teodorescu, M.; Raducan, A.; Stan, M.; Voicu, S. N.; Trica, B.; Ninciuleanu, C. M.; Nistor, C. L.; Mihaescu, C. I.; Petcu, C.; Cinteza, L. O. Novel Gel Microemulsion as Topical Drug Delivery System

for Curcumin in Dermatocosmetics. *Pharmaceutics* **2021**, *13* (4), 505. https://doi.org/10.3390/pharmaceutics13040505.
(83) Zhai, K.; Brockmüller, A.; Kubatka, P.; Shakibaei, M.; Büsselberg, D. Curcumin's Beneficial Effects on Neuroblastoma: Mechanisms, Challenges, and Potential Solutions. *Biomolecules* **2020**, *10* (11), 1469. https://doi.org/10.3390/biom10111469.
(84) Marchese, A.; Orhan, I. E.; Daglia, M.; Barbieri, R.; Di Lorenzo, A.; Nabavi, S. F.; Gortzi, O.; Izadi, M.; Nabavi, S. M. Antibacterial and Antifungal Activities of Thymol: A Brief Review of the Literature. *Food Chemistry* **2016**, *210*, 402–414. https://doi.org/10.1016/j.foodchem.2016.04.111.
(85) Kaulmann, A.; Bohn, T. Carotenoids, Inflammation, and Oxidative Stress—Implications of Cellular Signaling Pathways and Relation to Chronic Disease Prevention. *Nutrition Research* **2014**, *34* (11), 907–929. https://doi.org/10.1016/j.nutres.2014.07.010.
(86) Luo, L.; Lane, M. E. Topical and Transdermal Delivery of Caffeine. *International Journal of Pharmaceutics* **2015**, *490* (1–2), 155–164. https://doi.org/10.1016/j.ijpharm.2015.05.050.
(87) Shakeel, F.; Ramadan, W. Transdermal Delivery of Anticancer Drug Caffeine from Water-in-Oil Nanoemulsions. *Colloids and Surfaces B: Biointerfaces* **2010**, *75* (1), 356–362. https://doi.org/10.1016/j.colsurfb.2009.09.010.
(88) Puglia, C.; Offerta, A.; Tirendi, G. G.; Tarico, M. S.; Curreri, S.; Bonina, F.; Perrotta, R. E. Design of Solid Lipid Nanoparticles for Caffeine Topical Administration. *Drug Delivery* **2016**, *23* (1), 36–40. https://doi.org/10.3109/10717544.2014.903011.
(89) Ravetti; Clemente; Brignone; Hergert; Allemandi; Palma. Ascorbic Acid in Skin Health. *Cosmetics* **2019**, *6* (4), 58. https://doi.org/10.3390/cosmetics6040058.
(90) Gref, R.; Deloménie, C.; Maksimenko, A.; Gouadon, E.; Percoco, G.; Lati, E.; Desmaële, D.; Zouhiri, F.; Couvreur, P. Vitamin C–Squalene Bioconjugate Promotes Epidermal Thickening and Collagen Production in Human Skin. *Sci Rep* **2020**, *10* (1), 16883. https://doi.org/10.1038/s41598-020-72704-1.
(91) Ramöller, I. K.; Tekko, I. A.; McCarthy, H. O.; Donnelly, R. F. Rapidly Dissolving Bilayer Microneedle Arrays – A Minimally Invasive Transdermal Drug Delivery System for Vitamin B12. *International Journal of Pharmaceutics* **2019**, *566*, 299–306. https://doi.org/10.1016/j.ijpharm.2019.05.066.
(92) Green, R.; Allen, L. H.; Bjørke-Monsen, A.-L.; Brito, A.; Guéant, J.-L.; Miller, J. W.; Molloy, A. M.; Nexo, E.; Stabler, S.; Toh, B.-H.; Ueland, P. M.; Yajnik, C. Vitamin B12 Deficiency. *Nat Rev Dis Primers* **2017**, *3* (1), 17040. https://doi.org/10.1038/nrdp.2017.40.

(93) *Cosmeceuticals and Cosmetic Practice*; Farris, P. K., Ed.; John Wiley & Sons Ltd: Chichester, West Sussex, UK, 2014.
(94) Kristiansen, K. A.; Potthast, A.; Christensen, B. E. Periodate Oxidation of Polysaccharides for Modification of Chemical and Physical Properties. *Carbohydrate Research* **2010**, *345* (10), 1264–1271. https://doi.org/10.1016/j.carres.2010.02.011.
(95) Kim, U.-J.; Kuga, S.; Wada, M.; Okano, T.; Kondo, T. Periodate Oxidation of Crystalline Cellulose. *Biomacromolecules* **2000**, *1* (3), 488–492. https://doi.org/10.1021/bm0000337.
(96) Muchová, M.; Münster, L.; Vávrová, A.; Capáková, Z.; Kuřitka, I.; Vícha, J. Comparison of Dialdehyde Polysaccharides as Crosslinkers for Hydrogels: The Case of Poly(Vinyl Alcohol). *Carbohydrate Polymers* **2022**, *279*, 119022. https://doi.org/10.1016/j.carbpol.2021.119022.
(97) Sarwat, F.; Qader, S. A. U.; Aman, A.; Ahmed, N. Production & Characterization of a Unique Dextran from an Indigenous *Leuconostoc Mesenteroides* CMG713. *Int. J. Biol. Sci.* **2008**, 379–386. https://doi.org/10.7150/ijbs.4.379.
(98) Maia, J.; Carvalho, R. A.; Coelho, J. F. J.; Simões, P. N.; Gil, M. H. Insight on the Periodate Oxidation of Dextran and Its Structural Vicissitudes. *Polymer* **2011**, *52* (2), 258–265. https://doi.org/10.1016/j.polymer.2010.11.058.
(99) Münster, L.; Fojtů, M.; Capáková, Z.; Muchová, M.; Musilová, L.; Vaculovič, T.; Balvan, J.; Kuřitka, I.; Masařík, M.; Vícha, J. Oxidized Polysaccharides for Anticancer-Drug Delivery: What Is the Role of Structure? *Carbohydrate Polymers* **2021**, *257*, 117562. https://doi.org/10.1016/j.carbpol.2020.117562.
(100) Fraser, J. R. E.; Laurent, T. C.; Laurent, U. B. G. Hyaluronan: Its Nature, Distribution, Functions and Turnover. *Journal of Internal Medicine* **1997**, *242* (1), 27–33. https://doi.org/10.1046/j.1365-2796.1997.00170.x.
(101) Fallacara, A.; Baldini, E.; Manfredini, S.; Vertuani, S. Hyaluronic Acid in the Third Millennium. *Polymers* **2018**, *10* (7), 701. https://doi.org/10.3390/polym10070701.
(102) Boeden, H.-F.; Pommerening, K.; Becker, M.; Rupprich, C.; Holtzhauer, M.; Loth, F.; Müller, R.; Bertram, D. Bead Cellulose Derivatives as Supports for Immobilization and Chromatographic Purification of Proteins. *Journal of Chromatography A* **1991**, *552*, 389–414. https://doi.org/10.1016/S0021-9673(01)95956-4.
(103) Maekawa, E.; Koshijima, T. Properties of 2,3-Dicarboxy Cellulose Combined with Various Metallic Ions. *J. Appl. Polym. Sci.* **1984**, *29* (7), 2289–2297. https://doi.org/10.1002/app.1984.070290705.
(104) Gurvich, A. E.; Lechtzind, E. V. High Capacity Immunoadsorbents Based on Preparations of Reprecipitated Cellulose. *Molecular Immunology* **1982**, *19* (4), 637–640. https://doi.org/10.1016/0161-5890(82)90233-4.

(105) Wolf, B.; Finke, I. [The use of bead cellulose for controlled drug liberation. 5. Binding of benzocaine as a model drug to dialdehyde-bead cellulose and its in vitro liberation]. *Pharmazie* **1992**, *47* (2), 121–125.
(106) Li, J.; Wan, Y.; Li, L.; Liang, H.; Wang, J. Preparation and Characterization of 2,3-Dialdehyde Bacterial Cellulose for Potential Biodegradable Tissue Engineering Scaffolds. *Materials Science and Engineering: C* **2009**, *29* (5), 1635–1642. https://doi.org/10.1016/j.msec.2009.01.006.
(107) Patterson, J.; Siew, R.; Herring, S. W.; Lin, A. S. P.; Guldberg, R.; Stayton, P. S. Hyaluronic Acid Hydrogels with Controlled Degradation Properties for Oriented Bone Regeneration. *Biomaterials* **2010**, *31* (26), 6772–6781. https://doi.org/10.1016/j.biomaterials.2010.05.047.
(108) Li, S.; Pei, M.; Wan, T.; Yang, H.; Gu, S.; Tao, Y.; Liu, X.; Zhou, Y.; Xu, W.; Xiao, P. Self-Healing Hyaluronic Acid Hydrogels Based on Dynamic Schiff Base Linkages as Biomaterials. *Carbohydrate Polymers* **2020**, *250*, 116922. https://doi.org/10.1016/j.carbpol.2020.116922.
(109) Fu, Y.; Zhang, J.; Wang, Y.; Li, J.; Bao, J.; Xu, X.; Zhang, C.; Li, Y.; Wu, H.; Gu, Z. Reduced Polydopamine Nanoparticles Incorporated Oxidized Dextran/Chitosan Hybrid Hydrogels with Enhanced Antioxidative and Antibacterial Properties for Accelerated Wound Healing. *Carbohydrate Polymers* **2021**, *257*, 117598. https://doi.org/10.1016/j.carbpol.2020.117598.
(110) Babjaková, E.; Branná, P.; Kuczyńska, M.; Rouchal, M.; Prucková, Z.; Dastychová, L.; Vícha, J.; Vícha, R. An Adamantane-Based Disubstituted Binding Motif with Picomolar Dissociation Constants for Cucurbit[n]Urils in Water and Related Quaternary Assemblies. *RSC Adv.* **2016**, *6* (107), 105146–105153. https://doi.org/10.1039/C6RA23524G.
(111) Concheiro, A.; Alvarez-Lorenzo, C. Chemically Cross-Linked and Grafted Cyclodextrin Hydrogels: From Nanostructures to Drug-Eluting Medical Devices. *Advanced Drug Delivery Reviews* **2013**, *65* (9), 1188–1203. https://doi.org/10.1016/j.addr.2013.04.015.
(112) Kim, U.-J.; Lee, Y. R.; Kang, T. H.; Choi, J. W.; Kimura, S.; Wada, M. Protein Adsorption of Dialdehyde Cellulose-Crosslinked Chitosan with High Amino Group Contents. *Carbohydrate Polymers* **2017**, *163*, 34–42. https://doi.org/10.1016/j.carbpol.2017.01.052.
(113) Vatanpour, V.; Teber, O. O.; Mehrabi, M.; Koyuncu, I. Polyvinyl Alcohol-Based Separation Membranes: A Comprehensive Review on Fabrication Techniques, Applications and Future Prospective. *Materials Today Chemistry* **2023**, *28*, 101381. https://doi.org/10.1016/j.mtchem.2023.101381.
(114) Kamoun, E. A.; Chen, X.; Mohy Eldin, M. S.; Kenawy, E.-R. S. Crosslinked Poly(Vinyl Alcohol) Hydrogels for Wound Dressing Applications: A Review of Remarkably Blended Polymers. *Arabian Journal of Chemistry* **2015**, *8* (1), 1–14. https://doi.org/10.1016/j.arabjc.2014.07.005.
(115) Asy-Syifa, N.; Kusjuriansah; Waresindo, W. X.; Edikresnha, D.; Suciati, T.; Khairurrijal, K. The Study of the Swelling Degree of the PVA Hydrogel

with Varying Concentrations of PVA. *J. Phys.: Conf. Ser.* **2022**, *2243* (1), 012053. https://doi.org/10.1088/1742-6596/2243/1/012053.
(116) Chen, Y.; Li, J.; Lu, J.; Ding, M.; Chen, Y. Synthesis and Properties of Poly(Vinyl Alcohol) Hydrogels with High Strength and Toughness. *Polymer Testing* **2022**, *108*, 107516. https://doi.org/10.1016/j.polymertesting.2022.107516.
(117) Rodríguez-Rodríguez, R.; Espinosa-Andrews, H.; Velasquillo-Martínez, C.; García-Carvajal, Z. Y. Composite Hydrogels Based on Gelatin, Chitosan and Polyvinyl Alcohol to Biomedical Applications: A Review. *International Journal of Polymeric Materials and Polymeric Biomaterials* **2020**, *69* (1), 1–20. https://doi.org/10.1080/00914037.2019.1581780.
(118) Wang, M.; Bai, J.; Shao, K.; Tang, W.; Zhao, X.; Lin, D.; Huang, S.; Chen, C.; Ding, Z.; Ye, J. Poly(Vinyl Alcohol) Hydrogels: The Old and New Functional Materials. *International Journal of Polymer Science* **2021**, *2021*, 1–16. https://doi.org/10.1155/2021/2225426.
(119) Münster, L.; Vícha, J.; Klofáč, J.; Masař, M.; Hurajová, A.; Kuřitka, I. Dialdehyde Cellulose Crosslinked Poly(Vinyl Alcohol) Hydrogels: Influence of Catalyst and Crosslinker Shelf Life. *Carbohydrate Polymers* **2018**, *198*, 181–190. https://doi.org/10.1016/j.carbpol.2018.06.035.
(120) Bolto, B.; Tran, T.; Hoang, M.; Xie, Z. Crosslinked Poly(Vinyl Alcohol) Membranes. *Progress in Polymer Science* **2009**, *34* (9), 969–981. https://doi.org/10.1016/j.progpolymsci.2009.05.003.
(121) Miyazaki, T.; Takeda, Y.; Akane, S.; Itou, T.; Hoshiko, A.; En, K. Role of Boric Acid for a Poly (Vinyl Alcohol) Film as a Cross-Linking Agent: Melting Behaviors of the Films with Boric Acid. *Polymer* **2010**, *51* (23), 5539–5549. https://doi.org/10.1016/j.polymer.2010.09.048.
(122) Baker, M. I.; Walsh, S. P.; Schwartz, Z.; Boyan, B. D. A Review of Polyvinyl Alcohol and Its Uses in Cartilage and Orthopedic Applications. *J. Biomed. Mater. Res.* **2012**, *100B* (5), 1451–1457. https://doi.org/10.1002/jbm.b.32694.
(123) Mitura, S.; Sionkowska, A.; Jaiswal, A. Biopolymers for Hydrogels in Cosmetics: Review. *J Mater Sci: Mater Med* **2020**, *31* (6), 50. https://doi.org/10.1007/s10856-020-06390-w.
(124) Putro, P. A.; Sulaeman, A. S.; Maddu, A. Polyvinyl Alcohol-Based Hydrogel: A Systematic Literature Review on Thermal Properties by Differential Scanning Calorimetry. *J. Phys.: Conf. Ser.* **2021**, *2019* (1), 012101. https://doi.org/10.1088/1742-6596/2019/1/012101.
(125) Chu, L.; Liu, C.; Zhou, G.; Xu, R.; Tang, Y.; Zeng, Z.; Luo, S. A Double Network Gel as Low Cost and Easy Recycle Adsorbent: Highly Efficient Removal of Cd(II) and Pb(II) Pollutants from Wastewater. *Journal of Hazardous Materials* **2015**, *300*, 153–160. https://doi.org/10.1016/j.jhazmat.2015.06.070.

(126) Guo, Y.; Lu, H.; Zhao, F.; Zhou, X.; Shi, W.; Yu, G. Biomass-Derived Hybrid Hydrogel Evaporators for Cost-Effective Solar Water Purification. *Adv. Mater.* **2020**, *32* (11), 1907061. https://doi.org/10.1002/adma.201907061.
(127) Zhao, F.; Zhou, X.; Shi, Y.; Qian, X.; Alexander, M.; Zhao, X.; Mendez, S.; Yang, R.; Qu, L.; Yu, G. Highly Efficient Solar Vapour Generation via Hierarchically Nanostructured Gels. *Nature Nanotech* **2018**, *13* (6), 489–495. https://doi.org/10.1038/s41565-018-0097-z.
(128) Cavalieri, F.; Chiessi, E.; Villa, R.; Viganò, L.; Zaffaroni, N.; Telling, M. F.; Paradossi, G. Novel PVA-Based Hydrogel Microparticles for Doxorubicin Delivery. *Biomacromolecules* **2008**, *9* (7), 1967–1973. https://doi.org/10.1021/bm800225v.
(129) Ruiz, J.; Mantecón, A.; Cádiz, V. Investigation of Loading and Release in PVA-Based Hydrogels: Loading and Release in PVA-Based Hydrogels. *J. Appl. Polym. Sci.* **2002**, *85* (8), 1644–1651. https://doi.org/10.1002/app.10696.
(130) Chen, Y.; Song, J.; Wang, S.; Liu, W. PVA-Based Hydrogels: Promising Candidates for Articular Cartilage Repair. *Macromol. Biosci.* **2021**, *21* (10), 2100147. https://doi.org/10.1002/mabi.202100147.
(131) Husain, M. S. B.; Gupta, A.; Alashwal, B. Y.; Sharma, S. Synthesis of PVA/PVP Based Hydrogel for Biomedical Applications: A Review. *Energy Sources, Part A: Recovery, Utilization, and Environmental Effects* **2018**, *40* (20), 2388–2393. https://doi.org/10.1080/15567036.2018.1495786.
(132) Kamoun, E. A.; Loutfy, S. A.; Hussein, Y.; Kenawy, E.-R. S. Recent Advances in PVA-Polysaccharide Based Hydrogels and Electrospun Nanofibers in Biomedical Applications: A Review. *International Journal of Biological Macromolecules* **2021**, *187*, 755–768. https://doi.org/10.1016/j.ijbiomac.2021.08.002.
(133) Muchová, M.; Münster, L.; Capáková, Z.; Mikulcová, V.; Kuřitka, I.; Vícha, J. Design of Dialdehyde Cellulose Crosslinked Poly(Vinyl Alcohol) Hydrogels for Transdermal Drug Delivery and Wound Dressings. *Materials Science and Engineering: C* **2020**, *116*, 111242. https://doi.org/10.1016/j.msec.2020.111242.
(134) Münster, L.; Capáková, Z.; Fišera, M.; Kuřitka, I.; Vícha, J. Biocompatible Dialdehyde Cellulose/Poly(Vinyl Alcohol) Hydrogels with Tunable Properties. *Carbohydrate Polymers* **2019**, *218*, 333–342. https://doi.org/10.1016/j.carbpol.2019.04.091.
(135) Münster, L.; Vícha, J.; Klofáč, J.; Masař, M.; Kucharczyk, P.; Kuřitka, I. Stability and Aging of Solubilized Dialdehyde Cellulose. *Cellulose* **2017**, *24* (7), 2753–2766. https://doi.org/10.1007/s10570-017-1314-x.
(136) Veelaert, S.; de Wit, D.; Gotlieb, K. F.; Verhé, R. Chemical and Physical Transitions of Periodate Oxidized Potato Starch in Water. *Carbohydrate*

Polymers **1997**, *33* (2–3), 153–162. https://doi.org/10.1016/S0144-8617(97)00046-5.

(137) Trauer, S.; Patzelt, A.; Otberg, N.; Knorr, F.; Rozycki, C.; Balizs, G.; Büttemeyer, R.; Linscheid, M.; Liebsch, M.; Lademann, J. Permeation of Topically Applied Caffeine through Human Skin - a Comparison of *in Vivo* and *in Vitro* Data. *British Journal of Clinical Pharmacology* **2009**, *68* (2), 181–186. https://doi.org/10.1111/j.1365-2125.2009.03463.x.

(138) Bonina, F.; Bader, S.; Montenegro, L.; Scrofani, C.; Visca, M. Three Phase Emulsions for Controlled Delivery in the Cosmetic Field. *Int J Cosmet Sci* **1992**, *14* (2), 65–74. https://doi.org/10.1111/j.1467-2494.1992.tb00040.x.

(139) Santander-Ortega, M. J.; Stauner, T.; Loretz, B.; Ortega-Vinuesa, J. L.; Bastos-González, D.; Wenz, G.; Schaefer, U. F.; Lehr, C. M. Nanoparticles Made from Novel Starch Derivatives for Transdermal Drug Delivery. *Journal of Controlled Release* **2010**, *141* (1), 85–92. https://doi.org/10.1016/j.jconrel.2009.08.012.

(140) Pilloni, M.; Ennas, G.; Casu, M.; Fadda, A. M.; Frongia, F.; Marongiu, F.; Sanna, R.; Scano, A.; Valenti, D.; Sinico, C. Drug Silica Nanocomposite: Preparation, Characterization and Skin Permeation Studies. *Pharmaceutical Development and Technology* **2013**, *18* (3), 626–633. https://doi.org/10.3109/10837450.2011.653821.

LIST OF FIGURES

LIST OF TABLES

LIST OF ABBREVIATIONS AND SYMBOLS

ABBREVIATIONS

Alphabetically ordered

DXA	2,3 dialdehyde dextran
DAC	2,3-dialdehyde cellulose
3D	Three-dimensional
AGU	Anhydroglucose unit
ATR	attenuated total reflectance
BET	Brunauer-Emmet Teller
C1-C6	Numbered carbon atoms of D-anhydroglucopyranose unit
DAH	2,3-dialdehyde hyaluronate
DAPs	dialdehyde polysaccharides
DC	Dicarboxylated (appears in conjuction with other acronyms)
DH	degrees of hydrolysis
d_h	The hydrodynamic radii
DLS	dynamic light scattering
DO	degree of oxidation
DP	degrees of polymerization
DXI	2,3-dialdehyde dextrin
EWC	Equilibrium water content
FT-IR	Fourier-transform infrared spectroscopy
G	Shear modulus
GA	glutaraldehyde
GPC	Gel Permeation Chromatography
HA	Hyaluronic acid
HCl	Hydrochloric acid

HPLC	High-performance liquid chromatography
M_c	The average molecular weight between crosslinks
M_n	Number average molecular weight
M_w	molecular weight
$NaIO_4$	Sodium periodate
$n_{\text{-CHO}}$	Chemical amnout of crosslinkers reactive aldehyde groups
PDI	polydispersity index
pH	potential of hydrogen, le potentiel hydrogène
PNIPAm	Poly(N isopropylacrylamide)
PVA	poly(vinyl alcohol)
PVA/DAC	Poly(vinyl alcohol) hydrogel crosslinked by dialdehyde cellulose
PVA_c	Polyvinyl acetate
R	Gas constant
SC	*Stratum corneum*
SEM	scanning electron microscopy
T	Temperature
UV-VIS	ultraviolet
$V_{2,s}$	Polymer volume fraction
ζ	zeta potentials
ξ	network mesh size
ρ_c	the crosslink density

LIST OF PUBLICATIONS

Articles published in journals indexed on Web of Science:

Muchová, M.; Münster, L.; Vávrová, A.; Capáková, Z.; Kuřitka, I.; Vícha, J. Comparison of Dialdehyde Polysaccharides as Crosslinkers for Hydrogels: The Case of Poly(Vinyl Alcohol). *Carbohydrate Polymers* **2022**, *279*, 119022. https://doi.org/10.1016/j.carbpol.2021.119022.

Münster, L.; Fojtů, M.; Capáková, Z.; **Muchová, M.**; Musilová, L.; Vaculovič, T.; Balvan, J.; Kuřitka, I.; Masařík, M.; Vícha, J. Oxidized Polysaccharides for Anticancer-Drug Delivery: What Is the Role of Structure? *Carbohydrate Polymers* **2021**, *257*, 117562. https://doi.org/10.1016/j.carbpol.2020.117562.

Münster, L.; Fojtů, M.; **Muchová, M.**; Latečka, F.; Káčerová, S.; Capáková, Z.; Juriňáková, T.; Kuřitka, I.; Masařík, M.; Vícha, J. Enhancing Cisplatin Anticancer Effectivity and Migrastatic Potential by Modulation of Molecular Weight of Oxidized Dextran Carrier. *Carbohydrate Polymers* **2021**, *272*, 118461. https://doi.org/10.1016/j.carbpol.2021.118461.

Muchová, M.; Münster, L.; Capáková, Z.; Mikulcová, V.; Kuřitka, I.; Vícha, J. Design of Dialdehyde Cellulose Crosslinked Poly(Vinyl Alcohol) Hydrogels for Transdermal Drug Delivery and Wound Dressings. *Materials Science and Engineering: C* **2020**, *116*, 111242. https://doi.org/10.1016/j.msec.2020.111242.

Article already published with full citation, but not yet available on WoS

Důbravová, A.; Muchová, M.; Škoda, D.; Lovecká, L.; Šimoníková, L.; Kuřitka, I.; Vícha, J.; Münster, L. Highly Efficient Affinity Anchoring of Gold Nanoparticles on Chitosan Nanofibers via Dialdehyde Cellulose for Reusable Catalytic Devices. *Carbohydrate Polymers* **2023**, 121435. https://doi.org/10.1016/j.carbpol.2023.121435.

Manuscript under revision to the editors of international journals with an impact factor:

Káčerová S., **Muchová M**., Doudová H., Münster L., Hanulíková B., Víchová Z.,Valášková K., Kašpárková V., Kuřitka I., Humpolíček P., Vašíček O., Vícha J. Antibacterial, anti-oxidant, conductive, and anti-inflammatory polypyrrole/chitosan/dialdehyde cellulose hydrogel wound dressings

Conferences:

International conference - Active participation: **Monika Muchová** , Důbravová Alžběta, Lovecká Lenka, Kuřitka Ivo, Vícha Jan, Münster Lukáš. Pilot Preparation Study of Gold Nanoparticle-Chitosan Composite Catalyst. NANOCON (18-20 October 2023), Brno.

International conference: Káčerová Simona, Vícha Jan, Víchová Zdenka, **Muchová Monika**, Münster Lukáš, Vašíček Ondřej, Humpolíček Petr. Bioactive Films Based on Chitosan and Polypyrrole. ECIS 2022: 36th European Colloid & Interface Society Conference 4-9 September 2022 Chania, Crete, Greece, 2022

Proofs of concept:

Gold nanoparticles prepared using selectively oxidized polysaccharide. Vávrová Alžběta; Kuřitka Ivo; Vícha Jan; Münster Lukáš; **Muchová Monika**.

Antibacterial photocatalytic composites based on acetylated chitosans doped by ZnO. Münster Lukáš; Kuřitka Ivo; Vícha Jan; Masař Milan; **Muchová Monika**.

CURRICULUM VITAE

Personal information

Name	Monika Muchová
Address	Třída Obránců Mírů 2, Bruntál 792 01
E-mail	M_muchova@utb.cz
Nationality	Czech
Date of birth	01.08.1995

Education

2019-present – *Doctoral degree student*

Technology of macromolecular compounds, Tomas Bata University, Zlín, Czech Republic.

2017-2019 – *Mater´s degree*

Food Chemistry and Technology, Tomas Bata University in Zlín, Czech Republic

2014-2017 – *Bachelor´s degree*

Food Chemistry and Technology, Tomas Bata University in Zlín, Czech Republic

Education stays

September-November 2022

University of Aveiro, traineeship – Immobilization of oxidative enzymes on nanofibers,Universidade de Aveiro, 3810-193 Aveiro, Portugal

Work on projects

IGA/CPS/2023/006 "Preparation and characterization of advanced functional nanocomposite systems", Internal grant agency for specific research from Tomas Bata University in Zlín – member of project team

OP PIK
CZ.01.1.02/0.0/0.0/20_321/0025211-
Research and development of a new generation of anti-corrosion pigments that multiply the protection of metal surfaces

with an emphasis on their ecological and rational economic efficiency (2022-2023)

GAČR 23-07361S Synthesis of gold nanoparticles for SERS and catalysis guided by selectively oxidized polysaccharides

IGA/CPS/2022/002 "Preparation and characterization of advanced nanocomposite systems", Internal grant agency for specific research from Tomas Bata University in Zlín – member of project team

IGA/CPS/2021/002 "Preparation and characterization of nanocomposite systems", Internal grant agency for specific research from Tomas Bata University in Zlín – main investigator

IGA/CPS/2020/003 "Preparation and characterization of nanoparticles for advanced applications", Internal grant agency for specific research from Tomas Bata University in Zlín – member of project team

Pedagogic activities

Participation on teaching in laboratory classes of "The Basics of Food Packaging", TCPM/TP5ZB (FT, UTB).

Appendix I

Muchová, M.; Münster, L.; Capáková, Z.; Mikulcová, V.; Kuřitka, I.; Vícha, J. Design of Dialdehyde Cellulose Crosslinked Poly(Vinyl Alcohol) Hydrogels for Transdermal Drug Delivery and Wound Dressings. Materials Science and Engineering: C 2020, **116**, 111242. https://doi.org/10.1016/j.msec.2020.111242.

Materials Science & Engineering C 116 (2020) 111242

Contents lists available at ScienceDirect

Materials Science & Engineering C

journal homepage: www.elsevier.com/locate/msec

Design of dialdehyde cellulose crosslinked poly(vinyl alcohol) hydrogels for transdermal drug delivery and wound dressings

Monika Muchová, Lukáš Münster, Zdenka Capáková, Veronika Mikulcová, Ivo Kuřitka, Jan Vícha*

Centre of Polymer Systems, Tomas Bata University in Zlín, tř. Tomáše Bati 5678, 760 01 Zlín, Czech Republic

ARTICLE INFO

Keywords:
Poly(vinyl alcohol)
Dialdehyde cellulose
Transdermal
Hydrogel
Drug delivery
Wound dressing

ABSTRACT

2,3-Dialdehyde cellulose (DAC) was used as an efficient and low-toxicity crosslinker to prepare thin PVA/DAC hydrogel films designed for topical applications such as drug-loaded patches, wound dressings or cosmetic products. An optimization of hydrogel properties was achieved by the variation of two factors – the amount of crosslinker and the weight-average molecular weight (M_w) of the source PVA. The role of each factor to network parameters, mechanical, rheological and surface properties, hydrogel porosity and transdermal absorption is discussed. The best results were obtained for hydrogel films prepared using 0.25 wt% of DAC and PVA with M_w = 130 kDa, which had a high porosity and drug-loading capacity (high water content), mechanical properties allowing easy handling, best adherence to the skin from all tested samples and improved transdermal drug-delivery. Hydrogel films are biocompatible, show no cytotoxicity and have no negative impact on cell growth and morphology in their presence. Furthermore, hydrogels do not support cell migration and attachment to their surface, which should ensure easy removal of hydrogel patches even from wounded or damaged skin after use.

1. Introduction

Hydrogel-based biomaterials receive steadily growing attention due to their similarity to living tissues in terms of mechanical properties, porosity and high content of water. The last two qualities allow hydrogels to accommodate, store, and later release various substances, making them excellent materials for a wide range of drug-delivery applications in both medicine and cosmetics, i.e. from injectable drug-delivery depots to dermal patches, or from drug-loaded wound dressings to hydrating masks. In contrast to implantable drug depots, topically applied hydrogels could be easily removed and replaced after their content is depleted, which is ideal for sustained, painless, and controlled delivery of biologically active compounds [1].

Hydrogel films are also excellent wound dressing materials as they naturally hydrate the skin and keep the wound zone moist and wettable, which accelerates healing [2], soothes and cools burns and reduces pain and inflammation [3]. Hydrogels loaded with antibiotics and anti-inflammatory agents can also deliver the active compounds directly to the wounded area, reducing the risk of infection.

Necessary characteristics of hydrogels intended for topical applications include: biocompatibility, large loading capacity (equilibrium water content), good adherence to the skin (bioadhesivity), which increases dermal absorption of compounds loaded in the hydrogel, [4] and mechanical stability sufficient for easy removal. Hydrogels intended as wound dressings should not interfere with the cell growth and formation of new tissues. Simultaneously, they should not support cell migration and attachment to their surface or bulk, which may complicate their removal from the wounded area and lead to the disturbance of tender healing tissue.

To successfully balance all these qualities is not an easy task. For instance, purely biopolymer-based hydrogels often have poor mechanical properties in the swollen state, which make them difficult to handle and to remove from skin. Hydrogels based on artificial polymers have well-defined structure and properties but may suffer from other disadvantages. For instance, hydrogels based on poly(vinyl alcohol), PVA, are used for preparation of immunotherapeutic anticancer gels and transdermal patches, [5,6] wound dressings [3], drug-delivery patches [7] and contact lenses [8]. However, properties of PVA hydrogels are difficult to optimize – they tend to have poor elasticity, high stiffness and relatively low hydrophilicity. Possible solution is to use hybrid hydrogels composed of two polymers of both natural and artificial origin [3]. Properties of hybrid hydrogels are generally better defined than in case of purely biopolymer-based analogs and their individual attributes can be more easily optimized than those of synthetic polymer-based hydrogels.

* Corresponding author.
E-mail address: jvicha@utb.cz (J. Vícha).

https://doi.org/10.1016/j.msec.2020.111242
Received 22 March 2020; Received in revised form 18 June 2020; Accepted 24 June 2020
Available online 26 June 2020

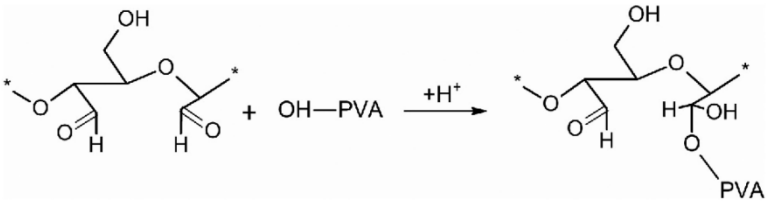

Fig. 1. Simplified reaction scheme between –CHO and –OH groups of 2,3-dialdehyde cellulose and PVA in an acidic environment.

In this work we investigate hydrogel films composed of PVA crosslinked by 2,3-dialdehydecellulose, DAC, which is prepared by regioselective periodate oxidation of hydroxyl groups of cellulose at C2 and C3 of pyranose cycle [9,10]. Structure of DAC and simplified reaction scheme between DAC and PVA is given in Fig. 1. Raw DAC is insoluble in aqueous media and must be solubilized by hot water prior to its utilization in solution-based processes [11]. DAC features two highly reactive aldehyde groups per each oxidized unit, which can be used for crosslinking of polymers bearing hydroxyl side groups (Fig. 1). However, DAC was deemed to be rather unstable in solution [12]. The presumed need to prepare a fresh crosslinker for every use reduced its potential in practical applications [13]. Only recently, we have shown that the stabilization of an aldehyde group content over a prolonged period can be achieved by decreasing the pH of the solution to 3.5 [10].

DAC has several advantages over currently used organic crosslinkers such as glutaraldehyde (GA). Firstly, DAC can be prepared using cellulose from renewable resources [14] and consumed periodate salt can be easily regenerated and re-used making the whole process sustainable [15]. Secondly, DAC is considerably less toxic than GA, [16] which is particularly important to the preparation of biomaterials for medical and cosmetic sector. Last but not least, DAC is more effective crosslinker than GA at the same concentration of aldehyde groups. [17] This is a result of "two-phase" network topology found in DAC hydrogels. [16–18] Briefly, while small GA molecules are uniformly distributed through the hydrogel network, much larger DAC macromolecules can crosslink numerous PVA chains simultaneously, thus creating regions with very high crosslink density, which are embedded in PVA matrix. Resulting PVA/DAC hydrogels thus have better mechanical properties than PVA/GA counterparts [18].

Here, DAC is used as a crosslinker for preparation of thin hydrogel films optimized for transdermal drug delivery, wound dressings and cosmetic products. The role of varied amount of crosslinker and different weight-average molecular weight (M_w) of PVA to the network parameters, porosity, viscoelastic properties, cytotoxicity and biocompatibility of prepared thin films is discussed together with release kinetics and transdermal absorption of two model drugs, rutin and caffeine.

Rutin is the glycoside composed of quercetin and rutinose (α-L-rhamnopyranosyl-(1 → 6)-β-D-glucopyranose). It is a flavonoid found in a wide variety of plants including buckwheat, tea and citrus fruit. It is highly versatile in its biological activity because it exhibits antioxidative, cytoprotective, vasoprotective, anticarcinogenic, neuroprotective and cardioprotective properties [19]. It finds numerous applications in cosmetics, because it stabilizes the vascular walls, prevents them from cracking and counteracts the manifestation of dilated veins. It is also utilized in wound dressing and healing applications because it shows anti-microbial and anti-inflammatory activity and reduces oxidative stress in the wounded area [20,21].

Caffeine is a stimulant of the central nervous system and is often used as a model drug for studying the penetration of hydrophilic substances across the skin barrier [22,23]. Caffeine-saturated hydrogels can stimulate the nervous system, support lymphatic system, prevent excessive fat accumulation in the skin and help to protect the skin from photodamage [22,23].

2. Experimental

2.1. Materials

Two types of poly(vinyl alcohol) (PVA) with 88% degree of hydrolysis with different M_w (130 and 31 kDa, respectively) were used (Sigma Aldrich Co.). Alpha cellulose (M_w = 109 kDa) [24] (Sigma Aldrich Co.), sodium periodate ($NaIO_4$) (Penta, Czech Republic), ethylene glycol, hydrochloric acid (HCl) (Penta, Czech Republic) were employed in the synthesis of 2,3-dialdehydecellulose (DAC) and in the subsequent preparation of hydrogels. The prepared PVA/DAC hydrogels were saturated with rutin and caffeine (Sigma Aldrich Co.). The mouse embryonic fibroblast cell line (NIH/3T3, ECACC) was used for the determination of biological properties. DMEM (Biosera, France) containing 10% of calf serum (Biosera, France) and 100 U/mL Penicillin/Streptomycin (Biosera, France) was used as a culture media. Cells were incubated at 37 °C in a 5% CO_2 humid atmosphere. Phosphate buffer saline (PBS) (Invitrogen, USA) was used for cells washing. Cells were cultured on Techno plastic (TPP, Switzerland), using Tetrazolium kit (MTT cell proliferation assay, Duchefa Biochemistry, The Netherlands). The other chemicals used in biological testing include formaldehyde (Penta, Czech Republic), Triton X (Sigma Aldrich Co.), Hoechst 33258 (Invitrogen, USA) and ActinRed™ 555 (Thermo Fisher Scientific, USA). For transdermal testing gentamicin sulfate (HiMedia Laboratories), formic acid (HCOOH), and methanol (Penta, Czech Republic) were used. All chemicals were of analytical purity and were used as received without further purification. Demineralized water was used throughout the experiments.

2.2. Preparation of crosslinked PVA/DAC hydrogels

In the first step, the 2,3-dialdehydecellulose (DAC) was prepared by oxidation of alpha cellulose by $NaIO_4$ using a 1:1.2 M ratio of reactants (DAC:periodate) following earlier works [10,17,18,25]. Briefly, to achieve high conversion of cellulose to DAC, 10 g of cellulose was suspended in 250 mL of water containing 16.5 g of sodium periodate. The mixture was then stirred in the dark for 72 h at 30 °C. The oxidation was stopped by addition of 10 mL of ethylene glycol and the product washed and filtered. Resulting raw DAC was suspended in 175 mL of water and solubilized at 80 °C for 7 h [11]. Next, the solubilized DAC was cooled, centrifuged (10 min, 10,000 RPM) and the solution was transferred to a 200 mL volumetric flask. The weight concentration of solubilized DAC was determined (42.3 ± 1.3 mg/mL) by simple weight analysis (i.e. solution evaporation and residue weighted). The prepared DAC solution of known concentration served for crosslinking of PVA.

In the second step, 10 g of each PVA type (M_w 31,000 or 130,000 g/mol) was dissolved in 80 mL of water at 90 °C. Subsequently, the catalyst (10 mL of 1.3 M HCl) and defined amount of DAC corresponding to 0.25 wt% and 1 wt% (with respect to the weight of PVA) was added. The prepared reaction mixtures were thoroughly stirred and poured onto Petri dishes (d = 140 mm) and left to dry at 30 °C until constant weight. The crosslinking reaction between PVA and DAC occurs during the drying of the reaction mixture, where dehydration of –CHO groups

Table 1
Designation of PVA/DAC samples, their composition and M_w of the PVA used.

Sample	PVA (g)	M_w PVA (kDa)	DAC (wt%)	DAC (g)
L-31	10	31	0.25	0.025
H-31	10	31	1	0.1
L-130	10	130	0.25	0.025
H-130	10	130	1	0.1

of DAC causes the formation of hemiacetals with hydroxyl groups of PVA. Simplified reaction scheme between –CHO of DAC and –OH group of PVA in an acidic environment is shown in Fig. 1.

The prepared thin films were then thoroughly washed in water to remove uncrosslinked material, and disc-shaped samples of 15 and 50 mm in diameter were cut out and stored in aseptic medium (70% ethanol solution) until used. A small part of the PVA/DAC samples was left unwashed for determination of network parameters (gel fraction). Designation and composition of the prepared PVA/DAC samples are listed in Table 1.

The estimation of network parameters, measurement of viscoelastic properties, BET and SEM analysis, drug release kinetics, cytotoxicity and transdermal absorption of prepared hydrogels were subsequently investigated.

2.3. Network parameters

The network parameters were estimated based on the measurements of swelling and weight change of prepared 15 mm disc-shaped PVA/DAC xerogel samples (6 specimens for each). Unwashed discs were weighed and then thoroughly washed for one week with regular changing of water. Subsequently, the swollen discs were gently dried to remove excess water, weighed and dried at 30 °C till constant weight. The network parameters were determined using equilibrium swelling theory suggested by Flory and Rehner [26]. The constants used for the calculation of network parameters include the specific volume of PVA polymer $\nu = 0.788\ cm^3/g$, the PVA density $\rho_p = 1.27\ g/cm^3$, the molar volume of water (V_1) at 25 °C = 18.069 cm^3/mol, the polymer-solvent interaction parameter (χ_1) = 0.464, the average bond length $l = 1.54$ Å, the characteristic ratio of PVA chain $C_n = 8.9$ and the molecular weight of PVA unit $M_r = 44$ g/mol. Following equations were used to calculate network parameters [10,27].

Equilibrium swelling (%) was obtained according to Eq. (1), where M_E is the mass of the hydrogel swollen to the equilibrium state, and M_0 is the mass of the washed and dried hydrogel [28].

$$\text{Equilibrium swelling (\%)} = \frac{M_E - M_0}{M_0} \times 100 \quad (1)$$

Equilibrium water content (*EWC*) describes the maximum amount of water absorbed by the hydrogel. M_s is the mass of the sample swelled under equilibrium conditions, and M_0 is the mass of the washed and dried hydrogel [29].

$$\text{EWC (\%)} = \frac{M_s - M_0}{M_s} \times 100 \quad (2)$$

The gel fraction was calculated using Eq. (3), where M_0 is the weight of the dried hydrogel after extraction of the soluble fraction in the hydrogel and M_{int} is the weight of the dry and non-washed hydrogel [28].

$$\text{Gel fraction (\%)} = \frac{M_0}{M_{int}} \times 100 \quad (3)$$

The average molecular weight between crosslinks (M_c), where M_n is the average number molecular weight of the initial uncrosslinked polymer, ν is the specific polymer volume, V_1 is the molar volume of water, $V_{2,s}$ is the polymer volume fraction and χ_1 is the polymer-solvent interaction parameter [26].

$$\mathrm{M_c\ (g/mol)} = \frac{M_n}{2} - \frac{\left[(V_{2,s})^{\frac{1}{3}} - \frac{V_{2,s}}{2} \right]}{\left(\frac{\nu}{V_1}\right)[\ln(1 - V_{2,s}) + V_{2,s} + \chi 1 (V_{2,s})^2]} \quad (4)$$

Polymer fraction ($V_{2,s}$), where M_s/M_0 is the weight ratio of dry to swollen hydrogel at equilibrium, ρ_p is the density of the polymer and ρ_w is the density of water [30].

$$\mathrm{V_{2,s}} = \left[1 + \frac{\rho_p}{\rho_w} \left(\frac{M_s}{M_0} - 1 \right) \right]^{-1} \quad (5)$$

Calculation of the crosslink density (ρ_c) [26,31].

$$\rho_c\ (mol/cm^3) = \frac{1}{\nu M_c} \quad (6)$$

The mesh size (ξ):

$$\xi\ (\text{Å}) = V_{2,s}^{-1/3} (\bar{r}_0^2)^{1/2} \quad (7)$$

where $(\bar{r}_0^2)^{1/2}$ is the end-to-end distance of the unperturbed (solvent-free) state.

$$(\bar{r}_0^2)^{1/2} = l \left(\frac{2 \times M_c}{M_r} \right)^{1/2} \times C_n^{3/2} \quad (8)$$

2.4. Measurement of viscoelastic properties

Disc samples (d = 15 mm, 6 specimens per sample) were measured in an equilibrium swollen state using a rotational rheometer Anton Paar MCR 502 (Anton Paar, Austria) equipped with D-PP15 shaft using a roughened aluminium plate with 15 mm diameter and ground plate with glued sandpaper both used to prevent slipping of samples during measurement. The measurement was performed at laboratory temperature in oscillation mode in frequency sweep from 1 to 10 Hz by applying a constant strain of 1%.

2.5. BET and SEM analysis

Lyophilized PVA/DAC cryogels were initially degassed at 75 °C for 24 h. Specific surface area (a_{BET}), total pore volume (V_p) and mean pore diameter of cryogels was determined by multipoint Brunauer-Emmet-Teller (BET) analysis of adsorption isotherms recorded at 77 K utilizing high precision surface area analyzer Belsorp-mini II (BEL Japan Inc., Japan). The measurement was carried out in triplicates. These materials were also analyzed by scanning electron microscopy (SEM) employing Nova NanoSEM 450 microscope (FEI, Czech Republic) operated at 5 kV accelerating voltage. Ahead of SEM imaging, cryogels were sputtered with gold-palladium nanoparticles to suppress the charge accumulation effect.

2.6. Loading and release

H-31, L-130 and H-130 samples of approximately 500 mg and 15 mm in diameter were loaded by biologically active compound by submerging into a 50 mL of stock solution of 0.1 mg/mL (rutin) or 10 mg/mL (caffeine) and shaken for 72 h at 37 °C. Loaded samples were then used to study the drug release kinetics. For this purpose, three samples from each hydrogel were placed in separate closed containers containing 10 mL of demineralized water and shaken at 37 °C in the dark. Aliquots of 1 mL were collected in given times over 96 h and analyzed using UV-VIS spectrometer Perkin Elmer Lambda 1050 (Perkin Elmer Inc., USA) using characteristic peaks at 353 nm (rutin) and 273 nm (caffeine). The experiments were performed in triplicates.

2.7. Cytocompatibility of hydrogels

The cytocompatibility tests included 1) evaluation of cytotoxicity of hydrogel extracts and 2) cell growth in the presence of hydrogel and in direct contact with their surfaces. The cytotoxicity was tested according to ISO 10 993-5. All tests were performed in quadruplicates.

1) Extracts from L-130, H-130 and H-31 specimens were prepared according to ISO 10993-12 in the concentration of 0.1 g of swollen gels per 1 mL of culture media. The tested samples were extracted in culture medium for 24 h at 37 °C under constant shaking. The parent extracts (100%) were then diluted in culture medium to obtain a series of dilutions with concentrations of 75, 50, 25, 10, and 1%. The mouse embryonic fibroblast (NIH/3T3) cells were seeded into 96 well plates in concentration 10^5 cells per mL and placed to the incubator for pre-cultivation for 24 h at 37 °C. After the pre-incubation period, the extracts were added and cells incubated for another 24 h. Determination of cell viability after exposure time was performed by MTT assay. The reference wavelength was set to 570 and 690 nm, respectively. The results are presented as the relative cell viability compared to the reference (cells cultivated on tissue plastic only in culture medium), where reference corresponds to 1 (100% cell viability).
2) For the test of cell growth in the presence of hydrogels, cells were seeded on culture plastic plates in concentration 10^5 cells per mL and pre-incubated till they reached sub-confluence. The hydrogels were placed in the centre over the adherent cells. Cells were checked every day by an inverted phase-contrast microscope Olympus IX 81 (Olympus, Japan) until the reference reached full confluency (96 h). Cell viability was measured by MTT assay in the same conditions as in the cytotoxicity of hydrogel extracts after 48 and 96 h.

For the determination of cell adherence and growth on the surface of hydrogels, cells were seeded directly on the samples surfaces in concentration 5×10^4 cells per cm^2. After 48 h samples were fixed with 4% formaldehyde for 15 min, washed with PBS, permeabilized with 0.5% Triton X for 5 min and subsequently stained with Hoechst 33258 and ActinRed™ 555 for 30 min in the dark. Cells were observed using an inverted fluorescence phase-contrast microscope Olympus IX 81 (Olympus, Japan).

2.8. Transdermal absorption tests in vitro

Tests were conducted according to the OECD Test Guideline for Skin Absorption: In vitro method, using the skin from pig ear. The pig's ear lobe was shaved and the inner part of the auricle was separated from the underlying cartilage. Square skin samples of 3 × 3 cm were cut out from the separated skin. The skin samples were then placed in test cells and their skin integrity was determined using a UNI-T UT71D multimeter. Samples with a resistance below 5 mΩ were excluded.

Disc-shaped samples of individual hydrogels were added to the prepared skin samples. Prior to insertion, the hydrogels were loaded with caffeine by shaking for 120 h at 37 °C in 10 mg/mL caffeine. Testing was performed on an automated diffusion cell system with the continuous flow of receptor liquid through samples Fraction Collector FC33 (Permegear, USA). All experiments were performed in triplicates. The receptor fluid (PBS buffer and 0.05% gentamicin sulfate) was collected for 24 h at a constant flow rate of 2 mL/h. After completion of the measurements, the fractions obtained at pre-set times (1–24 h) were stored at −20 °C until analysis. The individual samples were then filtered and analyzed by liquid chromatography employing HPLC chromatograph Breeze 1525 with UV-VIS detector (Waters Corporation, USA). Chromatographic separation of the caffeine within the samples was carried out isocratically on a Kinetex C18 100A column (150 × 4.6 mm, 2.6 μm) (Phenomenex, USA). The mobile phase consisted of 0.2% HCOOH and methanol in a 75/25 ratio, the temperature was set to 30 °C, the flow rate 0.7 mL/min. The wavelength used for detection was 272 nm.

3. Results and discussion

Four types of hydrogel samples differing in concentrations of DAC and M_w of PVA were prepared, see Table 1. Only the network parameters were determined for the sample L-31 (L stands for lower amount of the DAC, 0.25 wt%, number 31 is the molecular weight of PVA in kDa, cf. Table 1) because of its poor physical properties caused by combination of low crosslinker concentration and low M_w of PVA. Sample L-31 teared and disintegrated even during gentle manipulation, which prevented meaningful characterization as certain techniques would be influenced by macroscopic faults in hydrogel structure, making obtained data unreliable. Other three types of hydrogel samples (L-130, H-31 and H-130, H stands for higher concentration of crosslinker – 1 wt%, number 130 is the molecular weight of PVA in kDa, cf. Table 1) were characterized by full set of methods described above.

3.1. Network parameters

Based on the equations given in Section 2.3, the network parameters of all types of PVA/DAC hydrogel samples (L-130, H-130, L-31, H-31) were determined, Table 2. Unsurprisingly, the swelling of hydrogel matrices and *EWC* depends on both the amount of DAC and the M_w of PVA. The lower the amount of crosslinker and the lower the M_w of PVA, the more the hydrogel swells. Thus, sample L-31 has the largest swelling, equal to almost 80-times of its dry mass. On the other side, sample H-130 swells only about 3.5-times. Conversely, the gel fraction increases with increasing amounts of DAC and M_w PVA, thereby sample H-130 shows the largest gel fraction and sample L-31 the smallest one.

The dependence of average molecular weight between crosslinks (M_c), crosslink density (ρ_c), and mesh size (ξ) on both observed factors is, however, not so straightforward. As one may expect, decreasing the amount of DAC results in higher separation of crosslinked regions (higher M_c), which reduces ρ_c and increase the ξ of respective samples. However, the influence of M_w of PVA on M_c and ρ_c actually differs for different the amounts of crosslinker. Increased M_w of PVA is causing a significant decrease of M_c (an increase of ρ_c) in H-series (1% of DAC), but the opposite trend was found in L-series (0.25% of DAC). Notably, the ξ is smaller for PVA with M_w = 130 kDa in both series.

The variation of M_c and ρ_c between series is likely related to the nature of PVA/DAC network, which is composed of two types of interactions – the PVA/DAC chemical crosslinks complemented by

Table 2
Network parameters (the equilibrium swelling, the equilibrium water content *EWC*, the gel fraction, the average molecular weight between crosslinks M_c, the crosslink density ρ_c and the mesh size ξ) calculated for the prepared hydrogel samples. Data represent average of six measurements with standard deviations.

Sample	Equilibrium swelling (%)	EWC (%)	Gel fraction (%)	M_c (g/mol)	ρ_c (μmol/cm^3)	ξ (Å)
L-31	7900 ± 800	98.7 ± 0.1	12 ± 0.8	12380 ± 20	103 ± 1	508 ± 17
H-31	710 ± 20	87.6 ± 0.3	47.7 ± 0.9	6410 ± 160	198 ± 5	169 ± 4
L-130	1150 ± 90	92 ± 0.6	58.8 ± 1.8	20660 ± 1880	62 ± 6	352 ± 25
H-130	350 ± 10	77.8 ± 0.3	88.8 ± 0.2	2890 ± 90	440 ± 14	93 ± 2

residual physical interactions (hydrogen bridge network and chain entanglements) between the PVA macromolecules [17]. It is reasonable to assume that chemical crosslinking is more pronounced in H-series hydrogels, particularly for H-130 sample, where longer PVA chains offer considerably more crosslinking hot-spots. Thus, the sample H-130 exhibits the smallest M_c and ξ and the highest ρ_c of all. In more sparsely crosslinked L series, the effect of residual physical crosslinking of longer PVA (130 kDa) chains provides additional stabilization to the hydrogel network. Hence, despite L-130 sample having the lowest-density network with highest M_c and lowest ρ_c from all samples, its ξ is lower than in case of L-31, and its physical properties are sufficient for easy handling in contrast to sample L-31, which had to be excluded from further analyses.

To summarize, although the role of the amount of the crosslinker governs the network parameters of hydrogels (i.e. four-times less of DAC results in up to 10-times the swelling in L-31 vs. H-31), it is further accentuated by changing the M_w of PVA, which influences the hydrogel network mainly at the (macro)molecular level.

3.2. Analysis of viscoelastic properties

Oscillatory shear rheometry utilizing frequency sweep from 1 Hz to 10 Hz and constant strain of 1% was used to study the viscoelastic properties of prepared hydrogels. The dependence of storage modulus (G') and loss modulus (G'') on angular frequency is given in Fig. 2A. The G' values of PVA/DAC hydrogel samples range from more than 2100 Pa for sample H-130 to about 150 Pa for sample L-130, see Fig. 2B. The G'' values range from about 190 Pa for sample H-130 to about 4.3 Pa for sample L-130. As expected, [18] the results follow the trend of ρ_c (see Table 2), because the denser mesh have a higher elasticity than the sparser one, which will, in turn, have more viscous-like behavior. Hence, the lowest G' and G'' values were observed for the L-130 sample with the lowest crosslink density. The effect of the M_w of PVA is observable for H series hydrogels, where four-times lower M_w of PVA results in decrease of both G' and G'' by approx. 75%.

Analogous correlations between the amount of crosslinker and the M_w of PVA were found for the complex dynamic modulus (G^*) and the damping factor (tan δ). The complex modulus G^* was calculated as the square root of the sum of the square of storage and loss moduli in the selected range of oscillatory measurement at ambient temperature, Fig. 2C. The range of G^* values is from more than ~2200 Pa for H-130 to ~150 Pa for sample L-130. The *tan δ* is defined as the ratio between loss and storage modulus (G''/G') and gives a measure of viscous to elastic component of the material. The damping factor ranges from 0.09 for sample H-130 (most elastic) to 0.03 for sample L-130 (the most viscous), Fig. 2D.

To summarize, the most viscous and the least elastic material is the least crosslinked sample L-130. The most elastic is sample H-130. Notably, viscoelastic properties of sample H-31 are generally closer to L-130 than to H-130 despite being prepared by using the same amount of crosslinker as the latter. This demonstrates a considerable influence of the PVA matrix on the rheological properties of the hydrogels.

3.3. BET and SEM analysis

Samples of PVA/DAC hydrogels were lyophilized, and their specific surface area (α_{BET}), total pore volume (V_p), mean pore diameter and adsorbed volume of nitrogen (V_a) measured, see Fig. 3. The α_{BET} value for sample L-130 (31.1 ± 0.9 m^2/g) is an order of the magnitude higher than the values for samples H-130 (2.0 ± 0.1 m^2/g) and H-31 (2.2 ± 0.1 m^2/g). The total pore volume (V_p) exhibits the same trend as α_{BET} being about ten times higher for L-130 (0.218 ± 0.007 cm^3/g) than for H-series hydrogels (H-130 = 0.021 ± 0.001 cm^3/g and H-31 = 0.031 ± 0.002 cm^3/g, see Fig. 3C). This difference is closely related to the extent of cavitation induced by the lyophilization and indirectly linked to the water absorption capability of the hydrogel. Interestingly, mean pore diameter do not follow described trend. Largest pore diameter was observed for H-31 sample (54.6 ± 3.3 nm), followed by H-130 sample (41.5 ± 2.1 nm) and L-130 sample (28.1 ± 0.8 nm). The H-series cryogels thus have fewer larger pores, while L-130 contains a larger number of smaller pores in its structure.

Cryogel samples were further analyzed by scanning electron microscopy (SEM). In agreement with α_{BET} values, surface of L-130 cryogel was found to be highly porous, see Fig. 3D, while the H-31 sample showed slightly larger surface pores than the H-130 sample, but the difference is not very significant.

To summarize, while both α_{BET}, V_p and V_a increase significantly with the decreasing amount of DAC, the M_w of PVA seems to influence the mean pore size. It should be noted that combination of the low amount of DAC and high-molecular-weight PVA allowed preparing highly

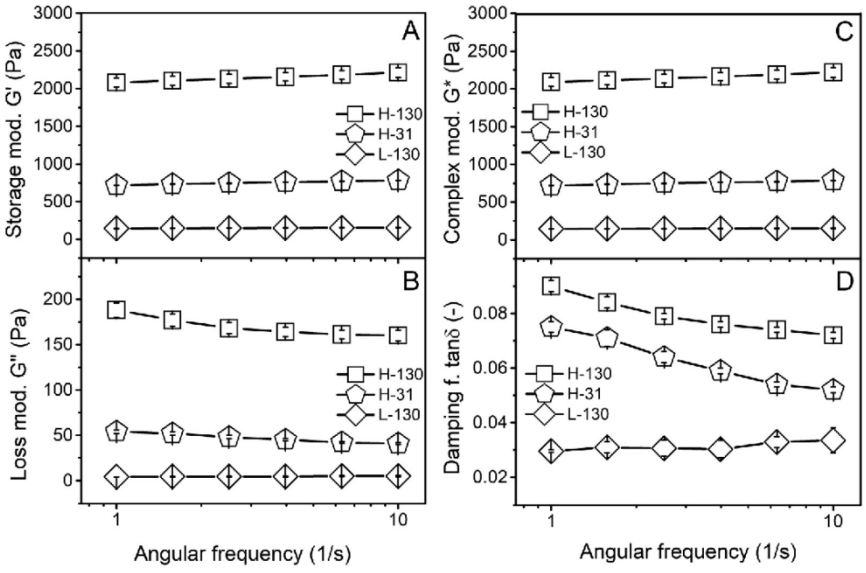

Fig. 2. Dependence of the storage modulus (G') and the loss modulus (G'') of PVA/DAC hydrogel samples on the angular frequency (part A and B), dependence of the calculated complex modulus (G^*, part C) and the damping factor ($tan\delta$, part D) on the angular frequency. Measurements were repeated six times; error bars express standard deviations.

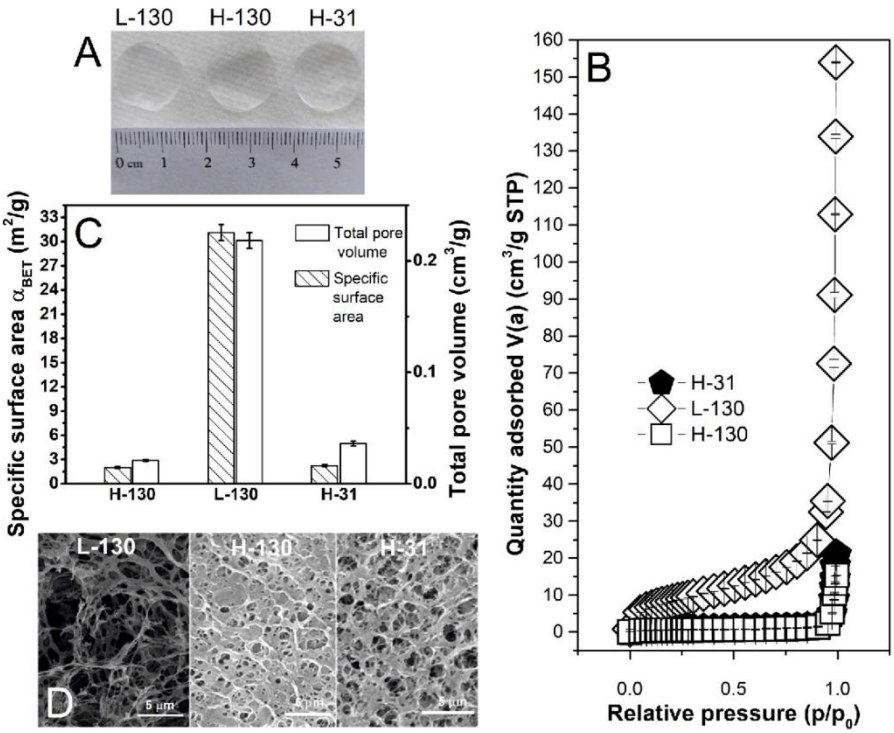

Fig. 3. Photographs of swollen hydrogel samples (part A), dependence of quantity of the adsorbed volume of nitrogen per cryogels mass (V_a) on the relative pressure p/p_0 (part B), the specific surface area α_{BET} and total pore volume (V_p) of prepared PVA/DAC cryogels (part C), and micrographs of individual PVA/DAC samples taken with SEM at 30.000× magnification (part D). Measurements were performed in triplicates; error bars represent standard deviations.

porous materials with mechanical properties allowing reasonable handling, which was not possible by using PVA with lower molecular weight (sample L-31).

3.4. Loading and release study

Samples of individual hydrogels were loaded with rutin or caffeine, see Section 2.6 for more details. The loaded hydrogel samples were subsequently put into separate containers containing 10 mL of water and release of rutin (Fig. 4A) and caffeine (Fig. 4B) evaluated by UV-VIS spectroscopy.

Release rates of relatively small caffeine molecules (M = 194 g/mol, Fig. 4B) from all three tested materials are identical within the experimental error. The effect of the network parameters is only observable for larger rutin (610 g/mol), where fastest release after 8 h was observed for H-31 sample, while both 130-series samples showed nearly identical release kinetics. This might be related to lower M_w of PVA influencing the pore size (see previous section), but the difference is relatively minor and more tests would be needed to confirm this observation.

Small overall differences in burst release kinetics are most likely caused by low thickness of prepared hydrogel films. Because most of the drug is situated in the vicinity of the thin film surface, the diffusion path is very short, which together with hydrogel mesh size being significantly larger than the diameter of studied molecules (100–350 Å, Table 2), minimizes the impact of hydrogel network to the drug release rate. This may be improved by employing thicker films or by modification of drug loading procedure.

Nevertheless, the observed burst release kinetics with up to 90% of compounds released in 8 h is considered to be suitable for topical drug delivery, where expected time of application is in order of hours rather than days.

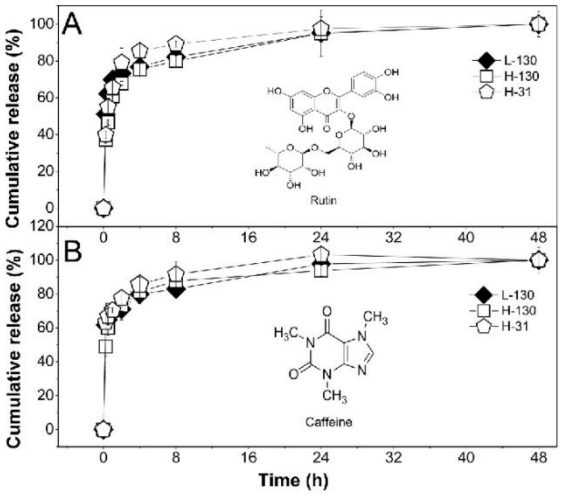

Fig. 4. Cumulative release of rutin (part A) and caffeine (part B) from L-130, H-31 and L-130 hydrogel samples. All experiments were performed in triplicates; error bars represent standard deviations.

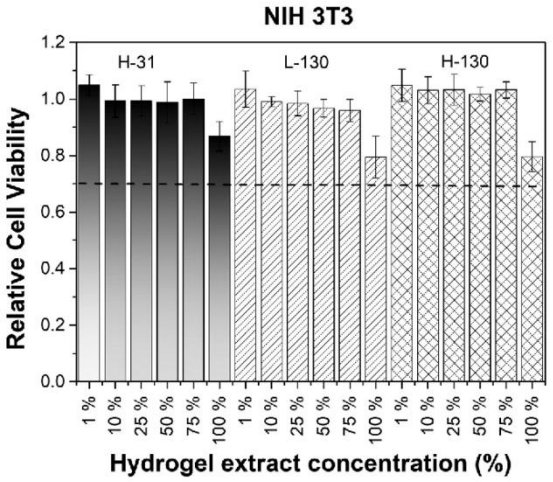

Fig. 5. Relative cell viability of mouse embryonic fibroblast cells (NIH/3T3) incubated with PVA/DAC hydrogel extracts of different concentrations (1–100%). Measurements were performed in quadruplicates; error bars represent standard deviations.

3.5. Biological testing

Biological evaluation included (i) determination of cytotoxicity of hydrogel extracts in culture media prepared according to ISO 10993-12 and (ii) observation of cell growth and morphology in the presence of hydrogels as well as directly on the gel surface. Cytotoxicity of hydrogel extracts was evaluated using mouse embryonic fibroblast cell line (NIH/3T3) according to ISO 10 993-5, see Fig. 5.

The amount of DAC did not have any observable impact to the cytotoxicity of hydrogel extracts and all materials can be considered non-toxic according to ISO 10933-5.

Subsequently, the cell growth and morphology in the presence of hydrogels was studied for 96 h. Cell viability was quantified by MTT assay, and qualitative analysis was done by observation under the microscope. Cell morphology was checked every day until reference reached confluency. Results are shown in Fig. 6, together with micrographs of cells cultivated in the presence of hydrogels for 96 h.

The presence of hydrogel samples has no observable effect on cell growth or morphology. Cells were growing at the same rate in the presence of hydrogels as in their absence and reached full confluency at the same time (Fig. 6, top). Likewise, the morphology was not affected by the hydrogels in any way, and fibroblasts retained their typical elongated shapes, see micrographs in Fig. 6. Cells were also seeded directly to the hydrogel surface in an attempt to observe they growth and morphology in direct contact with the hydrogel. However, cells did not adhere to hydrogel surface at all, making the evaluation impossible.

It should be also noted that no degradation of hydrogels was observed during the tests or when samples were kept under *in vitro* conditions (submerged to culture medium, seeded with NIH/3T3 cells, 37 °C) for one week. Surface of samples remained smooth, without signs of weathering or degradation and no difference in weight of the samples before and after the tests was observed.

To summarize, absence of cell migration/attachment to the hydrogel surface, no observable impact of hydrogel presence on the cell growth together with no observable degradation supports the suitability of hydrogel films as wound dressings. Additional tests are however required before biosafety in vivo can be claimed.

3.6. Transdermal absorption study

Transdermal absorption was studied using caffeine-loaded hydrogel samples. Caffeine was selected as a model substance for the study of transdermal absorption of hydrophilic compounds [22]. Hydrogel samples (1 cm in diameter) were loaded with caffeine and transdermal absorption of caffeine studied using skin from pig's earlobe, see Section 2.8 for more details. Amount of absorbed caffeine was determined by HPLC analysis.

The total amount of caffeine in the samples and calculated dose per 1 cm^2 skin is given in Table 3. All samples were loaded by the same method, but the total dose of caffeine differs between samples because of their different EWC, gel fractions and equilibrium swelling. The highest amount of caffeine was loaded in the sample L-130 (~900 μg), while sample H-130 was able to absorb the smallest amount (~500 μg).

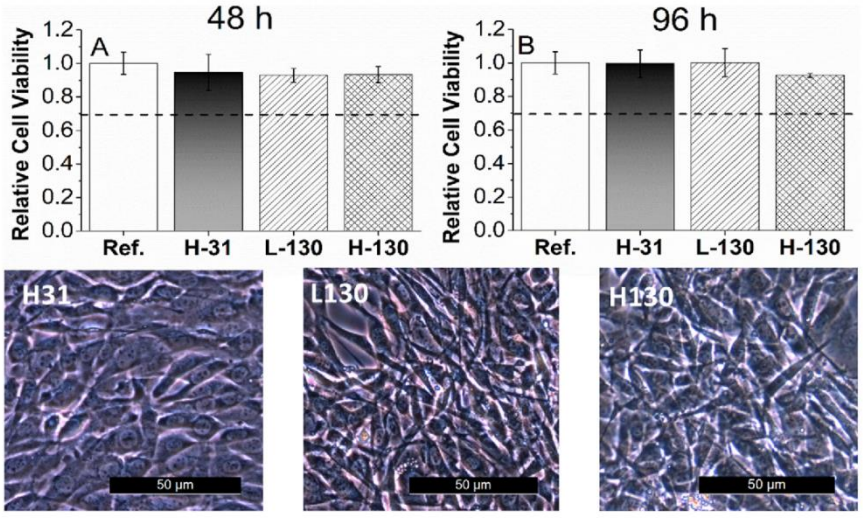

Fig. 6. Relative NIH/3T3 cell viability of cells incubated in the presence of hydrogel samples for 48 and 96 h, respectively, and micrographs of cells incubated for 96 h. Experiments were performed in quadruplicates; error bars represent standard deviations.

Table 3
The amount of caffeine in the samples (μg) and the dose of caffeine per cm^2 of skin.

Sample	Total dose of caffeine (μg)	Dose per cm^2 (μg/cm^2)
L-130	896 ± 8	1134 ± 10
H-31	660 ± 6	832 ± 7
H-130	495 ± 1	625 ± 1
Reference	250	320

The aqueous caffeine solution containing a total dose of 250 μg was used as a reference [23].

The total amount of transdermally absorbed caffeine (ng) is shown in Fig. 7A, the time profile of caffeine absorption (ng/mL) in Fig. 7B, total amount of transdermally absorbed caffeine relative to applied dose (%) in Fig. 7C and the time profile of caffeine absorption relative to applied dose (%) in Fig. 7D. Results show that caffeine penetrates the skin relatively slowly over the entire monitored time interval (24 h). According to Trauer et al. [23], this is a result of the absence of blood supply to the skin during the in vitro study because much faster absorption of caffeine through the skin of a living organism was observed. As a result, only between 0.07% and 0.2% of total caffeine dose crosses the skin barrier within 24 h under the employed setup (Fig. 7C and D). Caffeine hydrophilicity is thus clearly making its penetration through *stratum corneum* challenging [32]. This is in agreement with findings of other authors, including Trauer et al. [23], Bonina et al. [33], Santander-Ortega et al. [34] and Pilloni et al. [35] who also observed the transdermal caffeine absorption in the order of tenths of the percent of the applied dose using a variety of different carriers.

Despite the relatively low amount of transdermally absorbed caffeine, differences between the samples are clearly visible. The highest total amount of absorbed caffeine (1400 ng/0.15%) was observed for the L-130 sample, while only between 350 and 450 ng (0.06–0.07%) of caffeine was absorbed from H-series samples over 24 h. This corresponds to the average caffeine penetration of 72.1 ng·cm^2/h for L-130, 24.3 ng·cm^2/h for H-31, 19.3 ng·cm^2/h for H-130 and 18.1 ng·cm^2/h for caffeine solution. On the other hand, when the differences in applied dose are considered (Fig. 7C), only the sample L-130 overcomes the reference solution in terms of total caffeine absorption with respect to applied dose. However, while the amount of the drug absorbed from the caffeine solution linearly increases with time, the amount of caffeine absorbed from the hydrogels peaks between 8 and 12 h, respectively (Fig. 7B and D) showing higher effectivity of initial caffeine absorption from all hydrogels.

Comparing individual hydrogel samples, higher effectivity of caffeine absorption from L-130 stands out. The amount of caffeine permeated from the L-130 sample is approximately twice larger than from H-series samples, Fig. 7C, D. The higher efficiency of sample L-130 is assumed to be caused by its physical properties, namely the lowest elasticity among all tested materials. While more elastic H-series samples tend to keep their original shape on uneven skin surface, the L-130

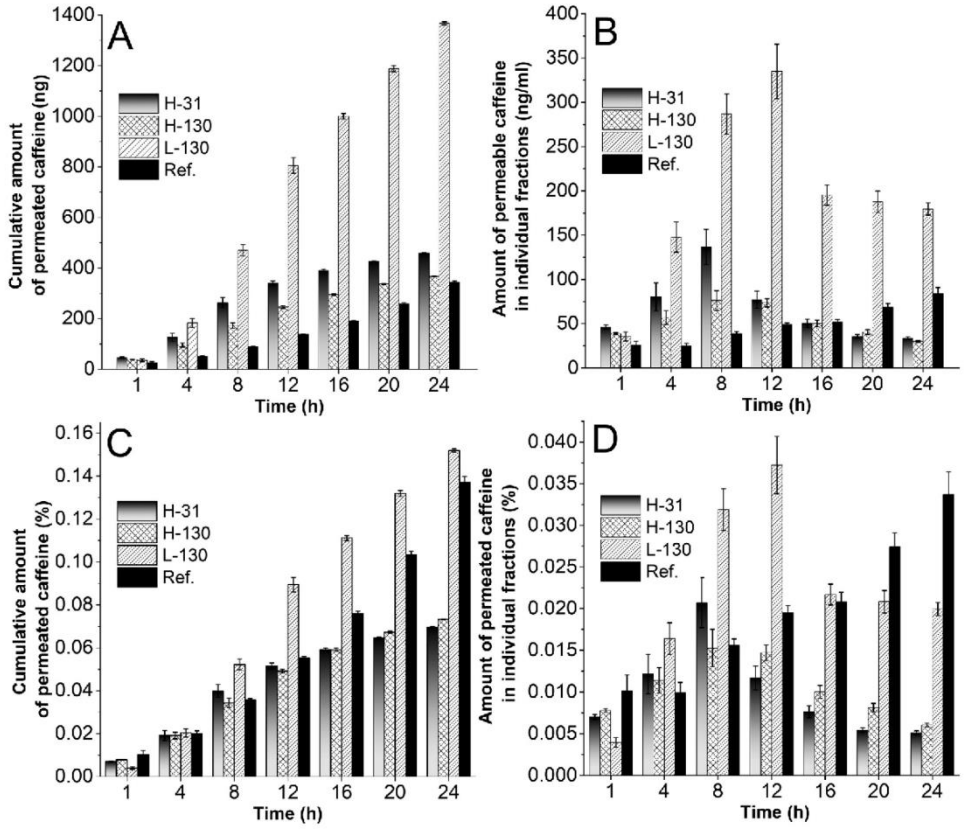

Fig. 7. The cumulative amount of permeated caffeine (ng) (part A), the time-dependent amount of permeated caffeine (ng/mL) (part B), total amount of transdermally absorbed caffeine relative to applied dose (%) (part C) and the time profile of caffeine absorption relative to applied dose (%) (part D). Ref. stands for the reference caffeine solution. Measurements were performed in triplicates; error bars represent standard deviations.

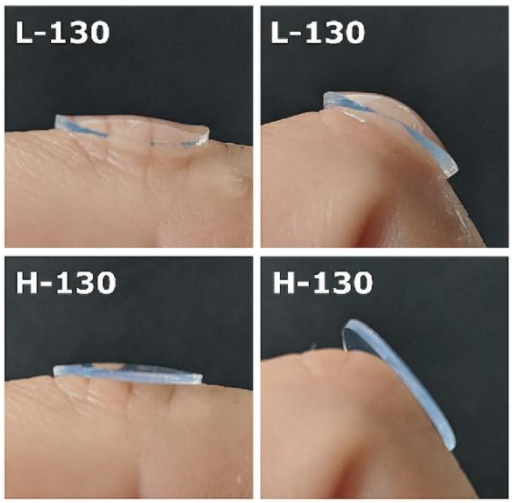

Fig. 8. The comparison of L-130 and H-130 hydrogels on the uneven skin surface.

adheres to the skin considerably better, see comparison of L-130 and H-130 hydrogel in Fig. 8. Because adherence to the skin is one of the key qualities dictating effectiveness of transdermal absorption, [4] this observation readily explain the improved transdermal delivery of caffeine from L-130 sample.

The hydrogel L-130 is thus assumed to be the most promising candidate for transdermal administration of biologically active substances from all tested materials without using any skin-penetration enhancers.

4. Conclusion

The combination of different concentration of crosslinker, 2,3-dialdehyde cellulose, DAC, and different molecular weight of the matrix, poly(vinyl alcohol), PVA, was used to optimize the properties of thin PVA/DAC hydrogel films towards topical applications. While changing the amount of crosslinker is a standard method for tuning the properties of hydrogels, simultaneous change of the molecular weight of the second hydrogel component provides another, yet often overlooked, degree of freedom which may be exploited to obtain the material with specific properties. Detailed analysis revealed that increased M_w of PVA influences hydrogel network parameters at (macro)molecular level (crosslink density, mesh size) providing additional stabilization. The impact of these molecular-scale changes on bulk properties of hydrogels is largest for equilibrium swelling capacity, viscoelastic characteristics and it also notably improves physical properties of L-130 films compared to L-31 ones (L-130 samples did not disintegrate during handling unlike the L-31). On the other hand, the specific surface area and the total pore volume of lyophilized samples is governed by the amount of crosslinker and does not depend on the type of PVA, which however influences the mean pore size. Neither the amount of crosslinker nor the molecular weight of PVA has a significant influence on drug release rates, likely because the role of hydrogel network density does not manifest in thin-film formulations. All hydrogels were non-cytotoxic under in vitro conditions, they did not affect the cellular growth and cell morphology or support the adherence of cells to their surface, which imply their suitability as biomaterials for transdermal drug delivery and wound dressings.

The best candidate for preparation of dermal patches and masks intended for transdermal delivery of biologically-active compounds is the hydrogel L-130, which is prepared using higher-molecular weight PVA matrix in combination with a lower concentration of crosslinker. It has high porosity and high water content (drug-loading capacity), physical properties allowing easy handling and the best adherence to the skin from all tested samples, which enhances its transdermal drug delivery properties. Conversely, a combination of higher M_w of PVA and a higher concentration of crosslinker leads to more elastic hydrogels with a denser network.

CRediT authorship contribution statement

Monika Muchová: Investigation, Visualization, Formal analysis, Writing - original draft. **Lukáš Münster:** Investigation, Visualization, Writing - original draft, Writing - review & editing. **Zdenka Capáková:** Investigation. **Veronika Mikulcová:** Investigation. **Ivo Kuřitka:** Resources, Funding acquisition. **Jan Vícha:** Conceptualization, Supervision, Writing - original draft, Writing - review & editing.

Declaration of competing interest

The authors declare that they have no known competing financial interests or personal relationships that could have appeared to influence the work reported in this paper.

Acknowledgement

This work was supported by the Ministry of Education, Youth and Sports of the Czech Republic Program NPU I (LO1504). M.M. was supported by the internal grant for specific research from Tomas Bata University in Zlín no. IGA/CPS/2020/003.

References

[1] E. Caló, V.V. Khutoryanskiy, Biomedical applications of hydrogels: a review of patents and commercial products, Eur. Polym. J. 65 (2015) 252–267, https://doi.org/10.1016/j.eurpolymj.2014.11.024.
[2] G.D. Winter, Formation of the scab and the rate of epithelization of superficial wounds in the skin of the young domestic pig, Nature 193 (1962) 293–294, https://doi.org/10.1038/193293a0.
[3] E.A. Kamoun, E.-R.S. Kenawy, X. Chen, A review on polymeric hydrogel membranes for wound dressing applications: PVA-based hydrogel dressings, J. Adv. Res. 8 (2017) 217–233, https://doi.org/10.1016/j.jare.2017.01.005.
[4] M.E. Parente, A.O. Andrade, G. Ares, F. Russo, Á. Jiménez-Kairuz, Bioadhesive hydrogels for cosmetic applications, Int. J. Cosmet. Sci. 37 (2015) 511–518, https://doi.org/10.1111/ics.12227.
[5] H. Ruan, Q. Hu, D. Wen, Q. Chen, G. Chen, Y. Lu, J. Wang, H. Cheng, W. Lu, Z. Gu, A dual-bioresponsive drug-delivery depot for combination of epigenetic modulation and immune checkpoint blockade, Adv. Mater. 31 (2019) 1806957, https://doi.org/10.1002/adma.201806957.
[6] C. Wang, J. Wang, X. Zhang, S. Yu, D. Wen, Q. Hu, Y. Ye, H. Bomba, X. Hu, Z. Liu, G. Dotti, Z. Gu, In situ formed reactive oxygen species–responsive scaffold with gemcitabine and checkpoint inhibitor for combination therapy, Sci. Transl. Med. 10 (2018), https://doi.org/10.1126/scitranslmed.aan3682.
[7] J.K. Li, N. Wang, X.S. Wu, Poly(vinyl alcohol) nanoparticles prepared by freezing–thawing process for protein/peptide drug delivery, J. Control. Release 56 (1998) 117–126, https://doi.org/10.1016/S0168-3659(98)00089-3.
[8] S.-H. Hyon, W.-I. Cha, Y. Ikada, M. Kita, Y. Ogura, Y. Honda, Poly(vinyl alcohol) hydrogels as soft contact lens material, J. Biomater. Sci. Polym. Ed. 5 (1994) 397–406, https://doi.org/10.1163/156856294X00103.
[9] U.-J. Kim, S. Kuga, M. Wada, T. Okano, T. Kondo, Periodate oxidation of crystalline cellulose, Biomacromolecules 1 (2000) 488–492, https://doi.org/10.1021/bm0000337.
[10] L. Münster, J. Vícha, J. Klofáč, M. Masař, P. Kucharczyk, I. Kuřitka, Stability and aging of solubilized dialdehyde cellulose, Cellulose 24 (2017) 2753–2766, https://doi.org/10.1007/s10570-017-1314-x.
[11] U.-J. Kim, M. Wada, S. Kuga, Solubilization of dialdehyde cellulose by hot water, Carbohydr. Polym. 56 (2004) 7–10, https://doi.org/10.1016/j.carbpol.2003.10.013.
[12] I. Sulaeva, K.M. Klinger, H. Amer, U. Henniges, T. Rosenau, A. Potthast, Determination of molar mass distributions of highly oxidized dialdehyde cellulose by size exclusion chromatography and asymmetric flow field-flow fractionation, Cellulose 22 (2015) 3569–3581, https://doi.org/10.1007/s10570-015-0769-x.
[13] J.A. Sirviö, H. Liimatainen, M. Visanko, J. Niinimäki, Optimization of dicarboxylic acid cellulose synthesis: reaction stoichiometry and role of hypochlorite scavengers, Carbohydr. Polym. 114 (2014) 73–77, https://doi.org/10.1016/j.carbpol.2014.07.

081.
[14] G. Yan, X. Zhang, M. Li, X. Zhao, X. Zeng, Y. Sun, X. Tang, T. Lei, L. Lin, Stability of soluble dialdehyde cellulose and the formation of hollow microspheres: optimization and characterization, ACS Sustain. Chem. Eng. 7 (2019) 2151–2159, https://doi.org/10.1021/acssuschemeng.8b04825.
[15] H. Liimatainen, M. Visanko, J.A. Sirviö, O.E.O. Hormi, J. Niinimaki, Enhancement of the nanofibrillation of wood cellulose through sequential periodate–chlorite oxidation, Biomacromolecules 13 (2012) 1592–1597, https://doi.org/10.1021/bm300319m.
[16] U.-J. Kim, Y.R. Lee, T.H. Kang, J.W. Choi, S. Kimura, M. Wada, Protein adsorption of dialdehyde cellulose-crosslinked chitosan with high amino group contents, Carbohydr. Polym. 163 (2017) 34–42, https://doi.org/10.1016/j.carbpol.2017.01.052.
[17] L. Münster, J. Vícha, J. Klofáč, M. Masař, A. Hurajová, I. Kuřitka, Dialdehyde cellulose crosslinked poly(vinyl alcohol) hydrogels: influence of catalyst and crosslinker shelf life, Carbohydr. Polym. 198 (2018) 181–190, https://doi.org/10.1016/j.carbpol.2018.06.035.
[18] L. Münster, Z. Capáková, M. Fišera, I. Kuřitka, J. Vícha, Biocompatible dialdehyde cellulose/poly(vinyl alcohol) hydrogels with tunable properties, Carbohydr. Polym. 218 (2019) 333–342, https://doi.org/10.1016/j.carbpol.2019.04.091.
[19] A. Ganeshpurkar, A.K. Saluja, The pharmacological potential of rutin, Saudi Pharm. J. 25 (2017) 149–164, https://doi.org/10.1016/j.jsps.2016.04.025.
[20] N.Q. Tran, Y.K. Joung, E. Lih, K.D. Park, In situ forming and rutin-releasing chitosan hydrogels as injectable dressings for dermal wound healing, Biomacromolecules 12 (2011) 2872–2880, https://doi.org/10.1021/bm200326g.
[21] J.K. Choi, S.-H. Kim, Rutin suppresses atopic dermatitis and allergic contact dermatitis, Exp. Biol. Med. (Maywood) 238 (2013) 410–417, https://doi.org/10.1177/1535370213477975.
[22] L. Luo, M.E. Lane, Topical and transdermal delivery of caffeine, Int. J. Pharm. 490 (2015) 155–164, https://doi.org/10.1016/j.ijpharm.2015.05.050.
[23] S. Trauer, A. Patzelt, N. Otberg, F. Knorr, C. Rozycki, G. Balizs, R. Büttemeyer, M. Linscheid, M. Liebsch, J. Lademann, Permeation of topically applied caffeine through human skin – a comparison of in vivo and in vitro data, Br. J. Clin. Pharmacol. 68 (2009) 181–186, https://doi.org/10.1111/j.1365-2125.2009.03463.x.
[24] P. Engel, L. Hein, A.C. Spiess, Derivatization-free gel permeation chromatography elucidates enzymatic cellulose hydrolysis, Biotechnol. Biofuels 5 (2012) 77, https://doi.org/10.1186/1754-6834-5-77.
[25] L. Münster, B. Hanulíková, M. Machovský, F. Latečka, I. Kuřitka, J. Vícha, Mechanism of sulfonation-induced chain scission of selectively oxidized polysaccharides, Carbohydr. Polym. 229 (2020) 115503, , https://doi.org/10.1016/j.carbpol.2019.115503.
[26] P.J. Flory, J. Rehner, Statistical mechanics of cross-linked polymer networks II. Swelling, J. Chem. Phys. 11 (1943) 521–526, https://doi.org/10.1063/1.1723792.
[27] N.A. Peppas, E.W. Merrill, Determination of interaction parameter χ_1, for poly (vinyl alcohol) and water in gels crosslinked from solutions, J. Polym. Sci. Polym. Chem. Ed. 14 (1976) 459–464, https://doi.org/10.1002/pol.1976.170140216.
[28] S.K.H. Gulrez, S. Al-Assaf G.O, Hydrogels: methods of preparation, characterisation and applications, in: A. Carpi (Ed.), Progress in Molecular and Environmental Bioengineering - From Analysis and Modeling to Technology Applications, InTech, 2011, , https://doi.org/10.5772/24553.
[29] B.J. Tighe, The role of permeability and related properties in the design of synthetic hydrogels for biomedical applications, Brit. Poly. J. 18 (1986) 8–13, https://doi.org/10.1002/pi.4980180104.
[30] N.A. Peppas, Y. Huang, M. Torres-Lugo, J.H. Ward, J. Zhang, Physicochemical foundations and structural design of hydrogels in medicine and biology, Annu. Rev. Biomed. Eng. 2 (2000) 9–29, https://doi.org/10.1146/annurev.bioeng.2.1.9.
[31] H. Omidian, S.-A. Hasherni, F. Askari, S. Nafisi, Swelling and Crosslink Density Measurements for Hydrogels, (n.d.) 6.
[32] M. Dias, A. Farinha, E. Faustino, J. Hadgraft, J. Pais, C. Toscano, Topical delivery of caffeine from some commercial formulations, Int. J. Pharm. 182 (1999) 41–47, https://doi.org/10.1016/S0378-5173(99)00067-8.
[33] F. Bonina, S. Bader, L. Montenegro, C. Scrofani, M. Visca, Three phase emulsions for controlled delivery in the cosmetic field, Int. J. Cosmet. Sci. 14 (1992) 65–74, https://doi.org/10.1111/j.1467-2494.1992.tb00040.x.
[34] M.J. Santander-Ortega, T. Stauner, B. Loretz, J.L. Ortega-Vinuesa, D. Bastos-González, G. Wenz, U.F. Schaefer, C.M. Lehr, Nanoparticles made from novel starch derivatives for transdermal drug delivery, J. Control. Release 141 (2010) 85–92, https://doi.org/10.1016/j.jconrel.2009.08.012.
[35] M. Pilloni, G. Ennas, M. Casu, A.M. Fadda, F. Frongia, F. Marongiu, R. Sanna, A. Scano, D. Valenti, C. Sinico, Drug silica nanocomposite: preparation, characterization and skin permeation studies, Pharm. Dev. Technol. 18 (2013) 626–633, https://doi.org/10.3109/10837450.2011.653821.

Appendix II

Muchová, M.; Münster, L.; Vávrová, A.; Capáková, Z.; Kuřitka, I.; Vícha, J. Comparison of Dialdehyde Polysaccharides as Crosslinkers for Hydrogels: The Case of Poly(Vinyl Alcohol). *Carbohydrate Polymers* **2022**, *279*, 119022. https://doi.org/10.1016/j.carbpol.2021.119022.

Carbohydrate Polymers 279 (2022) 119022

Contents lists available at ScienceDirect

Carbohydrate Polymers

journal homepage: www.elsevier.com/locate/carbpol

Comparison of dialdehyde polysaccharides as crosslinkers for hydrogels: The case of poly(vinyl alcohol)

Monika Muchová, Lukáš Münster, Alžběta Vávrová, Zdenka Capáková, Ivo Kuřitka, Jan Vícha *

Centre of Polymer Systems, Tomas Bata University in Zlín, tř. Tomáše Bati 5678, 760 01 Zlín, Czech Republic

ARTICLE INFO

Keywords:
Dialdehyde
Cellulose
Dextran
Dextrin
Hyaluronic acid
Crosslinking
Poly(vinyl) alcohol

ABSTRACT

A little is known about the link between the macromolecular architecture of dialdehyde polysaccharides (DAPs), their crosslinking capabilities, and the properties of resulting hydrogels. Here, DAPs based on cellulose, dextrin, dextran, and hyaluronate were compared as crosslinkers for poly(vinyl alcohol), PVA. The swelling, network parameters, viscoelastic properties, porosity, and cytotoxicity of PVA/DAP hydrogels were investigated concerning the crosslinker structure, molecular weight, aldehyde group density per macromolecule, and the size of spontaneously formed crosslinker nano-assemblies. Generally, crosslinkers based on linear polysaccharides (cellulose, hyaluronate) performed more reliably, while the presence of branching could be both beneficial (dextran) but also detrimental (dextrin) at lower crosslinker concentrations. For example, the hydrogel swelling differed by up to one-third (600 *vs.* 400%) and storage modulus even by up to one half (~7000 *vs.* ~3500 Pa) depending on crosslinker structure and properties. These differences were rationalized by variances in crosslinking modes derived based on obtained data.

1. Introduction

Hydrogels are three-dimensional networks of crosslinked macromolecules capable of absorbing large amounts of water. (Caló and Khutoryanskiy, 2015) Methods used for hydrogel crosslinking are numerous, ranging from purely physical crosslinking based *e.g.* on electrostatic interactions, hydrogen bonding, or hydrophobic association, to the formation of strong covalent bonds between the crosslinker and the polymer matrix. (Li and Mooney, 2016) Regarding the chemically crosslinked hydrogels, the choice of the crosslinker often depends on the nature of matrix polymer, particularly on its functional groups. Current methods of crosslinking are summarized in several reviews on this topic (Hennink and van Nostrum, 2012; Hu et al., 2019) and include photo-catalyzed bonding, enzyme-catalyzed reactions, and various methods of "click chemistry" such as Diels-Alder reactions, Michael-type addition, oxime reaction, and Schiff base formation. Given the broadness of this topic, in the following, we focus only on crosslinking of chosen matrix polymer, the poly(vinyl alcohol), PVA. The PVA is a biocompatible synthetic polymer used for the preparation of hydrogels for a variety of biomedical applications, in particular the wound dressings, systems for chronic wound management, drug delivery, and contact lenses. (Kamoun et al., 2015, 2017; Münster et al., 2019) Although the PVA can form physically crosslinked hydrogels by the freezing-thawing method, which induces the formation of crystallites and PVA chain entanglement (Peppas and Merrill, 1977), physically crosslinked PVA hydrogels are rather stiff materials with limited hydrophilicity and elasticity, which may hinder their biomedical applications. (Kamoun et al., 2015; Muchová et al., 2020) To overcome these limitations, PVA blends with various other (bio)polymers, as well as chemically crosslinked PVA hydrogels, were developed. (Kamoun et al., 2015) These include PVA hydrogels crosslinked by small-molecule organic dialdehydes, such as glutaraldehyde, GA. (Rudra et al., 2015) Dialdehydes are, in general, well-known crosslinkers capable of two major types of reactions: i) the Schiff base formation with substrates containing $-NH_2$ groups, such as chitosan (Hu et al., 2019; Kim et al., 2017), and ii) the hemiacetal bond formation between the reactive –CHO groups of the dialdehyde and –OH groups of the matrix, which is ideal for crosslinking of hydroxyl group-rich matrix polymers such as PVA (Dai and Barbari, 1999). The small molecule organic dialdehydes are, however, highly toxic even in residual amounts (Speer et al., 1980) which makes them ill-suited for rapidly developing biomedical applications. (Kim et al., 2017) Hence, dialdehyde polysaccharides (DAPs) emerged as an alternative to organic dialdehydes such as GA. DAPs are prepared by regioselective oxidation of source polysaccharides containing neighboring (vicinal)

* Corresponding author.
E-mail address: jvicha@utb.cz (J. Vícha).

https://doi.org/10.1016/j.carbpol.2021.119022
Received 16 September 2021; Received in revised form 8 December 2021; Accepted 13 December 2021
Available online 16 December 2021

–OH groups using periodate salt, which introduces a pair of reactive aldehyde groups in each oxidized unit, see Fig. 1A. For an overview of the chemistry and applications of DAPs see the recent review by Ding and Wu (2020), here we focus on their use as crosslinking agents for PVA. The DAPs are capable of PVA crosslinking *via* the same mechanism as small-molecule dialdehydes, *i.e.* the formation of hemiacetal bonds, see Fig. 1B for reaction scheme. Their biomacromolecular character, however, brings several key advantages over their organic counterparts. Because source polysaccharides can be obtained from renewable resources and consumed periodate can be regenerated using methods of green chemistry (Koprivica et al., 2016), the DAPs are considered to be a sustainable resource, which contributes to the rising interest in their various uses. (Yan et al., 2018) Each DAP macromolecule also contains multiple crosslinking sites which amount can be easily controlled by altering the degree of oxidation (*DO*). (Ding and Wu, 2020) Their macromolecular character has also been shown to lead to the formation of high-crosslink density regions formed around DAP macromolecules, which are embedded in otherwise mostly physically crosslinked (entangled) PVA matrix. (Münster et al., 2018) This crosslinking mode has been termed as a "two-phase network topology" and shown to significantly improve hydrogel physical properties compared to GA, particularly at lower crosslinker concentrations. It was also discovered that the molecular weight of used DAP influences the size of highly crosslinked domains and thus the properties of resulting hydrogels. (Münster et al., 2019) Essentially, the lower the average molecular mass of DAP is, the greater is the total number of highly crosslinked regions, but, the smaller the dimensions of highly crosslinked regions are, the fewer matrix chains can be crosslinked simultaneously.

Although the method of DAPs preparation has been intensively studied concerning different source materials (Kim et al., 2000; Kristiansen et al., 2010; Münster et al., 2020; Perlin, 2006), studies that would directly compare different DAPs in a given application(s), such as hydrogel crosslinking, are lacking. Hypothetically, it may be possible to exploit the structural differences between DAPs to enhance the properties of hydrogels towards the desired goal(s). Hence, in this contribution, we have prepared and investigated a set of DAPs derived from structurally different polysaccharides (cellulose, dextran, dextrin, and hyaluronic acid) and compared them as crosslinkers for the PVA. The PVA was selected as a model substrate due to its well-defined structure, well-understood chemistry, wide application potential (see above), easy handling, and our experience with the preparation of various PVA hydrogels. (Muchová et al., 2020; Münster et al., 2018, 2019) The impact of crosslinker macromolecular structure, molecular weight, density of –CHO groups, and size of its nano-assemblies on the physical (swelling, hydrogels network parameters, rheological properties, porosity) and biological (cytotoxicity) properties of PVA/DAP hydrogels have been studied, the differences between the crosslinkers are discussed and the best candidates for given applications are highlighted. The structures of source polysaccharides and respective dialdehydes are given in Fig. 1C (DAC – 2,3-dialdehyde cellulose, DAH – 2,3-dialdehyde hyaluronate, DXI – 2,3-dialdehyde dextrin, DXA – 2,3-dialdehyde dextran). Regarding the selected source polysaccharides, cellulose is the world's most widely occurring polysaccharide composed of linear chains of anhydroglucose units (AGUs) joined by β-(1 → 4) glycosidic bonds. Periodate oxidation of cellulose is characterized by the cleavage of the C2–C3 bond of the AGUs, leading to the formation of 2,3-dialdehyde cellulose (DAC). (Kim et al., 2000) DAC as a crosslinker has attractive properties for wound dressing applications. (Mayer et al., 2021; Mou et al., 2017; Muchová et al., 2020). Hyaluronic acid (HA) is a linear acidic glycosaminoglycan composed of D-glucuronic acid and *N*-acetyl-D-glucosamine connected by alternating β-(1 → 4) and β-(1 → 3) glycosidic bonds. Unlike cellulose, only D-glucuronic acid units of HA are oxidized, while *N*-acetyl-D-glucosamine units are resistant to periodate oxidation due to glycosidic bond at C3, see Fig. 1C. DAH has been used *e.g.* as a crosslinker for hydrogels designed for chronic wound management and tissue regeneration. (Gao et al., 2019; S. Li et al., 2020; Patterson et al., 2010) Dextrin has a branched structure composed of AGUs connected by α-(1 → 4) glycosidic bonds forming the main chain and

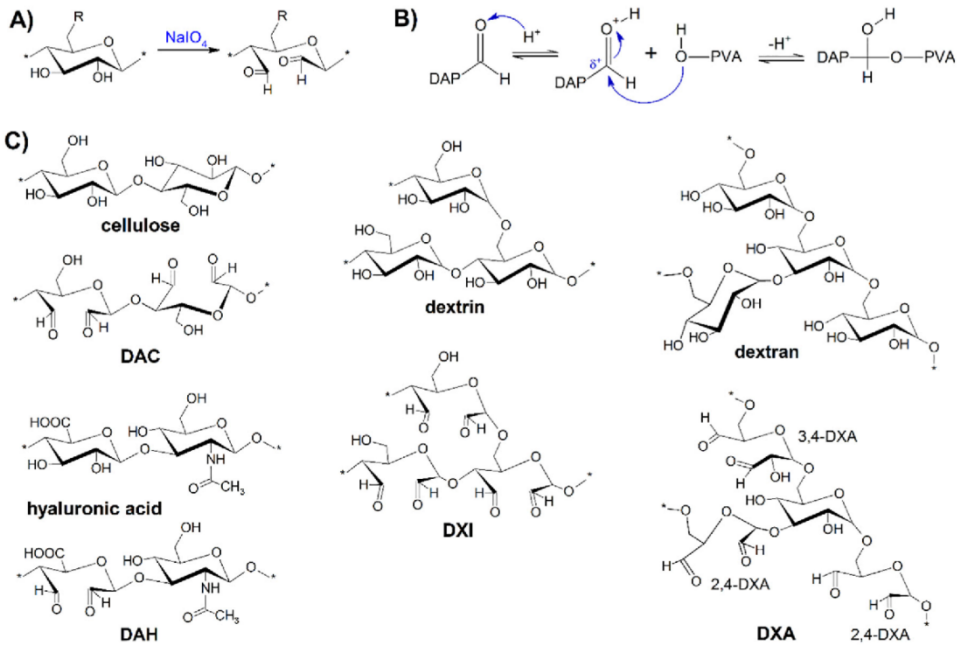

Fig. 1. A) Periodate oxidation of polysaccharide featuring vicinal diol group at C2 and C3; B) General scheme of hemiacetal bond formation between DAP and PVA; C) Structures of source polysaccharides (dextran, dextrin, cellulose, and hyaluronic acid) and corresponding dialdehyde derivatives.

short sidechains connected to the backbone *via* α-(1 → 6) glycosidic bonds. Periodate oxidation of dextrin leads to the formation of 2,3-dialdehyde dextrin (DXI). (Münster et al., 2020) Dextrans are composed of AGU chains bonded predominantly by α-(1 → 6) glycosidic bonds with a degree of α-(1 → 3) branching. They are produced by bacteria of the *Leuconostoc* and *Streptococcus* genera. Dextran-based hydrogels and nanogels are often used for biomedical applications, such as drug delivery (Münster, Fojtů, Muchová, et al., 2021; Su et al., 2021), and also exhibit high antibacterial activity (Zhang et al., 2021). Periodate oxidation of dextran leads to a mixture of 3,4-, 2,4- and 2,3-dialdehyde-dextran as described previously (Maia et al., 2011; Münster, Fojtů, Muchová, et al., 2021) Doubly oxidized 2,4-derivatives are the most abundant, while the 2,3-dialdehyde dextran is much less common. Moreover, α-(1 → 3) branched dextran units are resistant to periodate oxidation due to the absence of vicinal hydroxyl groups. For the sake of simplicity, all types of periodate oxidized dextran are referred to as dialdehyde dextran (DXA) in the following text.

2. Experimental

2.1. Materials

Following source polysaccharides were employed in this study: cellulose SigmaCell type 20 (weight-average molecular weight M_w = 76 kDa, degree of polymerization DP = 468, polydispersity index PDI = 4.7; Sigma Aldrich Co.), dextrin from corn starch type I (M_w = 52 kDa, DP = 325, PDI = 2.3; Sigma Aldrich Co.), dextran from *Leuconostoc spp.* (M_w = 71, DP = 449, PDI = 1.9; Sigma Aldrich Co.) and sodium hyaluronate (M_w = 1.5 MDa, DP = 3740, PDI = 4.3; Contipro Ltd., Czech Republic). The chemicals used in the primary and secondary oxidations of polysaccharides included sodium periodate ($NaIO_4$; Penta, Czech Republic), ethylene glycol (Penta, Czech Republic), sodium chlorite ($NaClO_2$, 80%; Sigma Aldrich Co.), acetic acid (CH_3COOH, ≥ 99.8%; Sigma Aldrich Co.), sodium acetate trihydrate ($CH_3COONa{\cdot}3H_2O$; Penta, Czech Republic) and sodium hydroxide (NaOH; Lachner, Czech Republic). Other chemicals involved in the characterization of DCPs included hydroxylamine hydrochloride (HAHCl; Sigma Aldrich), hydrochloric acid (HCl; Penta, Czech Republic), sodium nitrate ($NaNO_3$, Lachner, Czech Republic), and disodium phosphate dodecahydrate ($Na_2HPO_4{\cdot}12H_2O$, VWR, Czech Republic). Reagents used for the biological experiments included calf serum (CS) (mycoplasma-free), penicillin-streptomycin, trypsin, Dulbecco's Modified Eagle's Medium (DMEM), phosphate-buffered saline pH 7.2 (PBS, BioSera, France), 3-(4,5-dimethylthiazol-2-yl)-2,5-diphenyl tetrazolium bromide (MTT) reagent and dimethyl sulfoxide (DMSO, Sigma-Aldrich Co.). All chemicals were of analytical grade and were used without further purification. Demineralized water with a conductivity below 0.1 μS/cm was used throughout the experiments.

2.2. Preparation of crosslinkers (DAP) and hydrogels (PVA/DAP)

The flowchart of crosslinker and hydrogel preparation and characterization is given in Scheme S1. The 2,3-dialdehyde cellulose (DAC), 2,3-dialdehyde hyaluronate (DAH), 2,3-dialdehyde dextrin (DXI), and dialdehyde dextran (DXA) were prepared by oxidation of 1 gram of source polysaccharide dissolved in 50 mL of water using 1.65 g of sodium periodate. Reaction mixtures were stirred at 30 °C for 72 h (DAC), 24 h (DAH), 8 h (DXI), and 4 h (DXA) in the dark. The duration of each oxidation was previously established based on the kinetics of periodate consumption. (Münster, Fojtů, Capáková, et al., 2021) Reactions were stopped by the addition of 1 mL of ethylene glycol. The insoluble DAC was purified by centrifugation and repeated homogenization using WiseTis HG-15 homogenizer (Witeg, Germany). A partially soluble DXI sample was dialyzed for 1 day against demineralized water using dialysis tubing of 14 kDa molecular weight cut off (*MWCO*, Sigma Aldrich Co.). The resulting DAC suspension and DXI sample containing insoluble fraction was solubilized at 80 °C for 2 h in an oil bath under reflux. Obtained solutions were purified by centrifugation and filtration to remove residues of non-solubilized material and dialyzed again for 1 day using 14 kDa *MWCO* dialysis tubing. The soluble dialdehyde samples (DXA and DAH) were purified by filtration and dialyzed for 1 day using 14 kDa *MWCO* dialysis tubing. All purified materials were flash-frozen using an ethanol ice bath and lyophilized to obtain dialdehyde polysaccharide powders.

The following general procedure was utilized for the hydrogel preparation: 10 g of PVA was dissolved in 80 mL of water heated to 80 °C. Subsequently, the acidic catalyst (10 mL of 1.3 M HCl) was added and solutions thoroughly mixed. Next, solutions of DAPs containing i) 1.25 mmol/g of —CHO groups (corresponding to 0.1 wt% of crosslinker for DAC, DXI, and DXA and 0.25 wt% for DAH, which has 2.5× fewer —CHO groups per unit of mass) and, ii) 12.5 mmol/g (corresponding to 1 wt% of crosslinker for DAC, DXI, and DXA and 2.5 wt% for DAH) were added to acidified PVA solutions. Reaction mixtures were thoroughly stirred for 30 min, poured onto Petri dishes (d = 140 mm), and allowed to crosslink upon drying at 30 °C. Prepared films were then washed in water for 1 week to remove non-crosslinked material, and disc-shaped samples of 15 mm in diameter were cut out. Prepared hybrid hydrogel samples are generally referred to as PVA/DAP and are further divided and labelled according to the type of the crosslinker (DAC, DXI, DXA, or DAH) and by -L and —H index referring to lower (0.1/0.25 wt%) or higher (1/2.5 wt%) concentration of the crosslinker. Part of swelled PVA/DAP hydrogel samples (H-series) was moved to closed reaction flasks containing demineralized water, which were subsequently heated to 70 °C for 3 h (samples noted as DAP-HT). The goal of this treatment was to accentuate the role of chemical crosslinks by disrupting hydrogen bonding in residual crystallites which were formed between PVA chains during drying.

2.3. Methods of DAPs characterization

Qualitative FT-IR analysis (see Support Information SI, Fig. S1) was performed on prepared lyophilized DAPs powders using the infrared spectrometer Nicolet 6700 FT-IR (Thermo Fisher Scientific, USA) equipped with the diamond crystal in the ATR mode in a span of wavelengths 4000–700 cm^{-1} (res.: 4 cm^{-1}, scans: 64, the suppression of atmospheric gases enabled).

All prepared DAPs were characterized in the terms of their degree of oxidation (*DO*) by oxime reaction. Briefly, 0.1 g of each DAP was dissolved in 30 mL of demineralized water, and pH was set to 4.0 by 0.1 M HCl. A solution of HAHCl (20 mL containing 0.43 g of HAHCl) was basified using 0.1 M NaOH to pH 4.0 and mixed with each of acidified DAP solutions. The mixtures were then stirred at laboratory temperature for 24 h in closed containers. The conversion of aldehyde to oxime was determined by observing the consumption of 0.1 N NaOH. (Veelaert et al., 1997).

A gel permeation chromatography (GPC) study was conducted on dicarboxylated derivatives (DCPs) prepared from DAPs. The underlying reason is better-defined composition and higher stability of DCPs compared to their DAP precursors. This setup was employed previously with good results. (Münster et al., 2017) DCPs were prepared by slightly modified oxidation protocol of DAPs by $NaClO_2$ (—CHO: $NaClO_2$ molar ratio 1:4, assuming 12.5 mmol/g of —CHO in DAC, DXI, and DXA and 5.01 mmol/g of —CHO in DAH). The concentration of $NaClO_2$ was set to 0.2 M; the oxidation reactions were performed in the presence of 0.5 M CH_3COOH. The secondary oxidation started with the dropwise addition of concentrated $NaClO_2$ solution into the acidified solution of given dialdehyde and the reaction ran for 7 h at 30 °C in dark. Subsequent addition of 10 M NaOH to pH 8 terminated oxidation reaction, products were then purified by dialysis against demineralized water using 14 kDa *MWCO* dialysis tubing. After the dialysis, the pH of all samples was set to 7.4 by 0.1 M NaOH, solutions filtered, flash-frozen and lyophilized. Molecular weight analysis was carried out using a Waters HPLC Breeze

chromatographic system equipped with a Waters 2414 refractive index detector (drift tube $T = 60$ °C), a Tosoh TSKgel GMPW$_{XL}$ column (300 mm × 7.8 mm × 13 μm, $T = 30$ °C), and a mobile phase composed of 0.1 M of $NaNO_3$ and 0.05 M of $Na_2HPO_4 \cdot 12H_2O$ aqueous solution. A Pullulan polysaccharide calibration kit SAC-10 (Agilent Technologies, Inc.) in a span of M_w 342–805,000 g/mol was used for calibration.

Dynamic light scattering (DLS) analysis employed using a Zetasizer Nano ZS90 instrument (Malvern Instruments, UK) was used to determine zeta potential (ζ) and hydrodynamic radius (d_h) of DAP solutions. The measurements were performed on 1 mg/mL concentrated DAP samples at 25 °C using a DTS1070 cell and the Smoluchowski model.

2.4. PVA/DAP hydrogel network parameters

The network parameters were estimated based on the weight changes during swelling experiments on prepared 15 mm disc-shaped PVA/DAP hydrogel samples (DAP-L, DAP-H, and DAP-HT). The hydrogel discs were thoroughly washed in water for 1 week with regular changing of water. Subsequently, the swollen discs were gently dried to remove excess water, weighed, and dried at 30 °C in the oven till constant weight. The network parameters were determined using the equilibrium swelling theory proposed by Flory and Rehner (1943) as described in our previous works. (Münster et al., 2018, 2019).

2.5. Measurement of viscoelastic properties

Disc-shaped PVA/DAP hydrogel samples (d = 15 mm) were measured in an equilibrium swollen state using a rotational rheometer Anton Paar MCR 502 (Anton Paar, Austria) equipped with a D-PP15 shaft using a roughened aluminum plate with 15 mm diameter and ground plate with glued sandpaper both used to prevent slipping of samples during measurement. The measurement was performed at 37 °C in oscillation mode in frequency sweep from 1 to 10 Hz by applying a constant strain of 1%. The complex modulus G^* was calculated as the square root of the sum of the square of storage and loss modulus in the selected range of oscillatory measurement. The $tan\ \delta$ is defined as the ratio between loss and storage modulus (G''/G') and gives a measure of viscous to an elastic component of the material.

2.6. SEM and BET analysis of PVA/DAP cryogels

Before the scanning electron microscopy (SEM) analysis and measurements of specific surface area by multipoint Brunauer-Emmet-Teller (BET), hydrogel samples were lyophilized to form respective cryogels. PVA/DAP cryogels were then analyzed by scanning electron microscope Nova NanoSEM 450 (FEI, Czech Republic) operated at 5 kV accelerating voltage. All PVA/DAP sample specimens intended for SEM analysis were sputtered by gold-palladium nanoparticles to prevent the charge accumulation effect. BET analysis was conducted on PVA/DAP specimens degassed at 70 °C for 24 h evaluating absorption/desorption isotherms recorded at 77 K utilizing high precision surface area analyzer Belsorp-mini II (BEL Japan Inc., Japan).

2.7. XRD of PVA/DAP xerogels

X-ray diffraction analysis of PVA/DAP washed xerogels were performed on a Rigaku MiniFlex600 X-ray diffractometer in the diffraction 2θ angle range 5–95°, $Co_{K\alpha}$ ($\lambda = 1.789$ Å) radiation source was used with Kβ line filter.

2.8. Cytotoxicity

Thy cytotoxicity was assessed for crosslinkers as well as for pure hydrogels. Cytotoxicity in direct contact was determined for crosslinkers in concentrations of 0.05; 0.1; 0.5 and 1 mg/mL, while the cytotoxicity of hydrogels was measured on the sample extracts prepared according to the ISO 10993-12. Briefly, the extraction of 0.1 g hydrogel per 1 mL of culture media was carried out under stirring at 37 °C for 24 h. Extracts were tested in concentrations 50%, 75%, and 100% and were used immediately after their preparation. For both tests, mouse embryonic fibroblasts (NIH/3T3; ECCAC 93061524) were used. Firstly, the NIH/3T3 cells were seeded into the microtitration plates in concentration 1×10^5 per mL and let for pre-cultivation for 24 h. Subsequently, the solutions of crosslinkers and extracts were added to the cells and incubated for 24 h. All tests were performed in quadruplicates. After the incubation period, the cytotoxicity was measured using an MTT assay. The absorbance was measured at wavelength 570 nm on the multi-plate reader Infinite 200 PRO (Tecan, Switzerland). The results are presented in relative values where the absorbance of samples is compared to the reference (cells incubated in pure culture medium). The reference was set to 1 (meaning 100% viability). According to the ISO 10993-5 (2009), the decrease of cell mortality by 30% or more indicates a cytotoxic effect.

3. Results

3.1. Preparation and characterization of crosslinkers

DAPs were prepared as described in Section 2.2. Conditions of periodate oxidation were set to obtain fully oxidized materials (Münster et al., 2020; Münster, Fojtů, Capáková, et al., 2021), which were first characterized by FT-IR spectra, see Fig. S1 in SI. All prepared DAPs exhibit noticeable absorption bands around 1730 cm^{-1} (valence C=O vibrations from —CHO groups) and 875 cm^{-1} (symmetric valence —C—O—C— vibrations) in their IR spectra, signifying the presence of both free aldehyde groups and newly formed hemiacetal groups, respectively. Regarding the differences between DAPs, the dialdehydes of cellulose, dextran, and dextrin are composed of similar building blocks (*i.e.* oxidized glucopyranose units) and thus share very similar spectral patterns. On the other side, DAH exhibits typical absorption bands associated with the presence of —COOH groups in the glucuronic unit, namely the asymmetric valence —COO vibration around 1600 cm^{-1} and deformation vibration of —OH from —COOH around 1380 cm^{-1}. Contrary, the glucuronic acid fingerprint vibration band at 893 cm^{-1} (C—H deformation of the GlcA ring) is not present in the spectra of DAH, in which the C2–C3 bond is disrupted, indicating their quantitative oxidation.

The *DO* of individual DAPs, defined as a percentage of the total amount of basic structural units (monosaccharides for AGU-based materials and disaccharides for DAH) being oxidized to dialdehydes, was determined by oxime reaction, see Section 2.3 for methodology and Table 1 for results. While the DAH, DAC, and DXI are nearly fully oxidized (*DO* > 95%), the maximum *DO* of DXA is limited to ~85% by the presence of 15% of oxidation-resistant branched units. Note, however, that *DO* does not directly reflect the absolute amount of —CHO groups per unit of crosslinker mass (n_{-CHO}). The n_{-CHO} is given by the structure of the source polysaccharides, namely by the presence of vicinal —OH groups in their units. The fully oxidized cellulose and the dextrin thus contain 12.5 mmol/g of —CHO groups each, while the DXA oxidized from 85% contain 12.3 mmol/g of —CHO groups, which is comparable with DXI and DAC within the experimental error. On the other side, the presence of oxidation-resistant *N*-acetyl-D-glucosamine units in DAH reduces maximum —CHO content to 5.0 mmol/g, *i.e.* 2.5× lower than in the case of tested homoglycans. Hence, the amount of DAH crosslinker used during hydrogel preparation was increased by 2.5× to better assess the impact of molecular weight, structure, and —CHO group density of individual DAPs. Although this would somewhat increase the overall polymer concentration, the impact of this change on hydrogel properties should be much smaller than using a lower amount of crosslinker but with a 2.5× lower number of crosslinking hotspots.

To reliably establish the molecular weight of prepared dialdehydes, these were converted to corresponding dicarboxylated derivatives

Table 1
Number average molecular weight (M_n), weight average molecular weight (M_w), polydispersity index (*PDI*), degrees of polymerization (*DP*) of dicarboxy and dialdehyde polysaccharides, their *DO*, and molar amount of —CHO groups per unit of crosslinker mass (n_{-CHO}).

DCP	M_n (kDa)	M_w (kDa)	*PDI*	*DP*	DAP	M_n (kDa)	M_w (kDa)	*DO* (%)	n_{-CHO} (mmol/g)
DCDXA	44.1	84.8	1.92	420	DXA	30.2	58.0	85 ± 4	12.3 ± 0.4
DCH	24.8	47.8	1.92	103	DAH	21.4	41.2	99 ± 6	5.0 ± 0.3
DCDXI	16.9	36.9	2.17	157	DXI	11.5	25.2	98 ± 1	12.5 ± 0.2
DCC	16.9	31.2	1.84	132	DAC	11.5	21.2	95 ± 2	12.4 ± 0.3

(DCDXA – dicarboxy dextran, DCH – dicarboxy hyaluronate, DCDXI – dicarboxy dextrin, DCC – dicarboxy cellulose), see Section 2.3. Conversion of reactive dialdehydes to dicarboxylates was used in the past to study the structure and properties of DAPs and was shown to have minimal impact on the degree of polymerization of investigated molecules. (Kim et al., 2000; Münster et al., 2017) Here, it was employed to disrupt the hemiacetal bonds, which simulates processes occurring under the conditions of crosslinking reaction (drying, low pH), (Spedding, 1960) and thus more accurately describe the actual molecular weight distribution of DAPs during the crosslinking. The number average molecular weight (M_n), weight average molecular weight (M_w), polydispersity index (*PDI*), and degree of polymerization (*DP*) of dicarboxylated polysaccharides and corresponding M_n and M_w of DAPs are given in Table 1. The DXA exhibits the highest M_n of 30 kDa, followed by DAH (21 kDa), while DXI and DAC feature nearly identical M_n of ~12 kDa.

Besides the determination of molecular weight, the solutions of DAPs were investigated also using DLS to obtain the hydrodynamic radii (d_h) and zeta potentials (ζ) of DAP nano-assemblies which are spontaneously formed in their solutions (Table 2). Note, that measured d_h values do not follow the trend of the molecular masses of individual DAPs. Instead, nano-assemblies formed by linear molecules (DAC, DAH) are larger than those formed by branched crosslinkers despite these having the same (DXI) or significantly higher (DXA) M_n than their linear counterparts. The largest nano-assemblies are thus formed by DAH, while DAC produces similar results as DXA, despite nearly three times lower M_n. The size of DXI nano-assemblies is then nearly 1.5× smaller than those of DAC, despite having the same M_n. While the size distribution of DAC, DXI, and DAH nano-assemblies was relatively uniform (polydispersity between 0.35 and 0.4), the size distribution of DXA assemblies had a distinctly bimodal character, comprising of the dominant fraction (about 80%) of larger (d_h ~ 270 nm) and a minor fraction (about 20%) of smaller (~20 nm) nano-assemblies.

The formation of larger nano-assemblies by linear polysaccharides, particularly DAH, can be attributed to variances in macromolecular compaction between these and branched polysaccharides. The disruption of the C2–C3 bonds during the oxidation of pyranose rings introduces highly flexible elements into otherwise semi-rigid chains, as discussed by Kristiansen et al. (2013). The same authors also noted that the amount of compaction depends on the *DO*; the higher the *DO* is, the higher is the macromolecular compaction. The largest size of DAH nano-assemblies is thus attributed to the presence of non-oxidized *N*-acetyl-D-glucosamine units, which reduces the DAH chain flexibility compared to derivatives with completely oxidized chains. Stiffer macromolecules are not able to pack as tightly into nano-assemblies as the more flexible ones, which leads to larger sizes of their nano-assemblies. When AGU-based derivatives, *i.e.* the DAC, the DXI, and the DXA, are concerned, higher compaction of branched derivatives can be reasoned as follows.

Table 2
The hydrodynamic radii (d_h) and zeta potentials (ζ) of DAPs estimated by DLS.

	d_h (nm)	ζ (mV)
DXA	267 ± 19 (20 ± 3)	−14.6 ± 1.1
DAH	308 ± 1	−31.0 ± 1.9
DXI	170 ± 11	−23.6 ± 1.5
DAC	247 ± 28	−23.6 ± 1.1

The increased flexibility of oxidized sidechains in branched polysaccharides leads to the easier formation of hemiacetal bonds between the —CHO and —OH groups of polysaccharide backbone and sidechains. The DXA is, for instance, known to form a very dense network of highly stable intramolecular hemiacetals. (Maia et al., 2011) These bonds "tighten" the macromolecular structure by *de facto* "crosslinking" the sidechains with the main chain, which increases its compactness compared to branchless DAC.

Although the size distribution of nano-assemblies was measured in the neat crosslinker solutions, *i.e.* without the presence of PVA, which macromolecules would mask the signals of crosslinkers, it is reasonable to expect that nano-assemblies should be preserved also at least during the initial stages of crosslinking given their known stability in an acidic environment (Münster et al., 2017).

Regarding the stability of colloids, their ζ-potential values were between −15 mV for DXA and −31 mV for DAH. This is not surprising as DXA contains a fraction of non-oxidized (less polar) anhydroglucose units, while DAH bears also one carboxylic group per each basic structural unit increasing its negative charge. DLS and ζ-potential measurements of the samples were also repeated 1 week after their preparation, giving essentially the same results (not shown), thus implying a formation of stable colloids in aqueous solutions.

In the next step, cytotoxicity of crosslinkers was compared using mouse embryonic fibroblast cell line NIH/3T3 representing immortalized healthy tissue cells (Fig. 2). The cytotoxicity is defined by IC_{50} values, *i.e.* by the concentration of compound required to inhibit the NIH/3T3 cells growth by 50%.

All DAPs are non-cytotoxic up to the concentration of 0.1 mg/mL; DAH and DAC even support cell proliferation relative to culture plastic at this concentration. Overall, the DAH and DXA are the least cytotoxic, having IC_{50} 0.75 ± 0.04 mg/mL, and 0.73 ± 0.04 mg/mL, respectively. These are closely followed by DAC with IC_{50} = 0.65 ± 0.06 mg/mL. The most cytotoxic is DXI with IC_{50} 0.39 ± 0.03 mg/mL. The cytotoxicity of free crosslinkers might be related to the size of their nano-assemblies in neat solutions, which show similar dependence (DAH > DXA ~ DAC > DXI) and which likely influences their capability to cross the cellular membrane (cellular uptake). On the other hand, the cytotoxicity of the crosslinkers does not scale with the amount of reactive —CHO groups. For instance, the DXI, which has the same n_{-CHO} as DAC, is almost two

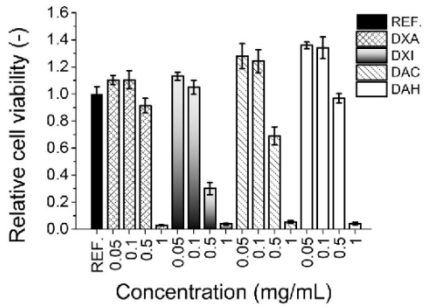

Fig. 2. Relative cell viability (NIH/3T3 cell line) after incubation in culture media containing 0–1 mg/mL of DAP for 24 h.

times more cytotoxic than other DAPs. Similarly, the DAH has essentially the same IC_{50} values as DXA and DAC despite having 2.5× lower amounts of —CHO groups. This may be related to previously reported adverse effects of low-molecular-weight HA on cells. (Tavianatou et al., 2019).

To put obtained cytotoxicity results into a better perspective, the cytotoxicity of glutaraldehyde was evaluated for comparison, see Fig. S2. GA was found severely toxic (relative cell viability <0.2) even at the lowest employed concentration of 0.05 mg/mL. Speer et al. even reported 99% inhibition of 3T3 fibroblast growth at 0.003 mg/mL concentration of GA. (Speer et al., 1980) All DAPs are thus many times less cytotoxic than GA.

3.2. Preparation of PVA/DAP hydrogels

Following the characterization of neat crosslinkers, PVA/DAP hydrogels were prepared using the well-established procedure described in Section 2.2. Two sets of hydrogels were prepared to investigate the effectiveness of the crosslinkers at low/high concentrations. The L-series hydrogels (L stands for Low amount of crosslinker) were prepared using 0.1 wt% of DAC, DXI, and DXA, and 0.25 wt% of DAH, respectively. Recall, that the amount of DAH was increased 2.5× to compensate for a proportionally lower amount of aldehyde groups as discussed in the previous section. The H-series samples (H stands for a High amount of crosslinker) were prepared in an analogous manner using 1 and 2.5 wt% of DAPs, respectively. Part of the swelled H-series samples was also heated in water to 70 °C for 2 h after thorough washing. Heat-treated hydrogels are designated with T, *e.g.* DXA-HT. Hydrogel samples were characterized in terms of network parameters, rheological properties, porosity, and cytotoxicity.

3.3. Network parameters

The equilibrium swelling of all hydrogels was determined and network parameters of all types of PVA/DAP hydrogel samples were calculated. Results are given in Fig. 3 and Fig. S3. The highest swelling among H-series samples has been observed for the DAH-H sample (~225%), followed by DXI-H and DAC-H samples which both swelled by about 200%, and the DXA-H sample with 170% swelling. Analogous trends are observed for equilibrium water content (*EWC*, Fig. S3), average molecular weight between crosslinks M_c and the mesh size ξ, while the crosslink density (ρ_c) increases in the opposite order (DXA-H has the highest crosslink density).

Heat treatment leads to a significant increase in hydrogel swelling, up to 480% for DAH-HT. The lowest swelling of 400% was observed for the DXA-HT sample. Overall trend thus remained the same as for H-series hydrogels. Other network parameters scaled accordingly; all were indicating a major decrease in crosslink density after heating. Although partial disruption of hemiacetal bonds during heating is a possibility, it is assumed that a major part of the observed decrease in crosslink density is caused by disruption of physical crosslinks in PVA, *i.e.* crystallites formed by hydrogen bonds between —OH groups of PVA chains during the preparation of hydrogel films. (Peppas and Merrill, 1977) Changes in hydrogel properties after heating demonstrate the importance of PVA physical crosslinks for hydrogel properties, which had to be taken into consideration for elucidation of individual crosslinking modes.

Contrary to H- and HT-series samples, the highest swelling in L-series was observed for DXI (620%), followed by DAH (500%) and DAC (480%) which are the same within experimental error, and DXA (420%), see Fig. 3. The swelling was thus larger and the hydrogel network sparser than in the previous series, which is attributed to i) lower number of chemical crosslinks and ii) decrease of the solid content of the hydrogels (and increase of EWC, see Fig. S3 in SI) given by the lower amount of crosslinker and as uncrosslinked chains are washed away during the purification of samples. The photographs of samples used for the analysis are given in Fig. S4.

3.4. Viscoelastic properties

The dependence of storage (G') and loss (G'') modulus of hydrogel samples on angular frequency is given in Fig. 4; for the dependence of complex modulus (G^*) and damping factor ($\tan\delta$) on angular frequency see Fig. 5.

All samples show a prevalence of elastic over the viscous component, as G' is larger than G'' and $tan\delta$ is lower than 1 for all samples. The G' values of H-series samples range from ~6500 Pa for the DXI-H sample to

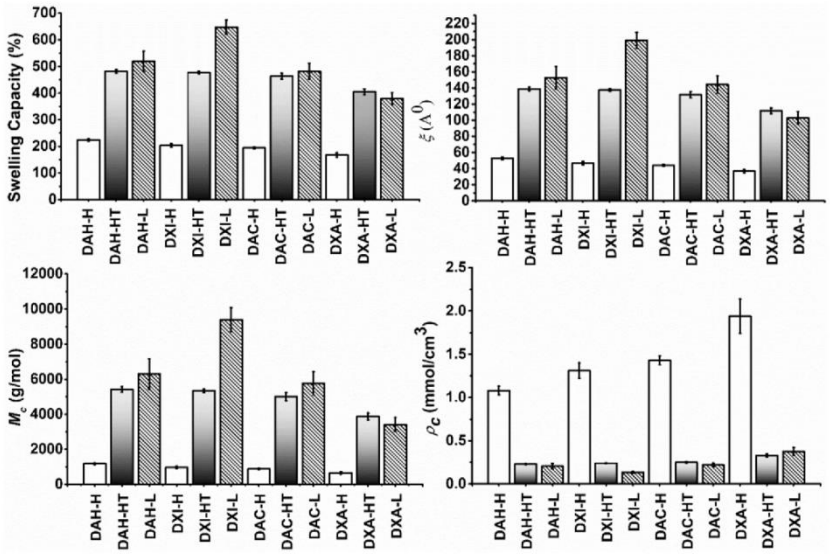

Fig. 3. Network parameters (the swelling capacity, the mesh size ξ, the average molecular weight between crosslinks M_c, the crosslink density ρ_c, and of individual PVA/DAP samples.

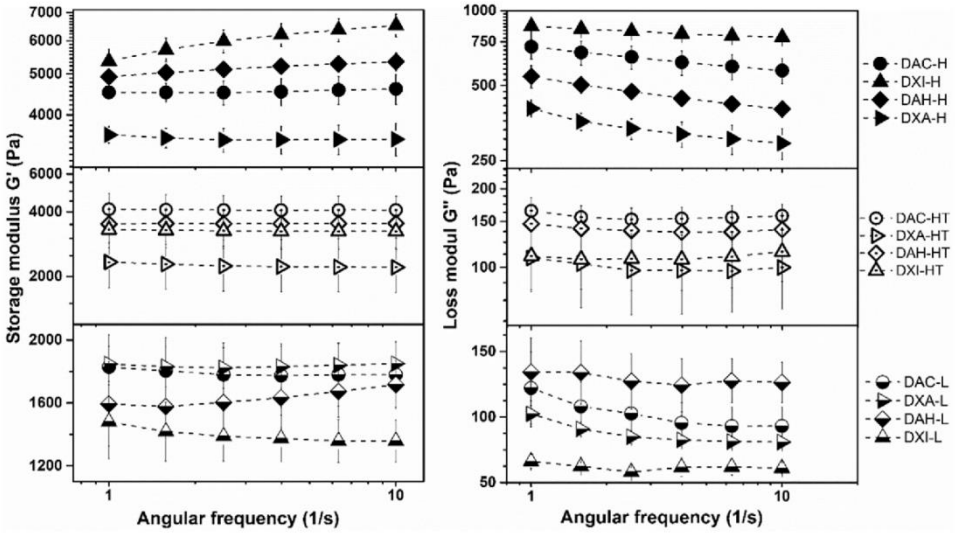

Fig. 4. Dependence of the storage modulus (G') and the loss modulus (G'') of PVA/DAP hydrogel samples on the angular frequency for H, HT, and L series hydrogels.

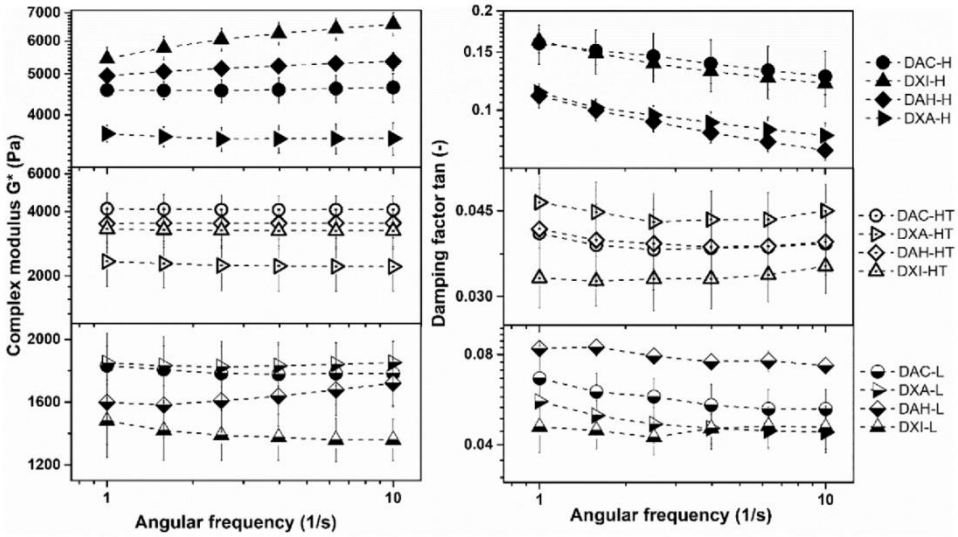

Fig. 5. Dependence of the calculated complex modulus G^* and the damping factor $tan\delta$ on the angular frequency.

~3500 Pa for the DXA-H sample (DXI > DAH > DAC > DXA). Note, that the DXA-H sample has the lowest G' values despite having the highest crosslink density; this issue is clarified in Section 4.

The G'' values follow a different trend than G', namely DXI > DAC > DAH > DXA. This is also reflected in damping factors, according to which DXI and DAC are the most elastic, while DAH and particularly DXA have more viscous characters (Fig. 4).

When hydrogel samples are heated, the G', G'' and $tan\delta$ values decrease relative to H-series samples in agreement with the loss of crosslinking. The largest decrease - nearly half of G' value relative to DXI-H - is observed for the DXI-HT sample, while the lowest relative decrease was observed for the DAC-HT sample. The G' values of DAC-HT, DAH-HT, and DXI-HT samples are the same within experimental error, while the DXA-HT sample remains the most viscous within the series. Analogical results were observed for G'' and $tan\delta$.

The decrease of storage and loss moduli and $tan\delta$ continues for L-series samples; the largest decrease compared to both H- and HT-series samples was again observed for the DXI-L sample, while the lowest decrease of storage modulus was observed for DXA-L and the lowest decrease of G'' (and thus the highest overall $tan\delta$) was obtained for DAH-L sample. Values of other samples in the L series are mostly comparable within experimental error, see Fig. 5.

3.5. BET and SEM

Samples of PVA/DAP hydrogels were lyophilized and resulting

cryogels were investigated by BET and SEM. Specific surface area (α_{BET}) and total pore volume (V_p) of the PVA/DAP samples are shown in Fig. 6. SEM micrographs of cryogels surfaces and cross sections can be found in Fig. S4 in SI.

The porosity of hydrogels increases from H-series to L-series samples. Among H-series hydrogels, the DAH-H sample has the highest and DAC-H the lowest α_{BET} and V_p values, being 3.9 m^2/g and 0.038 cm^3/g for DAH-H and 1.6 m^2/g and 0.001 cm^3/g for DAC-H, respectively. Correspondingly, the mean pore diameter (d_m) for DAH-H was highest, about ~35 nm, compared to the lowest found in DAC-H (~27 nm). The heating of the H-series samples led to an increase of α_{BET} and V_p in all cases. The α_{BET} values of HT-series samples are between 22.6 m^2/g (DAH-HT) and 16.9 m^2/g (DAC-HT), and V_p values between 0.32 cm^3/g (DAH-HT) and 0.16 cm^3/g (DAC-HT). The DAH-crosslinked sample thus remains the most porous even after the heating (see also SEM images in Fig. S4 in SI) and the DAC-crosslinked sample has the lowest overall porosity in both series. The decrease in crosslinker amount led to a dramatic increase in porosity for the DXI-L sample (α_{BET} = 39.8 m^2/g and V_p = 0.91 cm^3/g), which is the most porous from all tested samples. The least porous from L-series was the DXA-L sample with V_p and mean pore diameter 0.31 cm^3/g and 73 nm, respectively. Described differences between crosslinkers are visible also in SEM images (Fig. S4 in SI) both on the surface and on the cross section of individual samples, compare *e.g.* the DXA-L sample (the least porous) with the rest of the L-series.

3.6. Cytotoxicity of hydrogel extracts

Hydrogel extracts were prepared according to ISO 10 993-12, *i.e.* by extracting 0.1 g of swelled hydrogel samples per 1 mL of media. Cytotoxicity of hydrogel extracts was evaluated according to ISO 10 993-5 using mouse embryonic fibroblast cell line (NIH/3T3), see Fig. 7. Only results for 100% extracts are shown, as more diluted extracts were non-cytotoxic. Extracts are considered non-toxic according to ISO 10 993-5 if the relative cell viability is above 0.7 (dashed line in Fig. 7).

The cytotoxicity of hydrogel extracts only partially correlates with

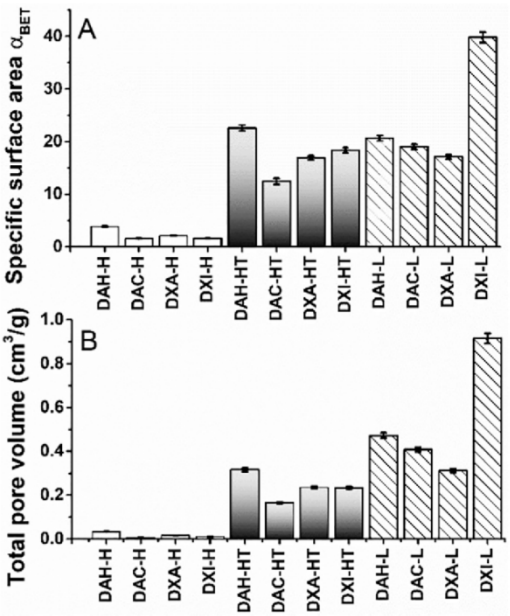

Fig. 6. The specific surface area (α_{BET}) and total pore volume (V_p) of prepared PVA/DAP cryogels.

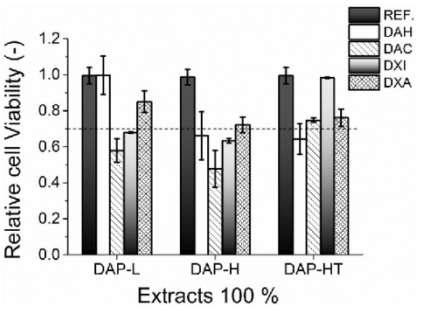

Fig. 7. Cytotoxicity of 100% hydrogel extracts evaluated according to ISO 10 993-5 using mouse embryonic fibroblast cell line (NIH/3T3). Relative cell viability 0.7 is marked by the dashed line.

the trends observed for free crosslinkers (Section 3.1) and depends on both the amount of crosslinker and the heating of the gel matrix. The least cytotoxic extracts were obtained from DAH and DXA-based hydrogels, respectively, which can be considered as non-cytotoxic (within experimental error) in all cases. Extracts from DAC and DXI-based hydrogels are both mildly cytotoxic in both L- and H-series; the DAC-H samples are the more cytotoxic, although the differences are not very large. The heat treatment of hydrogels significantly reduces the cytotoxicity of hydrogel extracts (particularly for DXI), likely because unreacted crosslinkers and partially crosslinked matrix fragments are better removed due to increased swelling of hydrogels at a higher temperature.

4. Discussion

Although all crosslinkers were used in doses containing the same amount of potential crosslinking hotspots (n_{CHO}), considerable differences between characteristics of individual hydrogels were observed. These can be attributed to the —CHO group density per macromolecule, the molecular weight, macromolecular architecture, and the size of nano-assemblies in the neat solutions of individual crosslinkers. A schematic overview of crosslinker characteristics is given in Fig. 8. The dimensions of crosslinker molecules and nano-assemblies are presented in scale relative to each other for better illustration; dimensions are based on measured *DP* (molecular weight) and d_h values (Section 3.1). The number of crosslinking hotspots per molecule represented by purple ovals reflects the relative ratio of –CHO groups between crosslinker molecules. Fig. 8 also schematically presents assumed binding modes for different crosslinkers which are rationalized below. Note, that a unified representation of the PVA matrix, which symbolizes the same concentration of PVA during the crosslinking, was used in all cases. The differences in the matrix (*e.g.* M_c values) of individual hydrogels were not implemented in Fig. 8 because these differ depending not only on crosslinker type but also on the crosslinker concentration, *i.e.* between series, which would complicate the presentation.

The characteristics and binding modes of individual crosslinkers derived from obtained results can be summarized as follows:

The DAC: Although the swelling and the crosslink density of DAC-based hydrogels are average compared to others, the storage modulus and damping factors are among the highest. Rheological properties of DAC-based hydrogels are also well retained after heating and at low crosslinker concentration, while the porosity of DAC xerogels is among the lowest across all series. Combined, all these facts indicate an evenly and effectively chemically crosslinked hydrogel network. This is in agreement with relatively large DAC nanodomains and high —CHO group density, which are comparable to those of almost three times heavier DXA and which allow for

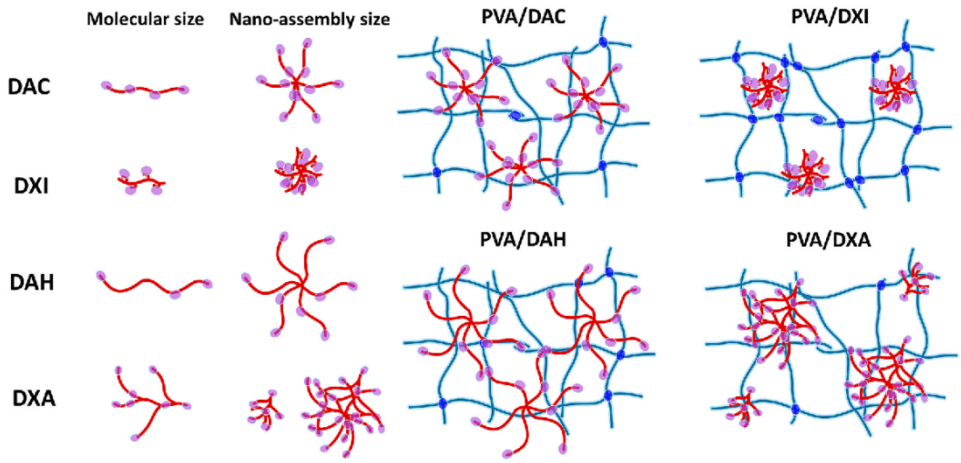

Fig. 8. Schematic representation of the size of the crosslinker molecules, n_{-CHO}, and hydrodynamic radii and assumed mode of crosslinking of PVA network. Crosslinking hotspots are in purple, residual physical crosslinks of the PVA matrix are given in blue. The sizes of individual macromolecules and nano-assemblies are reflecting the measured M_n and d_h, respectively, while the number of depicted crosslinking hotspots corresponds to the relative ratio of —CHO groups between crosslinker molecules. A unified representation of the PVA matrix, which symbolizes the same concentration of PVA during the crosslinking, was used for better clarity. Note, however, that sizes of PVA networks in swelled hydrogels differ as described in Section 3.3. (For interpretation of the references to colour in this figure legend, the reader is referred to the web version of this article.)

efficient crosslinking of even relatively distant PVA chains, see Fig. 8. Besides, the DAC crosslinking effectivity may be further enhanced by the presence of β-glycosidic bonds in its structure, resulting in an alternation of binding site directions along the DAC chain (see Fig. 1C). This allows efficient crosslinking of different PVA chains even by relatively close DAC units. The main disadvantage of DAC is the mild cytotoxicity of PVA/DAC hydrogel extracts, which can be however improved by heating of prepared hydrogels. DAC thus can be summarily described as a rather effective crosslinker because its hydrogels retain good properties even at low crosslinker concentrations or after the heating. On the other hand, DAC may not be the best choice for biological applications requiring higher porosity and excellent biocompatibility of prepared hydrogels, *e.g.* cellular scaffolds.

The DXI: Although the DXI has essentially the same M_n, n_{-CHO}, and chemical composition (AGU units) as DAC, the properties of DXI- and DAC-based hydrogels are markedly different due to their structure. For better illustration, selected hydrogel characteristics, namely swelling and storage modulus, were plotted against the M_n of the crosslinker, see Figs. S5 and S6 in SI. Given the same M_n of DAC and DXI, similar results might be expected. This is, however, not the case, as is best illustrated by the observed difference in swelling of the L samples. While the DXI-H sample features the highest storage modulus and damping factor despite having medium swelling and crosslink density, the properties of DXI-based hydrogels degrade rapidly after heating, *i.e.* when physical PVA crosslinks are disrupted, and decrease even further at low crosslinker concentration. DXI-L sample even features the highest swelling and porosity and the lowest network density and elasticity from all samples, thus being the polar opposite of DXI-H. Differences between DXI- and DAC-based hydrogels, which cannot be attributed to the different molecular weight or —CHO group density, can be justified by the smaller size of DXI domains. DXI-based hydrogels thus most likely contain comparatively smaller, but more numerous regions of very high crosslink density, embedded in otherwise physically crosslinked PVA network, see Fig. 8. A large fraction of physical crosslinks between the matrix chains improve hydrogel properties at high crosslinker concentrations, but these deteriorate quickly after heating (HT series – disruption of crystallites bound by hydrogel bonds) or when the amount of crosslinker is decreased. In the latter case, the compact DXI domains fail to crosslink more distant PVA chains which are more easily washed away. This decreases the solid content in the sample, which leads to the high porosity and low elastic component of DXI-L samples. DXI behaviour at lower concentrations thus resembles low-M_w crosslinkers. (Münster et al., 2018) This, in combination with one of the highest observed (yet still mild) cytotoxicity of DXI hydrogel extracts, makes DXI-based hydrogels the least interesting for biomedical applications of all tested species.

The DAH: Linear DAH macromolecules feature a significantly lower density of crosslinking hotspots per macromolecule than AGU derivatives due to their heteroglycan origin; only glucuronic acid units can be oxidized by periodate. The DAH thus forms a more loosely bound network than DAC even at high concentrations, which leads to the highest observed swelling, the lowest network density, the highest porosity, and the mediocre storage modulus of the DAH-H sample. At the same time, the properties of DAH-based hydrogels do not degrade as fast as those of DXI-based samples and even became comparable with DAC analogs at low crosslinker concentrations. This is ascribed to the large size of DAH nano-assemblies (and possibly also higher M_n of DAH macromolecules), which allows them to crosslink more distant PVA chains. Both DAH and DAH-based hydrogels also showed the lowest cytotoxicity from all samples. Overall, DAH-based hydrogels have a more viscous character, lower cytotoxicity, and higher porosity compared to other hydrogel samples, which makes them potentially interesting for the preparation of scaffolds for tissue engineering. Note, however, that a 2.5× higher amount of DAH is required to obtain hydrogels with physical qualities comparable to other crosslinkers.

The DXA: DXA-based hydrogel samples feature the lowest swelling and the highest crosslink density in every series. Hence, DXA-based hydrogels should also have the highest storage modulus and damping factors because the densest mesh should be able to store the most energy. This however applies only to the DXA-L sample, while the G' values of DXA-H and DXA-HT samples are the lowest within their respective series. The observed trend, *i.e.* the relatively small decrease of viscoelastic parameters with decreasing crosslinker

concentration, is thus the exact opposite of those found in another branched crosslinker, the DXI. The likely reason lies in the observed bimodal size distribution of DXA nano-assemblies. While the dominant fraction of relatively large (d_h ~ 270 nm) DXA nano-domains is capable to crosslink even distant PVA chains, numerous small (d_h ~ 20 nm) nano-domains act as a "secondary" crosslinker network, binding nearby PVA chains. Although the combination of dense and relatively short-range crosslinking with a decrease of viscoelastic parameters may seem counterintuitive, our recent solid-state NMR study revealed that the presence of a high amount of smaller crosslinker fragments evenly spread through the hydrogel network actually increases the distance of PVA chains and thus disrupts residual crosslinks between PVA chains. (Münster et al., 2018) The "secondary" short-range crosslinking is thus likely responsible for relatively low storage modulus of DXA-H/-HT samples as more distant PVA chains can more easily "slip" over each other and thus dissipate deformation energy more effectively than those involved in stiffer crystallites. Simultaneously, a large number of "short-range" crosslinks reduce the DXA hydrogels swelling, which agrees with obtained results. The importance of short-range "secondary" crosslinks decreases at low crosslinker concentration because thus crosslinked PVA chains are washed away more easily than those crosslinked by larger domains. Hence, the impact of long-distance crosslinks prevails in the DXA-L sample, resulting in properties comparable with the DAC-L sample of similar domain size and n_{-CHO}. To support the above-described reasoning, the crystallinity of dried-out DXI-H and DXA-H xerogel samples was compared. While the DXI-H sample showed 62% crystallinity, the crystallinity of DXA was only 54%. A higher amount of amorphous phase in the DXA sample indicates limited interaction of PVA chains and reduced formation of crystallites, which is in agreement with secondary short-range crosslinking. Regarding the biological properties, the DXA and DXA-based hydrogels show the lowest cytotoxicity from all AGU-based crosslinkers, comparable only with DAH. Overall, DXA produces hydrogels with comparatively lower swelling and better mechanical/rheological properties than DAH, particularly at low concentrations. This, in combination with low cytotoxicity, makes DXA-based hydrogels a potentially interesting alternative for DAH-based ones, which properties may not be up for the task at lower concentrations. The comparably lower swelling and porosity of DXA hydrogels may even present an advantage for some applications.

5. Conclusions

Properties of PVA hydrogels crosslinked by dialdehyde cellulose, dextrin, dextran, and hyaluronate were investigated and analyzed concerning the macromolecular and nanoscale architecture of the DAPs. Generally, our hypothesis has been confirmed as structural differences among source polysaccharides translated into dialdehyde derivatives had a pronounced impact on hydrogels characteristics. The most important factors were identified as (i) the —CHO group density (in this case also related to homo/heteroglycan origin of the crosslinker), (ii) the crosslinker structure (branched *vs.* linear) and molecular weight, and (iii) the size of crosslinker nano-assemblies spontaneously formed in their solutions.

The influence of —CHO group density of the crosslinker is, as expected, rather straightforward. The —CHO group density determines how many crosslinking hotspots are present in each crosslinker macromolecule. The lower density of —CHO groups increases hydrogel swelling and porosity while reducing hydrogel elasticity.

The influence of the crosslinker structure and the molecular weight is not as simple because both properties are mutually interconnected. The molecular weight of the crosslinker thus may not accurately reflect the properties of the resulting hydrogels when crosslinkers with the different architecture of macromolecular chains are considered. This is best illustrated by the case of DXI and DAC. While having the same M_n, the different architecture of their macromolecular chains results in significant variances in the properties of their hydrogels. Generally, the characteristics of hydrogels based on linear polysaccharides (DAC, DAH) are less dependent on concentration or heat treatment. The presence of branching may, however, be both beneficial (DXA) but also detrimental (DXI) at lower concentrations, depending on the sizes of the crosslinker nano-assemblies.

The size of crosslinker nano-assemblies, which reflects both the molar mass of crosslinker macromolecules as well as their structure, correlates with hydrogels properties and crosslinker binding modes rather well. Although it is not possible to unequivocally determine whether crosslinker nano-domains remain intact during the whole process of hydrogel preparation, the correlation between hydrogel properties and the size of nano-assemblies indicates that nano-assemblies were, at least partially, preserved even during the actual crosslinking. Generally, the crosslinkers with larger nano-assemblies remained effective even at lower concentrations due to their ability to bind even relatively distant matrix chains, while those with smaller ones excelled at higher concentrations, where they formed a dense network of relatively small chemically crosslinked domains complemented by physical interaction between matrix chains, but their properties deteriorated quickly at lower concentrations.

Regarding individual species, the DAC is a highly effective hydrogel crosslinker at both high and low concentrations, although low porosity and somewhat higher cytotoxicity of DAC-crosslinked hydrogels may limit its potential biological applications. The DXI, on the other side, is the least promising candidate from the whole set due to the strong dependence of DXI-based hydrogels properties on the amount of the crosslinker and the cytotoxicity of their extracts. DAH-based hydrogels feature comparatively higher porosity, more viscous character, and low cytotoxicity, which makes them particularly interesting for biomedical applications, although their mechanical/rheological properties might be lacking at lower concentrations. The DXA is the most effective crosslinker at low concentrations and produces the hydrogels with the lowest swelling. This, in combination with low cytotoxicity, makes DXA an interesting alternative for DAH-based hydrogels for the preparation of biomaterials, where better physical properties of the hydrogels are required.

Declaration of competing interest

The authors declare that they have no known competing financial interests or personal relationships that could have appeared to influence the work reported in this paper.

Acknowledgement

This work was supported by The Ministry of Education, Youth and Sports of the Czech Republic – DKRVO (RP/CPS/2020/006). M.M. was supported by the internal grant for specific research from Tomas Bata University in Zlín no. IGA/CPS/2021/002. Z.C. acknowledges the Czech Science Foundation grant 19-16861S.

Appendix A. Supplementary data

Supplementary data to this article can be found online at https://doi.org/10.1016/j.carbpol.2021.119022.

References

Caló, E., & Khutoryanskiy, V. V. (2015). Biomedical applications of hydrogels: A review of patents and commercial products. *Eur. Polym. J., 65*, 252–267. https://doi.org/10.1016/j.eurpolymj.2014.11.024

Dai, W. S., & Barbari, T. A. (1999). Hydrogel membranes with mesh size asymmetry based on the gradient crosslinking of poly(vinyl alcohol). *J.   Membr.   Sci., 156*(1), 67–79. https://doi.org/10.1016/S0376-7388(98)00330-5. Scopus.

Ding, W., & Wu, Y. (2020). Sustainable dialdehyde polysaccharides as versatile building blocks for fabricating functional materials: An overview. *Carbohydr. Polym., 248*, Article 116801. https://doi.org/10.1016/j.carbpol.2020.116801

Flory, P. J., & Rehner, J. (1943). Statistical Mechanics of Crosslinked Polymer Networks II. Swelling. *The Journal of Chemical Physics, 11*(11), 521–526. https://doi.org/10.1063/1.1723792

Gao, Z., Golland, B., Tronci, G., & Thornton, P. D. (2019). A redox-responsive hyaluronic acid-based hydrogel for chronic wound management. *J. Mater. Chem. B, 7*(47), 7494–7501. https://doi.org/10.1039/C9TB01683J

Hennink, W. E., & van Nostrum, C. F. (2012). Novel crosslinking methods to design hydrogels. *Adv. Drug Deliv. Rev., 64*, 223–236. https://doi.org/10.1016/j.addr.2012.09.009

Hu, W., Wang, Z., Xiao, Y., Zhang, S., & Wang, J. (2019). Advances in crosslinking strategies of biomedical hydrogels. *Biomater. Sci., 7*(3), 843–855. https://doi.org/10.1039/C8BM01246F

Kamoun, E. A., Chen, X., Mohy Eldin, M. S., & Kenawy, E.-R. S. (2015). Crosslinked poly (vinyl alcohol) hydrogels for wound dressing applications: A review of remarkably blended polymers. *Arab.J.Chem., 8*(1), 1–14. https://doi.org/10.1016/j.arabjc.2014.07.005

Kamoun, E. A., Kenawy, E.-R. S., & Chen, X. (2017). A review on polymeric hydrogel membranes for wound dressing applications: PVA-based hydrogel dressings. *J.Adv.Res., 8*(3), 217–233. https://doi.org/10.1016/j.jare.2017.01.005

Kim, U.-J., Kuga, S., Wada, M., Okano, T., & Kondo, T. (2000). Periodate oxidation of crystalline cellulose. *Biomacromolecules, 1*(3), 488–492. https://doi.org/10.1021/bm0000337

Kim, U.-J., Lee, Y. R., Kang, T. H., Choi, J. W., Kimura, S., & Wada, M. (2017). Protein adsorption of dialdehyde cellulose-crosslinked chitosan with high amino group contents. *Carbohydrate Polymers, 163*(Supplement C), 34–42. https://doi.org/10.1016/j.carbpol.2017.01.052

Koprivica, S., Siller, M., Hosoya, T., Roggenstein, W., Rosenau, T., & Potthast, A. (2016). Regeneration of aqueous periodate solutions by ozone treatment: A sustainable approach for dialdehyde cellulose production. *ChemSusChem, 9*(8), 825–833. https://doi.org/10.1002/cssc.201501639

Kristiansen, K. A., Potthast, A., & Christensen, B. E. (2010). Periodate oxidation of polysaccharides for modification of chemical and physical properties. *Carbohydr. Res., 345*(10), 1264–1271. https://doi.org/10.1016/j.carres.2010.02.011

Kristiansen, K. A., Dalheim, M.Ø., & Christensen, B. E. (2013). Periodate oxidation and macromolecular compaction of hyaluronan. *Pure Appl.Chem., 85*(9), 1893–1900. https://doi.org/10.1351/pac-con-13-01-05

Li, J., & Mooney, D. J. (2016). Designing hydrogels for controlled drug delivery. *Nature Reviews. Materials, 1*(12). https://doi.org/10.1038/natrevmats.2016.71

Li, S., Pei, M., Wan, T., Yang, H., Gu, S., Tao, Y., Liu, X., Zhou, Y., Xu, W., & Xiao, P. (2020). Self-healing hyaluronic acid hydrogels based on dynamic Schiff base linkages as biomaterials. *Carbohydr. Polym., 250*, Article 116922. https://doi.org/10.1016/j.carbpol.2020.116922

Maia, J., Carvalho, R. A., Coelho, J. F. J., Simões, P. N., & Gil, M. H. (2011). Insight on the periodate oxidation of dextran and its structural vicissitudes. *Polymer, 52*(2), 258–265. https://doi.org/10.1016/j.polymer.2010.11.058

Mayer, S., Tallawi, M., De Luca, I., Calarco, A., Reinhardt, N., Gray, L. A., Drechsler, K., Moeini, A., & Germann, N. (2021). Antimicrobial and physicochemical characterization of 2,3 dialdehyde cellulose-based wound dressings systems. *Carbohydr. Polym., 118506*. https://doi.org/10.1016/j.carbpol.2021.118506

Mou, K., Li, J., Wang, Y., Cha, R., & Jiang, X. (2017). 2,3-dialdehyde nanofibrillated cellulose as a potential material for the treatment of MRSA infection. *J. Mater. Chem. B, 5*(38), 7876–7884. https://doi.org/10.1039/C7TB01857F

Muchová, M., Münster, L., Capáková, Z., Mikulcová, V., Kuřitka, I., & Vícha, J. (2020). Design of dialdehyde cellulose crosslinked poly(vinyl alcohol) hydrogels for transdermal drug delivery and wound dressings. *Mater. Sci. Eng. C, 116*, Article 111242. https://doi.org/10.1016/j.msec.2020.111242

Münster, L., Vícha, J., Kloáč, J., Masař, M., Kucharczyk, P., & Kuřitka, I. (2017). Stability and aging of solubilized dialdehyde cellulose. *Cellulose, 24*(7), 2753–2766. https://doi.org/10.1007/s10570-017-1314-x

Münster, L., Vícha, J., Kloáč, J., Masař, M., Hurajová, A., & Kuřitka, I. (2018). Dialdehyde cellulose crosslinked poly(vinyl alcohol) hydrogels: Influence of catalyst and crosslinker shelf life. *Carbohydr. Polym., 198*, 181–190. https://doi.org/10.1016/j.carbpol.2018.06.035

Münster, L., Capáková, Z., Fišera, M., Kuřitka, I., & Vícha, J. (2019). Biocompatible dialdehyde cellulose/poly(vinyl alcohol) hydrogels with tunable properties. *Carbohydr. Polym., 218*, 333–342. https://doi.org/10.1016/j.carbpol.2019.04.091

Münster, L., Hanulíková, B., Machovský, M., Latečka, F., Kuřitka, I., & Vícha, J. (2020). Mechanism of sulfonation-induced chain scission of selectively oxidized polysaccharides. *Carbohydr. Polym., 229*, Article 115503. https://doi.org/10.1016/j.carbpol.2019.115503

Münster, L., Fojtů, M., Capáková, Z., Muchová, M., Musilová, L., Vaculovič, T., Balvan, J., Kuřitka, I., Masařík, M., & Vícha, J. (2021). Oxidized polysaccharides for anticancer-drug delivery: What is the role of structure? *Carbohydr. Polym., 257*, Article 117562. https://doi.org/10.1016/j.carbpol.2020.117562

Münster, L., Fojtů, M., Muchová, M., Latečka, F., Káčerová, S., Capáková, Z., Juriňáková, T., Kuřitka, I., Masařík, M., & Vícha, J. (2021). Enhancing cisplatin anticancer effectivity and migrastatic potential by modulation of molecular weight of oxidized dextran carrier. *Carbohydr. Polym., 272*, Article 118461. https://doi.org/10.1016/j.carbpol.2021.118461

Patterson, J., Siew, R., Herring, S. W., Lin, A. S. P., Guldberg, R., & Stayton, P. S. (2010). Hyaluronic acid hydrogels with controlled degradation properties for oriented bone regeneration. *Biomaterials, 31*(26), 6772–6781. https://doi.org/10.1016/j.biomaterials.2010.05.047

Peppas, N. A., & Merrill, E. W. (1977). Crosslinked poly(vinyl alcohol) hydrogels as swollen elastic networks. *J. Appl. Polym. Sci., 21*(7), 1763–1770. https://doi.org/10.1002/app.1977.070210704

Petlin, A. S. (2006). Glycol-cleavage oxidation. In D. Horton (Ed.), *60. Advances in Carbohydrate Chemistry and Biochemistry* (pp. 183–250). Academic Press. https://doi.org/10.1016/S0065-2318(06)60005-X.

Rudra, R., Kumar, V., & Kundu, P. P. (2015). Acid catalysed cross-linking of poly vinyl alcohol (PVA) by glutaraldehyde: Effect of crosslink density on the characteristics of PVA membranes used in single chambered microbial fuel cells. *RSC Adv., 5*(101), 83436–83447. https://doi.org/10.1039/C5RA16068E

Spedding, H. (1960). 628. Infrared spectra of periodate-oxidised cellulose. *J.Chem.Soc.*, 3147–3152. https://doi.org/10.1039/JR9600003147

Speer, D. P., Chvapil, M., Eskelson, C. D., & Ulreich, J. (1980). Biological effects of residual glutaraldehyde in glutaraldehyde-tanned collagen biomaterials. *Journal of Biomed. Mater. Res., 14*(6), 753–764. https://doi.org/10.1002/jbm.820140607

Su, H., Zheng, R., Jiang, L., Zeng, N., Yu, K., Zhi, Y., & Shan, S. (2021). Dextran hydrogels via disulfide-containing schiff base formation: Synthesis, stimuli-sensitive degradation and release behaviors. *Carbohydr. Polym., 265*, Article 118085. https://doi.org/10.1016/j.carbpol.2021.118085

Tavianatou, A.-G., Piperigkou, Z., Barbera, C., Beninatto, R., Masola, V., Caon, I., Onisto, M., Franchi, M., Galesso, D., & Karamanos, N. K. (2019). Molecular size-dependent specificity of hyaluronan on functional properties, morphology and matrix composition of mammary cancer cells. *Matrix Biol. Plus, 3*, Article 100008. https://doi.org/10.1016/j.mbplus.2019.100008

Veelaert, S., de Wit, D., Gotlieb, K. F., & Verhé, R. (1997). Chemical and physical transitions of periodate oxidized potato starch in water. *Carbohydr. Polym., 33*(2–3), 153–162. https://doi.org/10.1016/S0144-8617(97)00046-5

Yan, G., Zhang, X., Li, M., Zhao, X., Zeng, X., Sun, Y., Tang, X., Lei, T., & Lin, L. (2018). Stability of soluble dialdehyde cellulose and the formation of hollow microspheres: Optimization and characterization. *ACS Sustain.Chem.Eng.* https://doi.org/10.1021/acssuschemeng.8b04825

Zhang, M., Chen, G., Lei, M., Lei, J., Li, D., & Zheng, H. (2021). A pH-sensitive oxidized-dextran based double drug-loaded hydrogel with high antibacterial properties. *Int.J.Biol.Macromol., 182*, 385–393. https://doi.org/10.1016/j.ijbiomac.2021.03.169

Preparation of (bio)polymer matrices for substance transfer and study of their release

Příprava (bio)polymerních matric pro přenos látek a studium jejich uvolňování

Doctoral Thesis

Tomas Bata University in Zlin

Nám. T.G. Masaryka 5555, 760 01, Zlín

Typesetting by: Monika Muchová

This publication has not undergone any proofreading or editorial review.

Publication year: 2023